Forschungsbericht 2022-02

Physical interaction effects of out of plane waviness and impact damages of fiber composite structures

Nagham Al-Kathemi

Deutsches Zentrum für Luft- und Raumfahrt
Institut für Faserverbundleichtbau und Adaptronik
Braunschweig

DLR Deutsches Zentrum für Luft- und Raumfahrt

Forschungsbericht 2022-02

Physical interaction effects of out of plane waviness and impact damages of fiber composite structures

Nagham Al-Kathemi

Deutsches Zentrum für Luft- und Raumfahrt
Institut für Faserverbundleichtbau und Adaptronik
Braunschweig

117 Seiten
107 Bilder
17 Tabellen
50 Literaturstellen

Deutsches Zentrum
DLR für Luft- und Raumfahrt

Herausgeber:

Deutsches Zentrum
für Luft- und Raumfahrt e. V.
Wissenschaftliche Information
Linder Höhe
D-51147 Köln

ISSN 1434-8454
ISRN DLR-FB-2022-02

DOI: https://doi.org/10.57676/5bbk-dt97

Restfestigkeit nach Schlagschaden, Druckrestfestigkeit, Schadenstoleranz, Interaktionseffekt, Fertigungsdefekte, Aufprallschäden

Nagham Al-Kathemi
DLR, Institut für Faserverbundleichtbau und Adaptronik, Braunschweig

Physikalische Interaktionseffekte von Welligkeiten und Schlagschäden in Faserverbundstrukturen
Dissertation Universität Bremen

Diese Arbeit liefert experimentelle Untersuchungen für ein verbessertes physikalisches Verständnis des Interaktionsverhaltens zwischen Welligkeiten außerhalb der Ebene und Aufprallschäden niedriger Geschwindigkeit. Tests an quasi-isotropen Laminaten unterschiedlicher Kombination von Welligkeiten und Schlagschäden wurden durchgeführt, um den Einfluss auf die Druckrestfestigkeit zu untersuchen. Der Einfluss von Welligkeiten und Aufprallschäden wurde getrennt und simultan untersucht. Im Lastfall reiner Welligkeiten wurden zwei Dicken mit verschiedenen Welligkeitskonfigurationen getestet, um die kritischen Welligkeitsparameter sowie deren Dickenabhängigkeit zu identifizieren. Ein entsprechender Abminderungsfaktor wurde abgeleitet. Bei Kombination von Welligkeiten und Schlagschäden wurde eine Dicke ohne und mit unterschiedlichen Welligkeitskonfigurationen getestet. Die Tests führten zur Ableitung von drei Abminderungsfaktoren. Die experimentellen Untersuchungen zeigen, dass die Welligkeiten im untersuchten Aufprallenergieniveau nicht zwangsläufig zu einer Abminderung der betroffenen Abminderungsfaktoren führen. Welligkeitseffekte können Aufprallschädigungseffekte nicht kompensieren oder umgekehrt, dementsprechend stellt das Interaktionsverhalten näherungsweise eine multiplikative Beziehung dar, die durch Superposition von separat ermittelten Effekten angenähert werden kann.

Compression after impact (CAI), plain strength compression (PSC), damage tolerance (DT), interaction effect, manufacturing defects, low velocity impact

(Published in English)

Nagham Al-Kathemi

DLR, Institute of composite structures and adaptive systems, Braunschweig

Physical interaction effects of out plane waviness and impact damages of fiber composite structures
Dissertation University Bremen

This thesis provides the experimental investigations for an improved physical understanding of the interaction behavior between out of plane waviness (OoP) and low velocity impact damages. Plain strength compression (PSC), impact as well as compression after impact (CAI) tests on the compression strength of a quasi-isotropic laminates were conducted. The effects of OoP waviness and impact damages were considered separately and simultaneously. In the PSC case, two thicknesses with different waviness configurations were tested in order to identify the critical waviness parameters and their dependence on the thickness. A corresponding pure waviness Knock-Down-Factor (KDF) was derived. In the CAI case, one thickness with different waviness configurations as well as one configuration without waviness were tested. The CAI tests with and without waviness led to the derivation of three KDFs. The experimental results reveal that the waviness effect in the investigated impact energy level is present, even if the corresponding KDF is not always degraded. Waviness effects cannot compensate impact effects or vice versa, accordingly, the interaction behavior represents approximately a multiplicative relation which can be simplified by superposition of both effects individually.

TU Braunschweig – Niedersächsisches
Forschungszentrum für Luftfahrt

Berichte aus der Luft- und Raumfahrttechnik

Forschungsbericht 2022-06

Physical interaction effects of out of plane waviness and impact damages of fiber composite structures

Nagham Al-Kathemi

Deutsches Zentrum für Luft- und Raumfahrt
Institut für Faserverbundleichtbau und Adaptronik
Braunschweig

Diese Veröffentlichung wird gleichzeitig in der Berichtsreihe „NFL - Forschungsberichte“ geführt.

PHYSICAL INTERACTION EFFECTS OF OUT OF PLANE WAVINESS AND IMPACT DAMAGES OF FIBER COMPOSITE STRUCTURES

Dem Fachbereich Produktionstechnik
der
UNIVERSITÄT BREMEN

zur Erlangung des Grades
Doktor-Ingenieur
genehmigte

Dissertation
von
Dipl. Ing. Nagham Al-Kathemi

Gutachter: Prof. Dr.-Ing. Richard Degenhardt, Universität Bremen

Prof. Dr.-Ing. Dieter Meiners, Technische Universität Clausthal

Tag der mündlichen Prüfung: 17. Januar 2022

To my best friend and husband Lukas, my family and friends for believing in me…

Acknowledgments

The investigations were conducted under sponsorship between Airbus Operations and German Aerospace Center (DLR). The research leading to these results has received also follow-up funding from the European Community's Eighth Framework Programme (FP8/H2020), under Priority ERDF (European Regional Development Fund), Grant Agreement Number ZW 6-85038492. All support is gratefully acknowledged.

I would like to thank my Doktorvater Professor Dr.-Ing. Richard Degenhardt as well as Professor Dr.-Ing. Martin Wiedemann, Dr.-Ing. Tobias Wille, Dr.-Ing. Guido Kuhlmann, Dr. Ing. Hubert Temmen, M. Sc. Ümüt Görgülü, Dipl.-Ing. Bernd Räckers, Dr.-Ing. Achim Etzkorn, Dr.-Ing. Falk Heinecke, Dr.-Ing Raffael Marius Bogenfeld, Dipl.-Ing. Markus Kepke and Dipl.-Ing. Bernd Hildebrandt for their support.

I am also grateful to all other members of the doctoral committee, Professor Dr.-Ing. Dieter Meiners, Professor Dr.-Ing. Axel Herrmann, Dr.-Ing. Christian Willberg, Dipl.-Ing. Christoph Hoffmeister and Johannes Lämmle.

Nagham Al-Kathemi

Abstract

This thesis provides the experimental investigations for an improved physical understanding of the interaction behavior between manufacturing and in-service defects in composite structures. Out of plane waviness (OoP) as well as low velocity impact damages are very common defects in different industrial sectors, which lead individually to a serious reduction in the strength – in particular the compressive strength – and stiffness, and are therefore respected during design. Nevertheless, there is still a lack of knowledge in the interaction behavior of these defects.

An experimental campaign was defined considering the out of plane waviness and impact damages separately and simultaneously. There is no standard for waviness fabrication, that is why preliminary manufacturing trials were conducted enabling the development of a specific OoP waviness fabrication method. It covers industrial cases, in which the OoP waviness is induced by overlaps or inadvertently inserted foreign objects during the layup process. Appropriate testing methodologies were selected to enable the testing of wavy specimens. The experimental results were analysed and empirical relations related to the interaction behaviour were derived. Finally, the findings were verified by experimental results from literature.

Plain strength compression (PSC), impact as well as compression after impact testing (CAI) on the compression strength of a quasi-isotropic laminates were conducted according to the Airbus standards. In the PSC case, two thicknesses with different waviness configurations were tested in order to identify the critical waviness parameters as well as the dependency between the thickness and the critical waviness parameters. A corresponding pure waviness knock down factor ($KDF_{Wav,\ PSC}$) was derived. In the CAI case, one thickness with different waviness configurations as well as one configuration without waviness were tested. The CAI test with and without waviness led to the derivation of three KDFs, the influencing factors as well as a physical understanding of the interaction behavior. These KDFs are related to the effect of impact ($KDF_{Imp,\ CAI}$), waviness ($KDF_{Wav,\ CAI}$), and their interaction effect ($KDF_{Interaction,\ CAI}$) on compression strength. The comparison of these KDFs reveals that the waviness effect in the investigated impact energy level is present, even if the $KDF_{Interaction,\ CAI}$ is not always degraded. Waviness effects cannot compensate impact effects or vice versa, accordingly, the interaction behavior represents approximately a multiplicative relation which can be simplified by superposition of both effects individually $KDF_{Wav,\ PSC}$ and $KDF_{Imp,\ CAI}$. It does not mean that there is no interaction between both defects. However, this simplification is a useful mean for preliminary assessment of the interaction behavior.

The identified influencing factors reveal that it is the interplay between the waviness morphology, number of affected 0°-plies and waviness angles that are the relevant variables. They depend on the impact energy and impact direction relative to waviness orientation and position for reducing the compression strength and not just the waviness angle alone and projected delamination areas.

Zusammenfassung

Diese Arbeit liefert experimentelle Untersuchungen für ein verbessertes physikalisches Verständnis des Interaktionsverhaltens zwischen Fertigungs- und Betriebsbedingten Defekten in Faserverbundstrukturen. Welligkeiten (Out of plane waviness) sowie Aufprallschäden aufgrund niedriger Geschwindigkeit (Low Velocity Impact) sind sehr verbreitete Defekte in verschiedenen Industriebranchen. Diese können einzeln zu einer gravierenden Abminderung der Festigkeit – insbesondere der Druckfestigkeit – und Steifigkeit führen, weshalb sie bei der Auslegung berücksichtigt werden müssen. Dennoch mangelt es noch an Wissen über das Interaktionsverhalten dieser Defekte.

Eine experimentelle Kampagne wurde definiert, bei der Welligkeiten und Aufprallschäden getrennt und simultan berücksichtigt wurden. Es gibt keinen Standard für die Welligkeitsherstellung, deshalb wurden vorläufige Herstellungsversuche durchgeführt, die die Entwicklung einer spezifischen Welligkeitsherstellungsmethode ermöglichten. Sie deckt Industriefälle ab, bei denen die Welligkeit durch Überlappungen oder versehentlich integrierte Fremdkörper während des Layup-Prozesses hervorgerufen wird. Geeignete Testmethoden wurden ausgewählt, um das Testen von welligen Proben zu ermöglichen. Die experimentellen Ergebnisse wurden analysiert und empirische Zusammenhänge zum Interaktionsverhalten abgeleitet. Schließlich wurden die Ergebnisse durch experimentelle Ergebnisse aus der Literatur verifiziert.

Plain Strength Compression (PSC), Impact sowie Compression after Impact (CAI) Tests zur Untersuchung der Druckfestigkeit eines quasi-isotropen Laminats wurden nach Airbus-Standards durchgeführt. Im PSC Lastfall wurden Proben mit zwei Dicken mit unterschiedlichen Welligkeitskonfigurationen getestet, um die kritischen Welligkeitsparameter sowie die Abhängigkeit zwischen der Dicke und den kritischen Welligkeitsparametern zu identifizieren. Ein entsprechender Knock Down Faktor ($KDF_{Wav, PSC}$) für reine Welligkeit wurde abgeleitet. Im CAI Lastfall wurde eine Dicke mit unterschiedlichen Welligkeitskonfigurationen, sowie eine Konfiguration ohne Welligkeit getestet. Der CAI Test mit und ohne Welligkeit führte zur Ableitung von drei KDFs, den Einflussfaktoren sowie einem physikalischen Verständnis des Interaktionsverhaltens. Diese KDFs geben jeweils die Auswirkung der Aufschlagschäden ($KDF_{Imp, CAI}$), Welligkeit ($KDF_{Wav, CAI}$) und ihrem Wechselwirkungseffekt ($KDF_{Interaction, CAI}$) auf die Druckfestigkeit wieder. Der Vergleich dieser KDFs zeigt, dass der Welligkeitseffekt im untersuchten Aufprallenergieniveau vorhanden ist, auch wenn die $KDF_{Interaction, CAI}$ nicht immer beeinflusst bzw. abgemindert wird. Welligkeitseffekte können Aufprallschädigungseffekte nicht kompensieren oder umgekehrt, dementsprechend stellt das Interaktionsverhalten näherungsweise eine multiplikative Beziehung dar, die durch Superposition der beiden Effekte einzeln $KDF_{Wav, PSC}$ und $KDF_{Imp, CAI}$ vereinfacht werden kann. Es bedeutet nicht, dass es keine Wechselwirkung zwischen beiden Defekten gibt. Diese Vereinfachung ist jedoch ein nützliches Mittel zur vorläufigen Einschätzung des Interaktionsverhaltens.

Die identifizierten Einflussfaktoren zeigen, dass das Zusammenspiel zwischen Welligkeitsmorphologie, Anzahl der betroffenen 0°-Lagen und Welligkeitswinkeln die relevanten Variablen sind. Sie hängen von der Aufprallenergie und Aufprallrichtung relativ zur Welligkeitsorientierung und -position zur Reduzierung der Druckfestigkeit ab und nicht nur vom Welligkeitswinkel allein und projizierten Schadenflächen.

Contents

List of tables

List of Figures

List of Symbols

$\alpha_{0°}$	Number of affected 0°-plies ratio
α	Total number of affected plies ratio
A	Amplitude
A/L	Amplitude to wavelength ratio
c	Cross section centroid
E	Young's modulus
L	Wavelength
Θ	Waviness angle
Φ	Diameter of the projected delamination area
ε_x	Inplane strain in cartesian coordinate system
ε_z	Interlaminar normal strain in cartesian coordinate system
ε_{xz}	Interlaminar shear strain in cartesian coordinate system
$\sigma_1 = \sigma_\parallel$	Inplane stress in fiber direction in material coordinate system
$\sigma_2 = \sigma_\perp$	Inplane stress transverse to fiber direction in material coordinate system
$\sigma_3 = \sigma_\perp$	Interlaminar stress transverse to fiber direction in material coordinate system
σ_r	Peel stress
$\tau_{21} = \tau_{\perp\parallel}$	Inplane shear stress in material coordinate system
$\tau_{31} = \tau_{\perp\perp}$	Interlaminar shear stress in material coordinate system
t*	Increased thickness due to waviness

List of Abbreviation

AFP	Automatic fiber placement
ATL	Automatic tape lay-up
BVID	Barely visible impact damage
CAI	Compression after impact
CLT	Classical laminate theory
CODAC	Composite damage tolerance analysis code
DoF	Degree of freedom
DIC	Digital Image Correlation
GFP	Glass fiber reinforced plastic
FE	Finite element
FL	Failure load
Imp	Impact
IP	Inplane
ILNS	Interlaminar normal stress
ILSS	Interlaminar shear stress
KDFs	Knock down factors
Lam.	Laminate
Morph.	Morphology
QI	Quasi isotropic
OoP	Out of plane
Pos.	Position
PSC	Plain strength compression
Ref.	Reference
SSM	Single shell model
SpSM	Split shell model
UD	Unidirectional
Wav	Waviness

1 Introduction

Fiber composite materials are characterized by high weight-specific stiffness and strength properties, that is why they are increasingly used in different sectors like aviation, wind energy, automobile etc.. Although composite materials have excellent properties, they are very susceptible to manufacturing related defects and impact damages during operation (out of plane and inplane waviness, delamination, porosity, impact damages, etc.). In particular, the compression strength shows a strong dependency on these defects. Despite the greatest care, manufacturing induced defect and impact damages cannot be avoided in practice. This leads to high tolerance and quality requirements in the production which are associated with additional expenditure of time and costs caused by for instance repairs, additional engineering assessment, long processing, extended dwell times of the components and increased inventory.

Out of plane waviness (OoP) as well as low velocity impact damages are very common defects in different industrial sectors. Out of plane waviness can be caused for instance by overlaps, gaps, foreign objects as shown in Figure 1 and Figure 2 or by dropped off plies. In Figure 1 different sources for the development of waviness are illustrated. Depending on these causes, the initial inplane fiber orientation is disturbed by waviness, so that different number of affected plies and 0°-plies are influenced by waviness with different waviness angles. The 0°-plies are light-colored in this figure. As a consequence of this fiber misalignment, the nominal geometrical condition of the structure can be affected leading to a thickness increase in case of foreign object or overlaps or decrease in case of gaps. Additionally, OoP waviness is often accompanied by other structural health issues such as resin reach areas in case of gaps or fiber reach areas in case of overlaps. In both cases, the stiffness and the neutral axis position of the laminates are affected. Low velocity impact damage can be caused for instance by tooling drop during the manufacturing or assembly, or by stones impact during operation. Depending on the impact energy, the induced damages are often barely visible. Nevertheless, such impact damages are mostly accompanied by other defects like fiber breakage, matrix cracking or delamination. Consequently, OoP waviness and impact damages individually lead to a serious reduction in the strength and stiffness, and are therefore respected during design. In addition, both defects are challenging because both waviness and impact damage are usually difficult to detect. Impact further leads to barely visible damage.

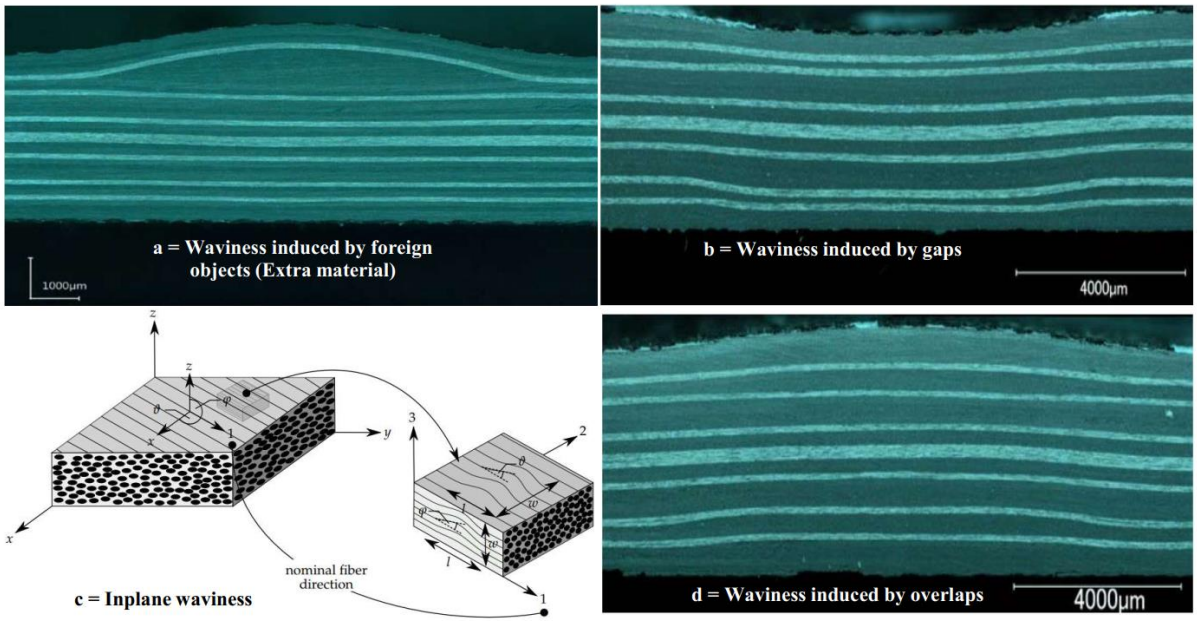

Figure 1: Waviness induced by foreign objects, waviness induced by gaps, waviness induced by overlaps, inplane waviness [1]

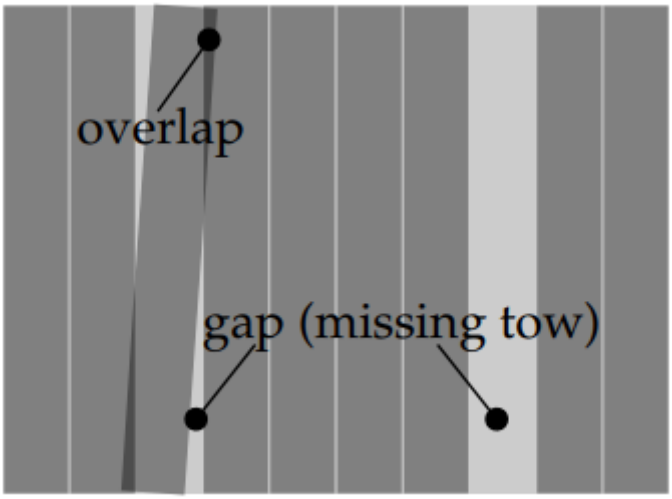

Figure 2: Gaps and overlaps caused by automatic fiber placement (AFP) [1]

The research fields of waviness and impact damages have attracted the attention of many researchers. Both fields were analyzed in detail analytically, numerically and experimentally, but the interaction between them is still unexplored. Experience has shown that both types of defects accumulate in different industrial sectors for instance aviation. Since aircraft structures must satisfy damage tolerance requirements, the worst case must be covered including interaction effect between waviness and impact. Damage tolerance to low velocity impacts is a key factor in the design of the aircraft structures due to the low out of plane strength of the composites. In addition, compression strength after impact is a critical factor in design due to its sensitivity to manufacturing defects. The lack of physical understanding results in conservative design requirements and tight tolerances in production. Thus, the composite potential cannot be exploited.

As a result, the focus of this thesis is the investigation of the interaction behavior between OoP waviness and low velocity impact damage experimentally aiming to derive and identify the relevant and critical influencing factors of both defects separately and in interaction under compression loading condition. This objective is achieved by defining a specific test campaign based on the reviewed literature which allows the investigation of the pure waviness effect in undamaged structure, pure impact effect on the damage resistance and damage tolerance as well as the waviness effect in an impacted structure. Accordingly, the test campaign consists of plain strength compression testing (PSC), impact testing as well as compression after impact testing (CAI). This intent requires a specific waviness fabrication method with predefined waviness parameters in multilayer laminate to cover industrial applications. Therefore, a waviness fabrication method was developed which enabled the investigation of different waviness angles, number of affected plies and number of affected 0°-plies in dependence of a critical waviness morphology for both load cases.

Despite increasing automation in the production of composite structures, manufacturing defects cannot be completely avoided. Therefore, there is a need for an improved understanding of the physical relations in case of interaction between impact damages and waviness defects. Building this physical based understanding represents an essential milestone in order to develop improved methods, to reduce conservatisms in design requirements as well as to avoid catastrophic failure mechanisms through the interaction on the one hand and to develop lighter, more efficient and more environmentally friendly aircraft on the other hand.

All results and findings including relations describing the interaction behavior as well as the majority of the graphs, tables, figure and text passages introduced in this thesis are based on the experimental investigation published by Al-Kathemi [2].

2 State-of-the-art

This chapter comprises common damages occurred in composite structures, reviewed literature emphasizing the lack of investigations regarding the interaction behavior as well as a brief introduction of relevant structural mechanical aspects related to the damage evolution.

2.1 Damages in composite structures

Although, fiber composite materials are characterized by high weight-specific stiffness and strength properties, nevertheless, compared to metallic structures the design is more challenging and the damage behavior is more complex. Different kind of damages can occur during manufacturing, assembly and in-service. These are briefly described below.

Manufacturing defects are usually waviness, overlaps, gaps, porosity, delamination, matrix cracking, fiber fracture and thickness deviations. **Assembly defects** are for instance impact damages due to the foreign objects and/or collision, scratches as well as delamination around holes and joints due to the drilling process. **In-service defects** are mainly impact damages caused by foreign objects like stones, hails etc., delamination caused by impact, temperature cycling and fatigue, fiber fracture caused by foreign object impact, lightning strike, scratches or abrasion.

Waviness is categorized in inplane (IP) and out of plane (OoP) waviness. The IP waviness represents an inplane fiber misalignment with respect to the nominal ply orientation as shown in Figure 1 (c). Out of plane waviness represents an out of plane fiber misalignment with respect to the nominal ply orientation affecting the geometrical condition of the structure component, which can lead to thickness deviation depending on the cause of the waviness as shown in Figure 1 (a, b and d). Waviness can be induced during the layup process, molding or curing process. In the filament winding process, waviness can be induced due to the non-uniform pressure between the plies. In the layup process of multidirectional laminates, residual longitudinal and transverse stresses can be the cause to induce waviness due to the mismatch of thermal coefficient expansion between polymer matrix, fiber and mold. In the molding process, waviness can be induced due to the deformation restraint of the plies in a multidirectional prepreg, resulting in IP and/ or OoP waviness. During the curing process, waviness can be induced due to the unintended presence of foreign objects.

Gaps and overlaps are common defects, which can be induced for instance during the automatic fiber placement (AFP) or automatic tape layup (ATL) due to the processing method and/or change in the geometry of the structure. Gaps induced by AFP are shown in Figure 2. These defects are the results of the material quality, the machine parameters, unintentionally programming error of the layup machine, respectively as well as complex part geometries and layups. Depending on the material quality each tow undergoes width deviation resulting in gaps and/or overlaps which can be occurred between tows and courses in AFP or ATL. Both overlaps and gaps can be the source for waviness, which are often accompanied by other structural health issues as described in Chapter 1.

Porosities are known as the volume fraction of voids in composite materials. Voids are induced by trapped air, volatiles and off-gassing, tool and bag leaks. Several types of voids of an un-debulked and uncured prepreg laminate are shown in Figure 3. These are fiber tow voids, which can be present within the fiber tow; interlaminar voids, which can be present between the plies and resin voids. After an accepted curing process most of these porosities are eliminated, nevertheless a small proportion remains, which often must be tolerated. Porosities also can be the source for development of waviness, because their presence can induce fiber misalignment.

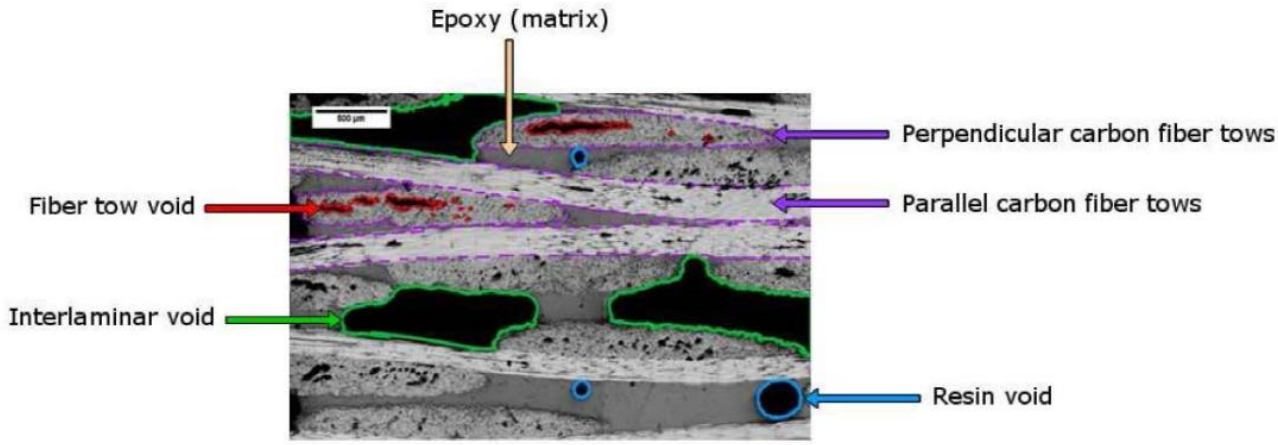

Figure 3: Types of voids of an un-debulked and uncured prepreg laminate [3]

Delaminations are manufacturing, assembly and in-service defects, which are defined as a separation between two successive plies. There are different sources for causing delaminations. During the layup process foreign objects such as Teflon foil or other aids used during the manufacturing process can get unintentionally into the laminate. During the curing process delaminations can be induced e.g. by leak in vacuum. During the assembly process, delaminations can be caused by e.g. the drilling process and impact induced by foreign objects. During the in-service, delaminations can be induced by impact loading with foreign objects such stones, hails etc.. Two damage types caused by two different impact energy levels are shown in Figure 4. Damage (a) is a matrix cracking caused by low energy level, which represents the starting point of delaminations. Damage (b) represents the typical delamination distribution in the through thickness direction of a structure component. Such delamination distribution is known as pine tree formation, which is usually caused by higher impact energy.

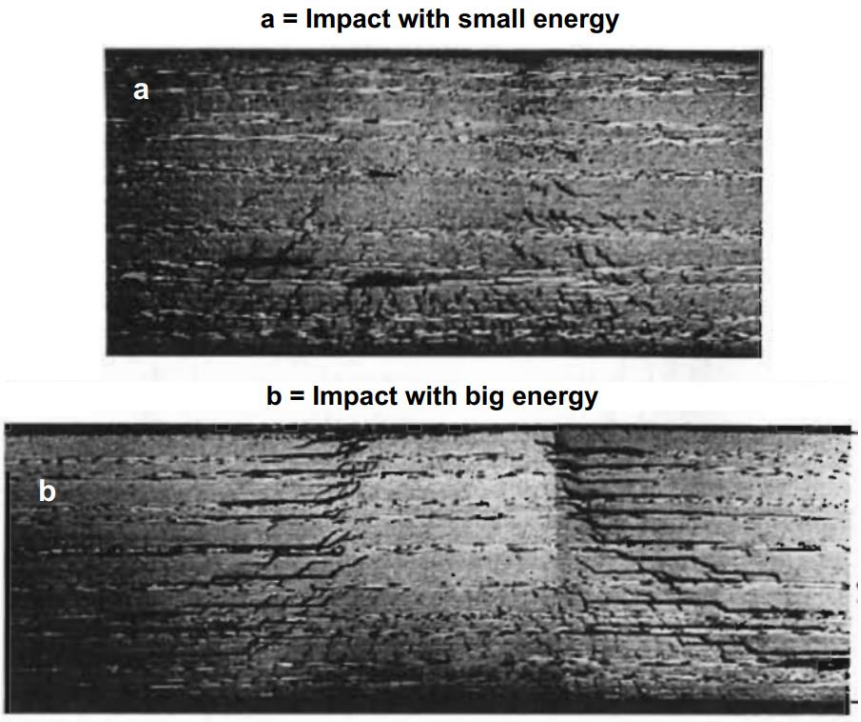

Figure 4: Delamination and matrix cracks caused by impact [4]

Matrix cracking is both a manufacturing and in-service defect**.** Matrix cracks can be categorized in intralaminar and interlaminar matrix cracks. Intralaminar matrix cracks represent a separation between the embedded fibers, either through the matrix and/or in the fiber-matrix interface (debonding) as shown in Figure 5. Interlaminar cracks are distributed in the through the thickness of the laminate, which can be induced by impact loading building the starting point for delaminations as shown in Figure 4 (a). Both matrix cracks categories can occur in laminates subjected to thermal cycling, tension and fatigue, too.

Fiber fracture is described as the simultaneous breakage of fiber bundles consisting of hundreds of individual fibers, which occurs when the tension or the compression strength is exceeded as shown in Figure 5. Fiber fracture is generally caused in in-service due to foreign-object impact, lightning strike, applied load, processing methods such as drilling process, scratches and abrasion. Fiber fracture also can be the result of manufacturing defects such as waviness which reduces the strength in load direction promoting early fiber fracture.

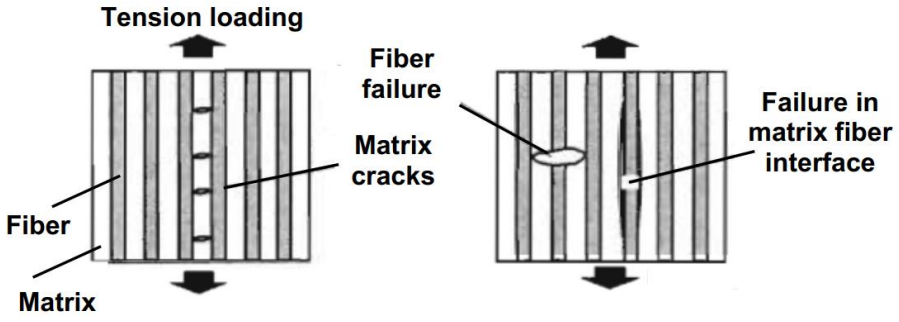

Figure 5: Matrix and fiber failure [4]

The defects briefly described above have attracted the attention of many researchers. They were analyzed in detail analytically, numerically and experimentally, however, mainly independently of each other. Nevertheless, there is still a lack of knowledge in the interaction behavior between manufacturing and in-service defects, especially with respect to the damage tolerance behavior.

Waviness as well as impact damages are very common defects, which lead individually to a serious reduction in the strength and stiffness. Since aircraft structures must fulfil damage tolerance requirements, the worst case must be covered including the interaction effect between waviness and impact. This leads to conservative design requirements and tight tolerances in production. Thus, the composite potential cannot be exploited. Therefore, this thesis focuses on the interaction effect between OoP waviness and low velocity impact damages.

2.2 Out of plane waviness

Table 1 highlights the main emphasis of the reviewed literature with regards to the investigated waviness parameters e.g. morphology type, waviness distribution (formation), layup type etc., as well as the availability of experimental data. Additionally, it provides a classification of the OoP waviness morphology that can occur depending on respective manufacturing processes. The term “investigated by” indicates, whether the categorized morphologies, the waviness parameters as well as the interaction effect on the compression strength are treated in the literature (✓) or not (✗).

Morphology A is characterized by its flat outer surfaces, B by a mix of flat and curved surfaces. The curved surfaces in case B can be either convex, showing a thickness increase in the structure component or concave, showing a thickness decrease in structure as shown in Figure 1 (a, b and d). Morphology B with a convex shape is induced by foreign objects or overlaps (a, d), meanwhile concave shape is induced by gaps or imprints (b). Morphology C is characterized by its curved outer surfaces, which represents the worst-case scenario of morphology B, because the entire plies of the component are affected by OoP waviness. The common parameters, which characterize the waviness severity are the amplitude (A), wavelength (L), waviness angle (Θ), respectively. The location of the maximum waviness angle shown in Figure 6 represents the inflection point of the ply wave, midway between the central trough and adjacent crest.

Investigated waviness distributions in case of morphology A are uniform, graded waviness as well as single and/or several distributed affected 0°-ply/plies. Uniform waviness means, that the amplitude (A) to wavelength (L) ratio A/L is constant in the entire laminate. Graded waviness means the amplitude decays linearly from a maximum at the laminate midplane to zero on the outer surfaces of the laminate according to [5] and [6]. Nevertheless, it is possible, that the maximum amplitude of a graded waviness starts from the outer surface and decays to zero on the other outer surface building morphology B. Possible waviness formation of morphology C is uniform waviness.

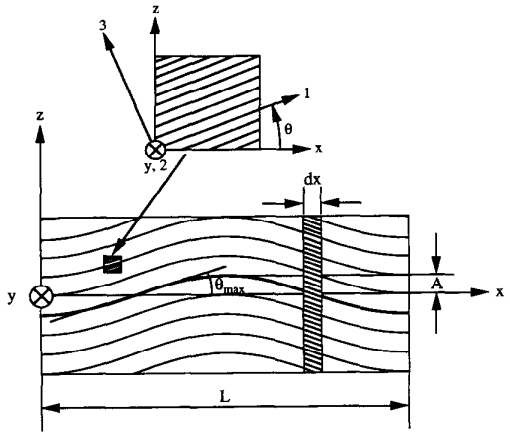

Figure 6: Waviness parameters; amplitude (A), wavelength (L), waviness angle (Θ) [5]

Some relevant investigations related to waviness are summarized in the following. The majority of the presented analytical, numerical and experimental works investigate the effect of waviness in dependence on A/L ratio on the stiffness and strength. Unidirectional laminates (UD) with uniform and graded waviness as well as cross ply laminates with specifically distributed waviness in and around the laminate midplane were investigated, in which one or several 0°-plies are affected by waviness. The effect of affected 0°-plies by waviness on the strength and stiffness reduction is intensively investigated for UD and cross ply laminates but not enough for multilayered laminates.

Morphology	A	B	C
Geometry	Flat 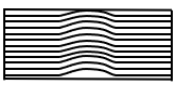	Curved - Flat 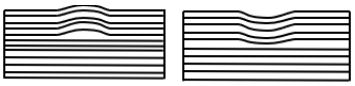	Curved 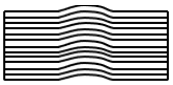
Investigated by	✓ [5], [6], [7], [8], [9], [10], [11],	×	✓ [12], [13]
Studied distribution	✓ Uniform, graded, specifically distributed 0°-ply	× Uniform, graded	✓ Uniform
Studied layup	✓ UD, Cross ply, QI	×	✓ UD, QI
Studied affected plies	×	×	×
Studied affected 0°-plies	✓	×	✓
Available experiments	✓	×	✓
Interaction effect with Damage tolerance	×	×	×
✓ = Treated in the literature		× = Not treated in the literature	

Table 1: Waviness morphology classification and main focus of the reviewed literature [2]

Rai [14] developed an analytical model for predicting the IP uniform waviness effect on the lamina modulus of elasticity as a function of A/L. The modulus of elasticity was used in an incremental loading scheme to predict the general stress strain response. Both, the modulus of elasticity and the stress strain response were validated experimentally. It was found, that the modulus of elasticity is decreased when A/L ratio is increased and the stress strain response is non-linear.

Bogetti [15] developed an analytical model based on the two-dimensional (2D) laminate theory using an unit cell model as shown in Figure 7. Its objective was the prediction of OoP waviness effect on the stiffness, strength and thermal expansion coefficient in a cross ply laminate. The investigated cross ply laminate consists of three plies, in which the 0°-ply is affected by waviness. The 90°-plies are assumed to be straight (Morphology A). The investigation showed that strength and stiffness reduction is increased when the amplitude is increased and the half wavelength is decreased. Greater stiffness reduction is expected in systems with higher material anisotropy. Ply waviness is shown to induce a significant interlaminar normal (σ_3) and interlaminar shear (τ_{13}) stresses within the 0°-ply at the depicted locations in Figure 8 (a and b), which results in a significant strength reduction. For comparison purpose the inplane axial stress (σ_1) is shown in the same Figure (c). Failure mechanisms and mechanical properties transverse to the waviness direction are not affected by the waviness. In [16] he investigated the nonlinear behavior of the stress strain response considering material nonlinearity based on the three-dimensional (3D) laminate theory using an unit cell model based on the same waviness configuration given in [15]. The nonlinear analysis prediction was compared with the linear analysis one. At low load level the overall stress strain response in both analyses was similar. However, the predicted failure load of the nonlinear analysis was beyond the linear analysis prediction. In the linear analysis the interlaminar shear stress was the contributor for the failure mechanism, which was identified at the highest inclination of the wavy ply. In contrast, in the nonlinear analysis the interlaminar shear was not the driver for failure mechanism. The continuous load increase ultimately led to final failure.

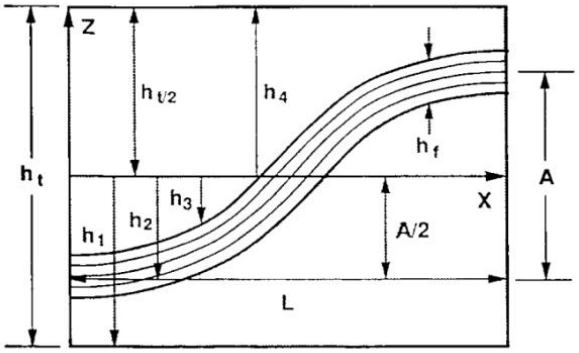

Figure 7: Unit cell geometry of the wavy ply configuration [15]

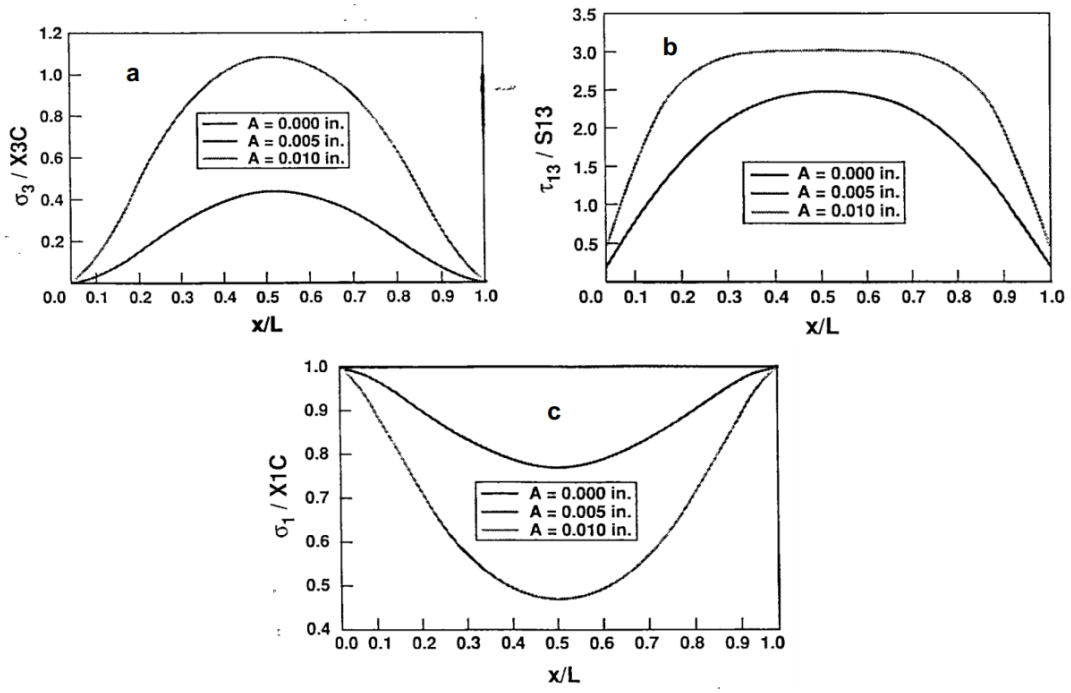

Figure 8: a= Interlaminar normal stress (σ_3); b= Interlaminar shear stress (τ_{13}); c= Inplane stress (σ_3) within a wavy 0°-ply under compression loading, [15]

Adams [7] examined the OoP waviness effect on the compressive strength in cross ply laminates analytically and experimentally. Different laminate thicknesses (2.3 - 4.1 mm) made of IM7/8551-7A were investigated, in which one to several 0°-plies were affected by waviness. The effect of affected wavy 0°-plies on the strength reduction was described by a factor. This factor is given as the number of affected wavy 0°-plies to the total number of 0°-plies. A manufacturing process was developed to produce flat specimens with isolated as well as specifically distributed waviness by means of single step method using strips of the same material and steel mold (Morphology A). The wavy 0°-plies were localized around the laminate midplane to simulate waviness in thick laminates and to minimize the out of plane bending due to the localized non-symmetry in the laminate. The investigation showed that laminates with higher number of affected 0°-plies lead to a stronger reduction in the strength. The final failure was sudden, catastrophic and without an indication of failure initiation. An angled fracture plane through the specimen thickness was evident, which indicates the presence of a shear failure mode as shown in Figure 9, in addition to the delamination failure mode. The wavy 0°-plies were commonly failed at or near the inflection point of the ply wave, midway between the central trough and adjacent crest as shown in Figure 9. In most specimens, the wavy 0°-plies were fractured in only one location. Further, it was found, if a maximum of 33 % of the 0 °-plies are affected by waviness, the percentage decrease in compressive strength is approximately equal to the percentage of the wavy 0 °-plies.

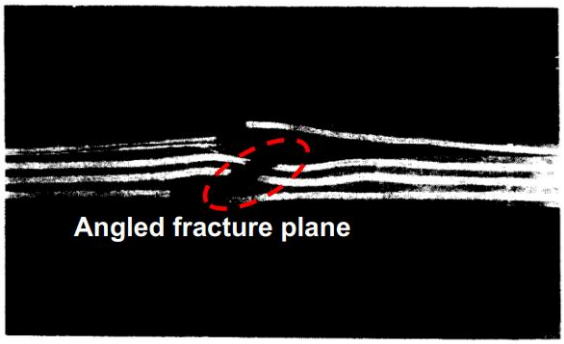

Figure 9: Failure of wavy 0°-plies near the inflection point of the ply wave, midway between the central trough and adjacent crest [7]

Hsiao [5] and [6] developed an analytical method for predicting the elastic properties and the compression strength of UD and cross ply laminates affected by three types of OoP waviness. These are uniform, graded and localized waviness (Morphology A). The analytical prediction was validated experimentally. The specimens with OoP uniform waviness with a thickness of 19 mm were manufactured by means of tape winding method. The specimens with graded waviness with a thickness of approximately 9 mm were fabricated by means of three step curing method. The cross ply laminate with central waviness in laminate midplane was manufactured by means of 90° strips, with a thickness of approx. 9 mm. It was found that the major Young's modulus and the strength are decreased significantly with increased A/L ratio, especially in the uniform waviness case. The normalized stresses for an UD laminate under compression loading are illustrated in Figure 10. It is experimentally observed that the failure mechanism is initiated by interlaminar shear stress (τ_{13}) at the location of the maximum waviness angle, followed by delamination and layer buckling, which leads to final failure as shown in Figure 11. It is stated, that τ_{13} is dominant, when laminates containing OoP waviness are subjected to compression loading. Experimental results were in good agreement with the analytical method.

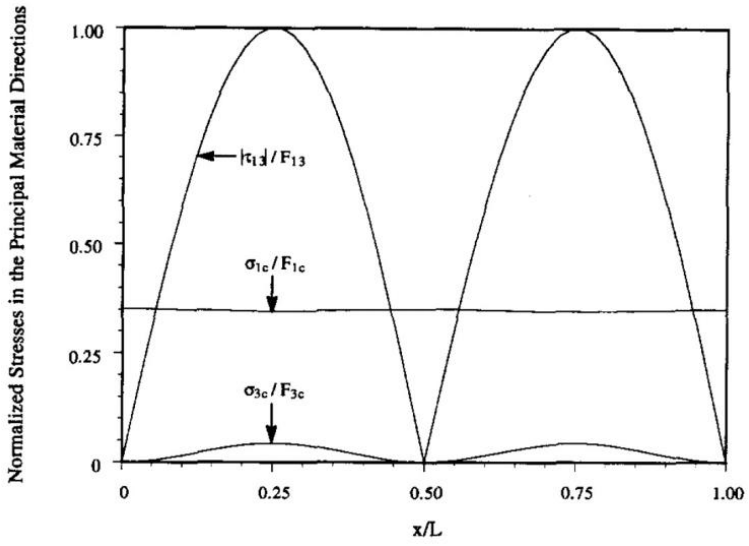

Figure 10: Normalized stresses in the principal material directions along the ply with the maximum waviness at midplane of UD laminate with graded waviness under compression [5]

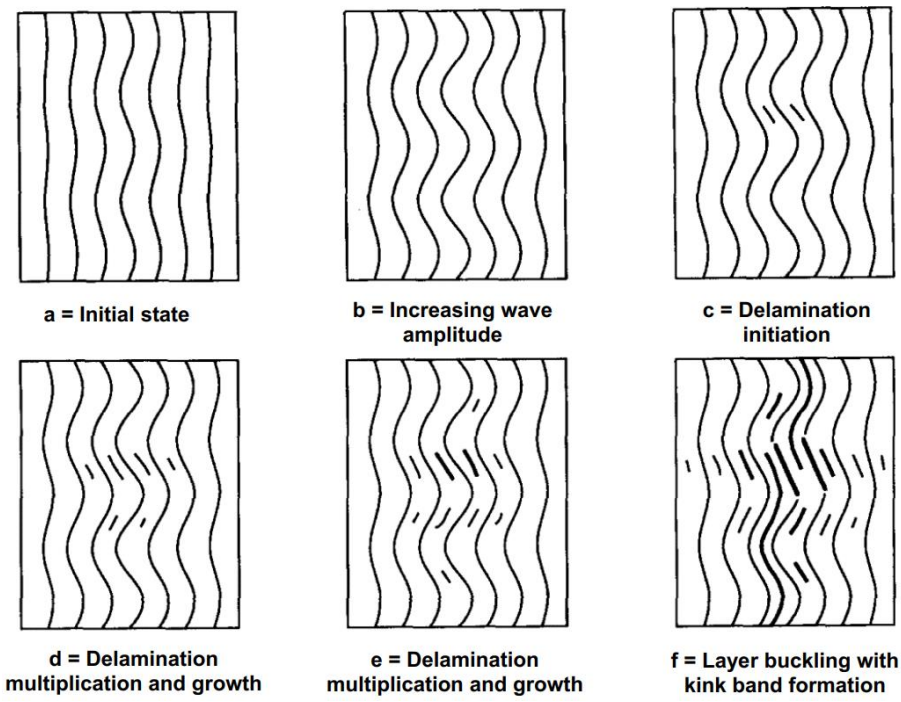

Figure 11: Failure progression in UD laminate with graded waviness under compression [5]

Chun [8] investigated the effect of OoP waviness on the nonlinear behavior of UD laminates using an analytical model for calculating the elastic properties. It considers material and geometrical nonlinearities caused by the three types of waviness; uniform, graded and localized waviness under compression and tension loading. The OoP uniform waviness was fabricated using several sets of two half molds (Morphology A). It was found that the major Young's moduli E_x is reduced with increased A/L ratio, E_z is increased with increased A/L and E_y is not affected by the waviness. The observed nonlinearity in the stress strain curves of the conducted experiments was concluded as geometric nonlinearity induced by the waviness.

Garnish [17] investigated the OoP uniform waviness effect on the elastic properties of a UD lamina by means of a finite element (FE) based micromechanics model. The findings of the investigations introduced in this section were confirmed by this FE model that waviness affects the elastic properties, in particular the elastic major Young's modulus E_x.

Duangmuan [9] developed a 2D FE model to predict the final failure of cross ply laminates affected by OoP waviness. Different thicknesses, which vary between 1.78 mm to 10.9 mm were considered. The material used is IM7-8551-7A. The OoP waviness was always introduced in the 0°-ply/plies to investigate different wavy 0°-ply distributions. Ply waviness was located at the laminate midplane, close to the laminate midplane, as well as separated multiple wavy plies around the midplane (Morphology A). Like Adams [7] a factor called wave fraction was introduced to describe the portion of the affected wavy 0°-plies to the total number of 0°-plies. The OoP waviness was fabricated by means of strips from the same material and a mold. The effectiveness of the FE approach for predicting the compression strength reduction and final failure was confirmed experimentally. Several findings were derived. Ply waviness induces delamination in the interfaces between the wavy ply and neighboring ply, which represents the first ply failure. Delaminations are caused due to high

interlaminar stresses. There are two critical regions of high interlaminar stresses as shown in Figure 12. The most critical region under compression loading was determined to be the region having the highest interlaminar tensile stresses, which is located above the wavy 0°-ply at the central trough of the wave. The second one is associated with the location of the maximum interlaminar shear stresses occurred within the wavy plies where the inclination has its maximum. The identified high interlaminar shear stresses at the inclination was observed by Hsiao [5] and [6], too. The regions of the maximum interlaminar stresses were considered as the critical regions for initial failure under compression loading. Further, the compression strength reduction depends on the ratio of the affected 0°-plies, the through the thickness waviness location and the laminate thickness.

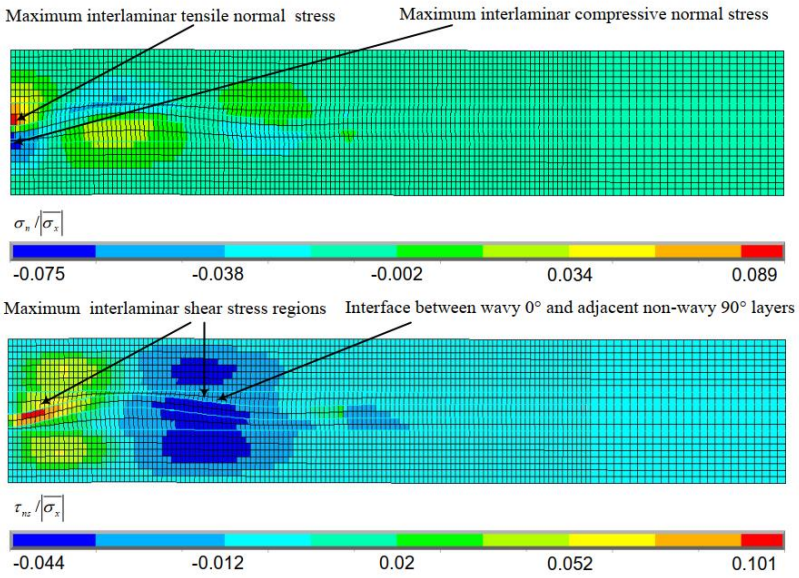

Figure 12: Critical interlaminar normal and shear stresses with one wavy 0°-ply at laminate midplane [9]

Khattab [11] developed an analytical approach based on the classical laminate theory (CLT) to predict the elastic properties at ply and laminate level. Different types of waviness were treated, namely ply with IP waviness, laminate with planar OoP ply waviness, laminate with 3D surface OoP waviness, as well as ply and laminate with localized IP and OoP waviness. Additionally, a 3D FE approach was used to predict the effect of the above-mentioned waviness types on the stiffness and strength of UD composite structures. A three-step manufacturing method was developed for the fabrication of predefined and reproducible OoP graded waviness (Morphology A). For this purpose, a special tooling with predefined A/L ratio was manufactured to fabricate thick flat UD tension specimens (10.8 mm) made of T800 - M21. The findings are: The analytical approach corrects the preceding analytical approach based on the compliance formulation. The FE approach predicts the failure onset properly, but the test force displacement curves were not reproduced. Further, the failure load detected in the experiment is two times higher than the failure load shown in the FE approach. The failure evolution under tension loading was detected by Digital Image Correlation system (DIC). It shows that delamination between the outer plies starts at early stage of the load history due to the tension and shear stresses in the outer plies of the wavy area as shown in Figure 13 (a).

The delamination is propagated further in the wavy as well as in the non-wavy region due to the increased tension loading, as shown in Figure 13 (b-d). As the tension loading is increased, interlaminar shear stresses are developed leading to the final fiber fracture.

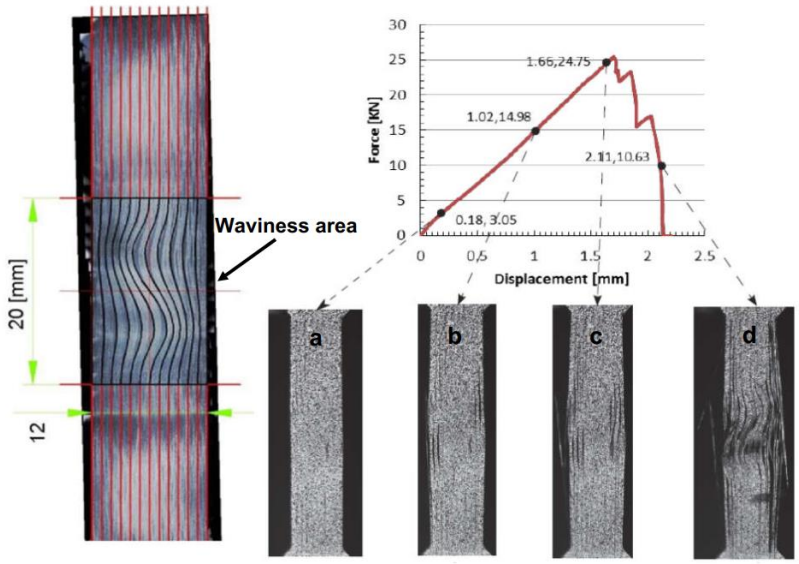

Figure 13: Frames captured by high-speed camera at different load stages, a-d delamination propagation due to the applied tension loading [11]

Gesell and Altmann [12], [18], and [19] investigated the effect of resin systems on the mechanical properties of structures affected by OoP waviness. UD Tensile and compression specimens were manufactured with and without uniform waviness made of glass fiber using different resin systems. The waviness was manufactured by means of an one-side tooling (Morphology C). The tension and compression experiments reveal that OoP waviness induces a 3D stress state in the material subjected to a simple uniaxial loading. Interlaminar shear and normal stresses are created because the geometry of the waviness, which leads to interlaminar damage of the material. The stress strain curves including the shear strain plots at different load stages (1 - 6) of the wavy specimens with different matrix systems under compression and tension loadings are illustrated in Figure 14 to Figure 15. In the compression case, interlaminar normal tension and interlaminar shear stresses are induced at the maximum inclination of the wavy shape. The shear strain is increased with the applied load as shown in Figure 14, so that the matrix is continuously stressed under shear and transverse loading (2-4). Stage (5) represents the phase before fiber kinking is built. At stage (6) after fiber kinking is built, final failure occurs. It is stated, that under compression loading, fiber kinking is the key failure mechanism induced by the nonlinear shear behavior of the matrix.

Under tension loading, it is observed that the wavy plies are straightened by the applied load, so that interlaminar normal tension and shear stresses are introduced, Figure 15. The author assumed without evidence, despite the usage of the DIC system, that stage 2 represents an interphase failure mechanism. Stage 3 represents the starting point of the nonlinear behavior announcing an interphase failure between fiber and matrix and the initiation of yielding. Nevertheless, it was difficult to prove the presence of cracks. The matrix cracks initiate

delamination as shown in stage 4. Further, delaminations at stage 5 occur at the maximum inclinations before final fiber failure occurs at stage 6. Comparing Figure 14 with Figure 15 shows that matrix properties affect strongly the failure mechanism under compression loading. In contrast, the failure mechanisms under tension loading are negligibly affected by the matrix properties.

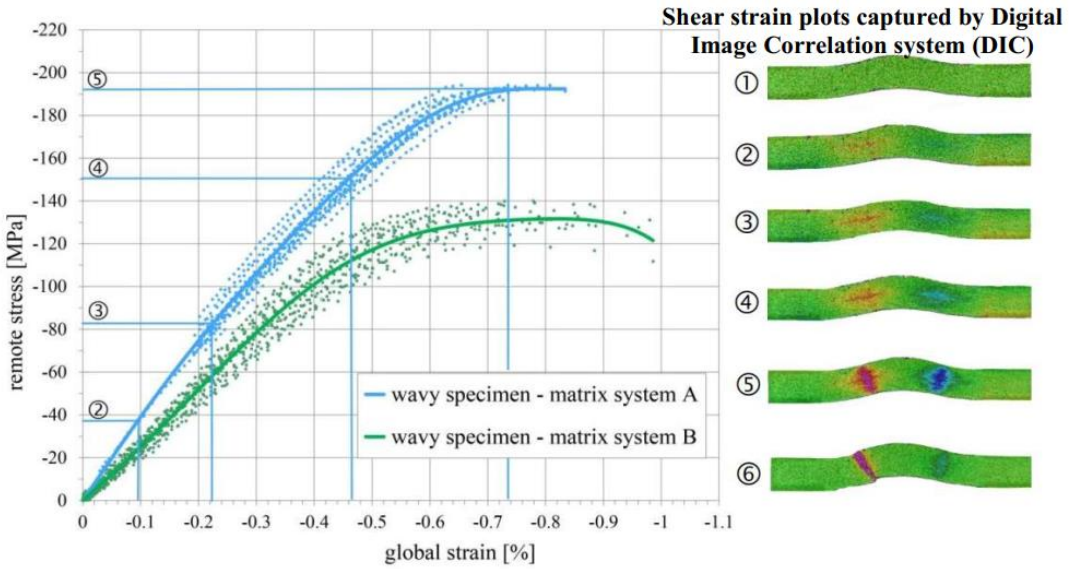

Figure 14: Stress strain curves of wavy specimens with different matrix systems and the corresponding shear strain plots captured by DIC system at different compression load stages [12]

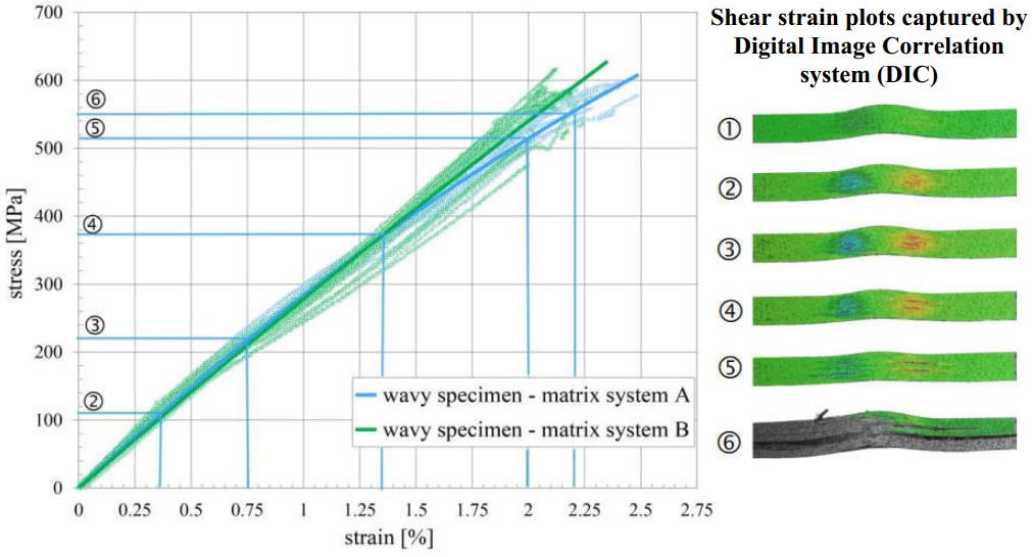

Figure 15: Stress strain curves of wavy specimens with different matrix systems and the corresponding shear strain plots captured by DIC system at different tensile load stages [12]

Eskandari [20] developed a 3D FE model considering material and geometric non-linearity. The objective is to investigate the effect of OoP uniform waviness on the stiffness and strength in a UD laminate (Morphology A). The FE model based on geometric non-linearity showed good agreement with the tests.

Recently QI laminates containing OoP waviness attract the attention of some researchers, [10], [21], [13] and [2]. The experimental investigation of Al-Kathemi [2] built the fundamental for this thesis.

Mukhopadhyay [10] and [21] developed a 3D FE model for predicting the position and sequence of the failure event up to final failure under tension and compression loading. A 6 mm QI laminate made of IM7-8552 material was involved which included a localized OoP waviness in laminate midplane (Morphology A). The OoP waviness in the 0°-plies was introduced artificially by means of an insert of the same material. The FE approach was validated by tension and compression experiments. A high-speed camera was used to capture the failure evolution and sequence. The FE approach was able to capture the location and sequence of damage events accurately. Under compression loading, the final failure was catastrophic. No load drop was observed in the stress displacement curves. It was observed that delamination, matrix cracking in the waviness vicinity and fiber kinking in the wavy 0°-plies are the governing failure modes for the final failure as shown in Figure 16. The location of the delamination was above the affected wavy 0°-ply at the inflection point of the ply wave, midway between the central trough of the wave and the adjacent crest. This finding correlates well with the observation done by Duangmuan [9], although both laminates investigated in both studies are different (Cross ply laminate [9] and QI laminate [10]). Thus, based on the observations of Mukhopadhyay [10] and the findings of Duangmuan [9], it can be assumed, that the region above the affected wavy 0°-ply represents the region of high interlaminar tensile stress, too. Under tension loading, failure was mainly delamination and matrix cracking located in the waviness region, which was observed after the first load drop. The final failure happened mainly due to fiber fracture.

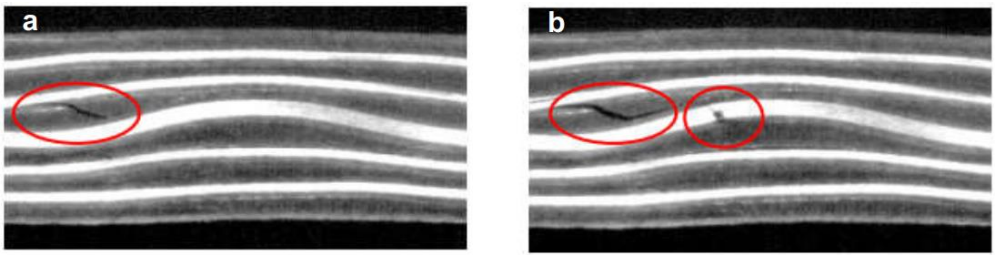

Figure 16: Frames captured by high-speed camera just before final failure, a = development of matrix crack and delamination, b = Fiber kinking in the wavy 0°-plies [10]

Thor [13] investigated the failure behavior of a structure containing waviness under compression and tension loading experimentally and numerically. UD (approx. 2 mm thick) and QI laminates (approx. 5 mm thick) made of IM7-8552 with and without uniform OoP waviness were fabricated by means of one side tooling (Morphology C). Two A/L ratios, waviness angles, respectively were fabricated in the investigated laminates. Wave 1 is with

high Θ (= 15°) and wave 2 is with low Θ (= 7.2°). The conducted experiments reveal that the compression and tension strength of the UD and QI laminates are decreased with increased waviness angles. Nevertheless, the strength reduction due to the presence of waviness in the UD laminate in comparison to QI laminate with comparable waviness parameters is higher due to the increased number of the affected 0°-plies.

The experimental and numerical results reveal, that failure modes evolution and final failure modes depends on waviness parameters, namely amplitude and the structure geometry namely the thickness as shown in Figure 17. In case of wave 1 with higher A/L ratio, the failure is determined by the bending moment, which is superimposed with the axial global loading. The bending moment results from the amplitude and thickness. In case of wave 2 with lower A/L ratio, the contribution of the bending moment is less in the superposition of the loading resulting in material failure as shown in Figure 17. Within the tested wave 1 configuration (a - c), it is observed that there is a transition from tension to compression of the inplane strain (ε_x) across the thickness under compression and tension loading. In contrast, wave 2 configuration (b) does not show this characteristic. Thus, the failure behavior is more determined by the material properties for lower amplitude to thickness ratios. Global compression load of wave 2 and the absence of notable bending moments leads to fiber kinking of the specimen as shown schematically in Figure 17 (b). The maximum interlaminar tensile strain (ε_z) under compression loading is located at the turning point of the sinusoidal wave as shown schematically in Figure 17 (a - b). In contrast, under tension loading the maximum ε_z is located in the center of the waviness as shown in (c). This interlaminar normal tension strain is the cause for the initiation of the delamination.

In Figure 18 the interlaminar shear strain (ε_{xz}) distributions of wavy UD specimens are depicted right before and after final damage for wave 1 (a) and wave 2 (b) under compression loading as wells as for wave 1 under tensile load (c). The detected interlaminar shear strain distribution is in accordance with the reviewed literature in [5], [6] and [19], which confirmed that the associated interlaminar shear stress τ_{13} is the most significant stress component for damage initiation in wavy composites under axial compression, which is followed by mode I delamination and layer wise buckling.

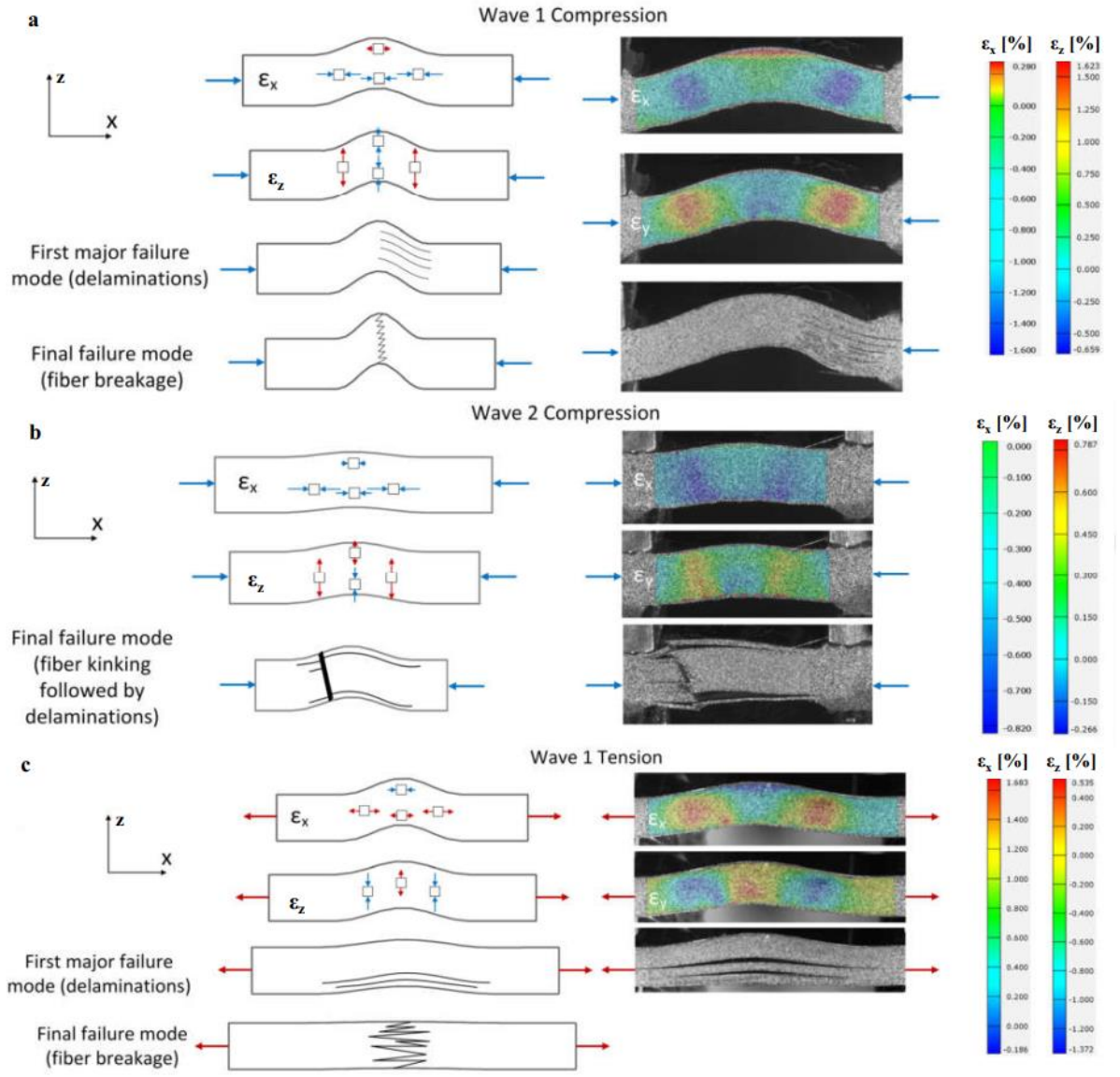

Figure 17: Inplane and through the thickness strain distribution schematic and Aramis presentation; First major and final failure in a = QI laminate with wave 1 (compression), b = QI laminate with wave 2 (compression), c = UD laminate with wave 1 (tension) [13]

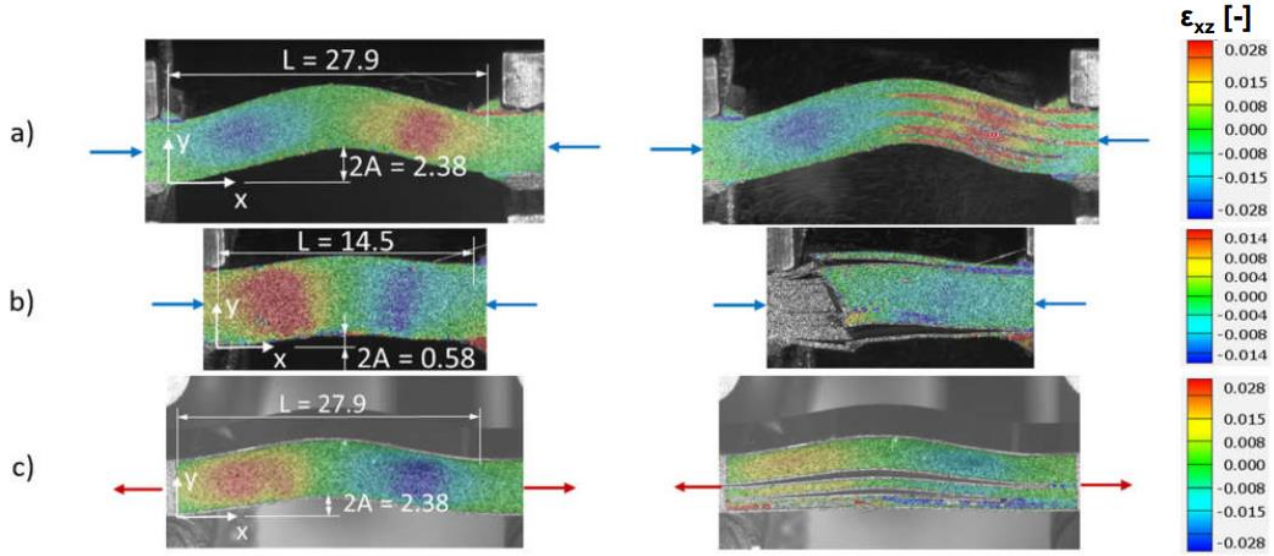

Figure 18: Interlaminar shear strain in wavy UD laminate configurations a = Wave 1 (Compression), b = Wave 2 (Compression), c = Wave 1 (Tension) [13]

In summary, based on the reviewed literature, the following conclusions are drawn: There is a need for more investigations, which consider more common laminates with stepwise increased number of affected plies and number of affected 0°-plies in dependence on different waviness angles as investigated in [2]. However, the literature lacks investigations on the behavior of common multilayered layups affected by waviness, since these are expected to show more complex failure behavior and are more relevant for the industrial applications.

Morphologies A and C are typically investigated but not morphology B as shown in Table 1. Morphology B is relevant for the industrial applications, too, because it can be induced by overlaps, gaps or foreign objects. Furthermore, the waviness morphology has to be considered in dependence on the above-mentioned parameters to cover geometrical effects induced by the waviness morphology as revealed by Thor [13] and Al-Kathemi [2]. Therefore, these parameters are in focus of the current experimental investigation.

The techniques to manufacture specimen with uniform or graded waviness usually require special tooling with predefined waviness parameters. The need for different tooling to cover different waviness angles or ratios A/L is disadvantageous. The final specimen geometry can be either flat or has sinusoidal shape (Morphology A and C). Another approach is to induce the waviness by means of inserts. By this technique, waviness can be distributed with flexible ratios A/L or waviness angles, respectively. The waviness morphology can be A or B. In this thesis, it was decided to choose the insert fabrication method without additional tooling to enable the fabrication of different waviness angles, different number of affected 0°-plies and total number of affected plies in dependence on morphology B. The developed fabrication method, waviness parameters; waviness angle, total number of affected plies and 0°-plies are described in Chapter 4. The present work deliberately omits the use of the ratio A/L. Instead, the waviness angle is used to characterize the waviness severity. In order to keep the number of parameters measured as small as necessary minimizing the source of error.

2.3 Low velocity impact

Impact damages are categorized in high and low velocity impacts. High velocity impact damages result in complete penetration of the composite structure as shown in Figure 19, which represents a bird strike damage. In this case, the component damaged has to be replaced. In contrast, low velocity impact damages are barely visible damages (BVID) and are often difficult to detect as shown in Figure 4 (cross section view). They might reduce the compressive residual strength significantly without giving any visible signs of damage at the surface of the impacted structure and are therefore of great concern from a damage tolerance and safety point of view. Damage tolerance is the ability of structures to continue to perform their intended functions with some tolerable level of damage. The design of damage tolerant structure is important to ensure that structures do not fail at least to the point of damage detectability. Therefore, the focus of this thesis is on the low velocity impact.

Figure 19: High velocity impact – Bird strike [22]

The following works related to low velocity impact should clarify the gap with regards to the interaction between manufacturing defects and impact damages. Abrate [23] describes most relevant aspects to the impact process, impact models, impact classification in low and high velocity impact, models for predicting damage impact and CAI behavior, as well as reviews of analytical and experimental procedures.

Baaran and Kärger [24] and [25] developed a 2D FE tool called composite damage tolerance analysis code (CODAC) for modeling the impact process, impact damages and CAI analyses for monolithic and sandwich structures. Three-layered shell elements are used to model the sandwich structure. The monolithic structure is modelled by single shell elements. Since impact is accompanied by different failure modes namely, fiber fracture, intralaminar and interlaminar matrix cracking as well as delamination, stress-based failure criteria are implemented to assess their effect on the strength of the monolithic and sandwich composite structure. Particular attention is paid to the delamination and growth, since these split the laminate into two or several sub-laminates as schematically shown in Figure 20, which strongly affect the bending stiffness, the stability behavior, the interlaminar shear distribution and thus the strength. The CODAC tool was validated by different tests, which revealed that this provides an acceptable and quick assessment of the residual strength capacity.

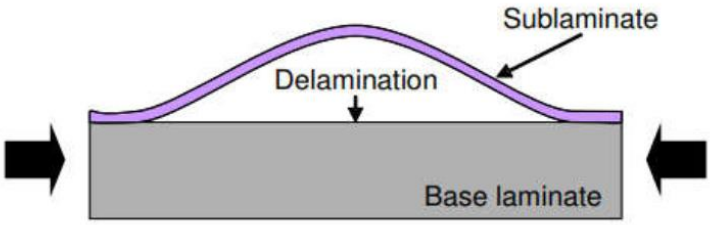

Figure 20: Sub-laminate buckling [24]

Mendes [26] investigated the numerical prediction of CAI strength in dependence of different impact energies for fabric laminates using two different modeling approaches; Single shell model (SSM) and split shell model (SpSM). In the SSM approach, shell elements are used to model the laminate without considering the delamination effects. In the SpSM approach, the delamination effects were considered. Two laminate thicknesses (2.1 mm and 4.2 mm) were incorporated, each of them was impacted with three different impact energies. The 2.1 mm laminate was impacted with 8 J, 16 J, 28 J, the 4.2 mm laminate with 12 J, 24 J; 32 J, respectively. CAI tests of impacted and non-impacted specimens were conducted. Experimental results showed that the split shell model provides better correlation than the single shell model due to the consideration of the delamination as a relevant failure mode.

Rivallant [27] developed a 3D FE model for simulating the CAI test in three steps; impact event, stabilization and applying the CAI boundary conditions, and thereafter conducting the CAI test. It considers the failure modes induced by the impact; fiber fracture, intra ply matrix cracking and delamination, which were modelled by 3D elements and cohesive elements, respectively. Impact and CAI tests with different impact energies (1.6, 6.5, 17, 26.5 and 29.5 J) were conducted to validate the FE model. The impact tests were performed in a drop tower system with a 2 kg – 16 mm diameter impactor according to the Airbus Test Method [28]. The specimens were made of T700-M21 with a thickness of 4.16 mm. The stacking sequence of the QI laminates is $[0_2,45_2,90_2, 45_2]_s$.

The inplane and out of plane stress displacement curves depicted in Figure 21 show that the FE model correctly represents the global behavior of the plate. The deflections correspond to the out of plane displacement at the center of the plate. The deflections on the impacted side were measured by means of a DIC system and those of the non-impacted side were measured by strain gauges. The deflection curves show the traditional local sub-buckling behavior of impacted plates, which is increased with the damage size or impact energy level. For the specimens impacted with 6.5 J, deflections on both faces are similar, due to the slight damage induced by this impact energy level. The curves of the impacted specimens with 29.5 J show clearly a difference in the deflection between the two sides of the plate due to the local sub-buckling of the partly delaminated plies. In [29] he investigated the role of impact-induced cracks on the failure evolution and final failure based on the experimental data given in [27]. It is observed that there is a dependency between the reduction in the compression strength and the change in the rupture mode. The presence of initial crack at the impact location leads to a rupture by propagation of the crack in the buckled plate. In contrast, when no crack is

observed, the rupture is sudden. The impact induced-crack is shown to play an essential role in the final failure of the laminate under compression.

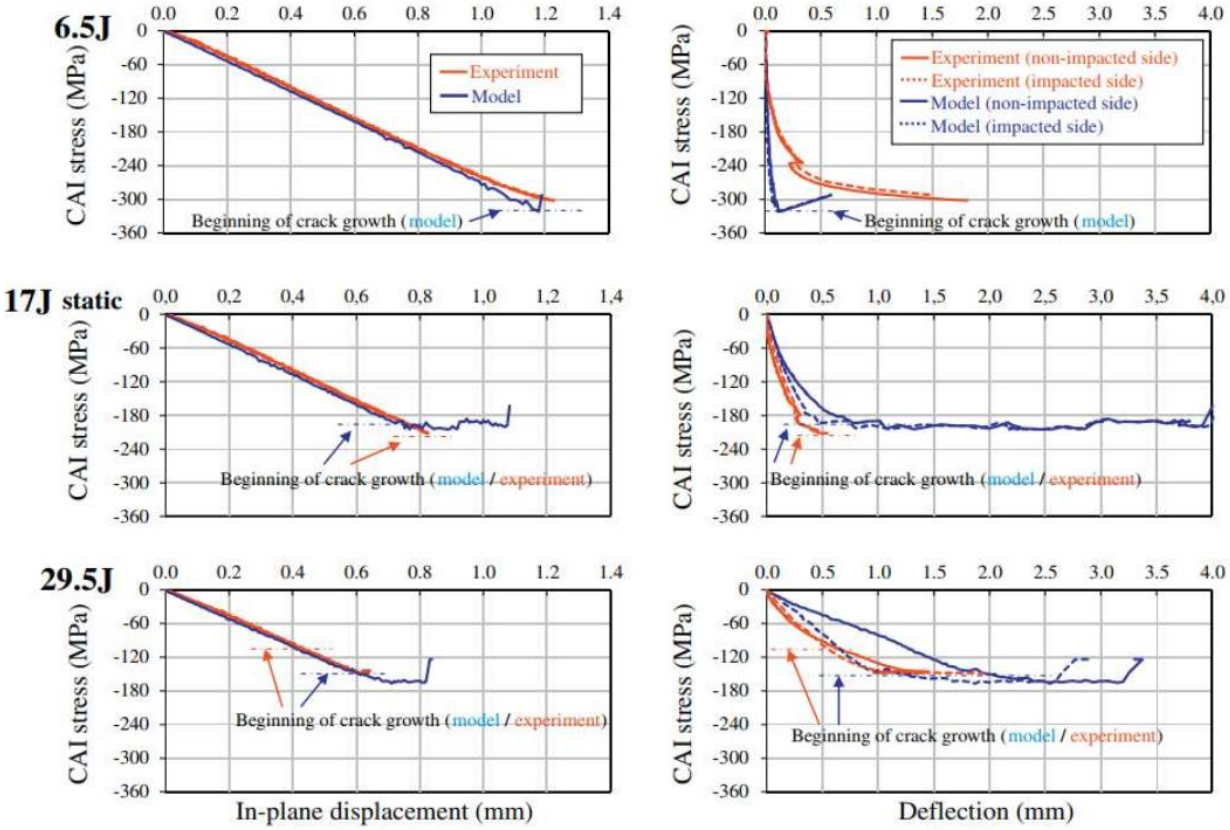

Figure 21: Inplane and out of plane stress displacement at different impact energies [27]

Abir [30] developed a 3D FE model for predicting the CAI strength and delamination growth in two steps aiming to understand the physics behind strength reduction and delamination growth. The procedure consists of modeling the impact event and thereafter the CAI testing. Fiber fracture and matrix cracking (intralaminar damage) induced by impact and CAI are considered by using a continuum damage model approach with stiffness degradation. Delamination is considered by using cohesive interface elements. This modeling method was validated against experimental data from [27]. The experimental and the FE results indicate that, failure during CAI was found to be triggered by impact-induced local buckling causing fiber damage and delamination growth that leads to rapid and sudden load drop. The FE analysis also shows that the damage does not grow before the onset of local sub-buckling, which is marked by a rapid increase in the out of plane displacement as shown in Figure 21. Immediately thereafter, delamination and fiber damage propagate rapidly resulting in the final load drop. He also found, that delamination size and through thickness position affects the compression strength. The failure load decreases with an increase in the delamination size, impact energy respectively. A smaller delamination size delays failure, as shown in the experiment conducted by Rivallant [27].

Tan [31] developed a 3D FE damage model to predict low velocity impact damage and compression after impact. To simulate both impact and compression after impact damages,

the damage model considers intralaminar and interlaminar damages, which includes improved non-linear shear response, unified matrix-dominated damage initiation and mixed-mode intralaminar damage progression. The results of this methodology were validated against experimental data from the literature [27].

Bogenfeld [32] presented an analytical scaling approach for low velocity impact in composite structures, which allows the analysis of structural impact scenarios on coupon level. In [33] he carried out a review of the existing analytical and numerical impact modeling methods for low velocity impact. Six modeling methods from the literature were selected and examined with regard to their predictions, advantages and disadvantages. These are the spring mass model (analytical), plate model (analytical), layered shell model, stacked shell model with cohesive elements, stacked solid model using cohesive elements or cohesive surfaces. The results from these 6 modeling methods were compared against experimental data. This comparison provided the following recommendations: Layered shell models are suitable for quick and rough estimates; Stacked shell/solid models are better than layered shell models, because despite the modeling effort, the impact process and the resulting damage are plausibly recorded. A disadvantage of the hi-fidelity models is the additional required material parameters such as energy release rates.

Huang [34] developed a fully analytical energy-based model for predicting the impact resistance and damage tolerance characteristics of composites plates. Its results were validated against tests, which were conducted according to the Boing standard. A QI laminates with approx. 5 mm thickness made of T300-PEI and AS4-PEEK were impacted with different impact energies 5 J – 30 J. Based on the performed tests, the analytical model provides high accurate predictions

Rhead [35] presented the results of a new analytical and experimental investigations that show the interaction effect between local sub-laminate buckling and global buckling on strain level at which delamination propagation and global buckling occur. Composite panels with a different range of stacking sequences were artificially delaminated by means of Teflon foil and subjected to compression testing in a fixture, which allowed local sub-laminate and global panel buckling modes to interact. The Teflon foils were embedded very close to the outer panel surface, so that each panel was divided into sub-laminate and base laminate with a predefined delamination geometry. The thickness of the sub-laminates varies between 0.5 mm to 0.75 mm. All panels are made of T700GC-M21 with a thickness of 4 mm. Additionally, panels without delamination were fabricated, which serve as a baseline. Compared to panels without delamination, it is observed that the interaction between local sub-laminate buckling and global buckling reduced the panel buckling strains by up to 29 % and the delamination propagation strains by up to 49 %. The cause for the panel buckling strains reduction is due to the loss of panel axial and bending stiffness initiated by local buckling of the sub-laminate.

In summary, the low velocity impact effect on the damage resistance and damage tolerance behavior is intensively and widely investigated, but not its effect on the interaction with manufacturing defects.

2.4 Interaction between waviness and impact

There are only very limited researches considering the interaction between manufacturing defects and low velocity impact damages. The main findings are summarized in the following.

Ehrlich [36] investigated the effect of weakly curved specimens made of QI laminate from IM7-8552 on the impact behavior analytically and experimentally. The specimen geometry is illustrated in Figure 22. The outlined circle in the middle of the specimen represents the curved region. Two types of curvature were manufactured and investigated; convex and concave. Additionally, flat samples were manufactured as a baseline to estimate the curvature effect on the damage resistance of the structure. The impact tests were conducted with different impact energies according to the airbus standard [28]. It was found out, that the curvature of the structure plays a crucial role on the damage resistance. The experimental results showed that convex specimens had much greater damage than plane ones. In contrast, concave specimens compared to plane ones were more tolerant against damage as shown in Figure 23. The purposely induced convex and concave curvature is treated in this thesis as a uniform OoP waviness with different waviness severity and different curvature orientation with respect to the impact direction. Work [36] will be treated in more detail in Chapter 6 to verify the experimental based findings of this thesis.

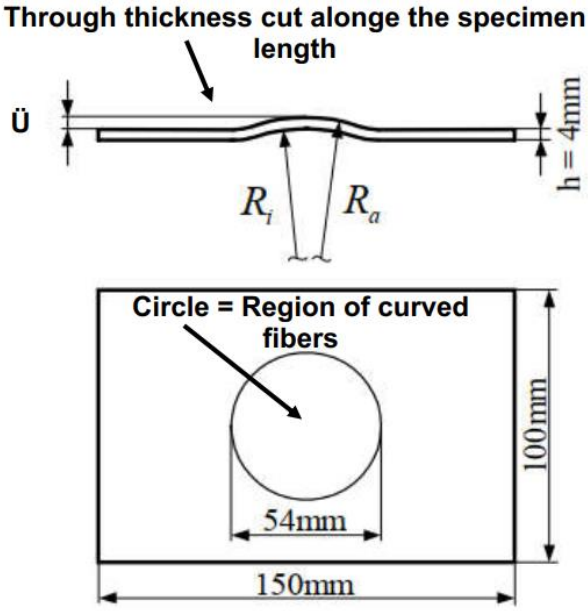

Figure 22: Impact specimen dimension with curved region, top and cut view [36]

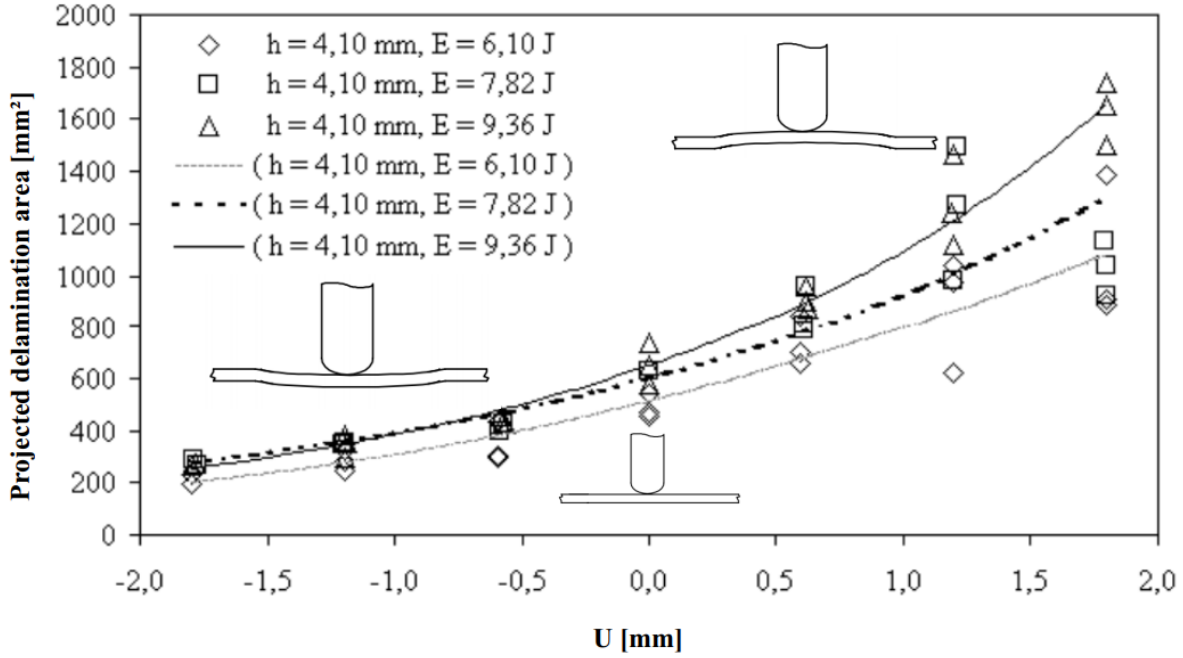

Figure 23: Impact experimental results – Projected delamination area [36]

Rhead [37] investigated the interaction effect between tow gaps induced by the AFP and impact damage on damage morphology and CAI strength. Two coupon configurations with different distributions of tow gaps were manufactured from IMA-M21. No coupons without gaps were fabricated. Figure 24 (a) contains the test fixture including the strain gauges positions. The schematic sketches of coupons A and B are depicted showing the position of tow gaps in (b) and (c). Dashed lines in Coupon A indicate the minimal surface distortion caused by the gap compared to the one in coupon B. In coupon A, the tow gaps were located close to the impact side. In coupon B, the tow gaps were located directly under the impact site near the non-impacted side. The nominal thickness of the coupons is 5.5 mm having the stacking sequence [±45/0/- 45/90/02/45/02/±45/02/45/02/90/-45/0/∓45]. The coupons were impacted with 18 J in a drop tower system with 16 mm diameter hemispherical impactor. US-scan method was used to assess the induced damage morphology. DIC system was involved to measure the strain distribution and the out of plane displacement of the laminates, which allowed the visualization of buckling modes and delamination growth in the investigated coupons. Additionally, the axial strains were recorded throughout the tests by two pairs of vertically aligned back-to-back strain gauges as shown in Figure 24.

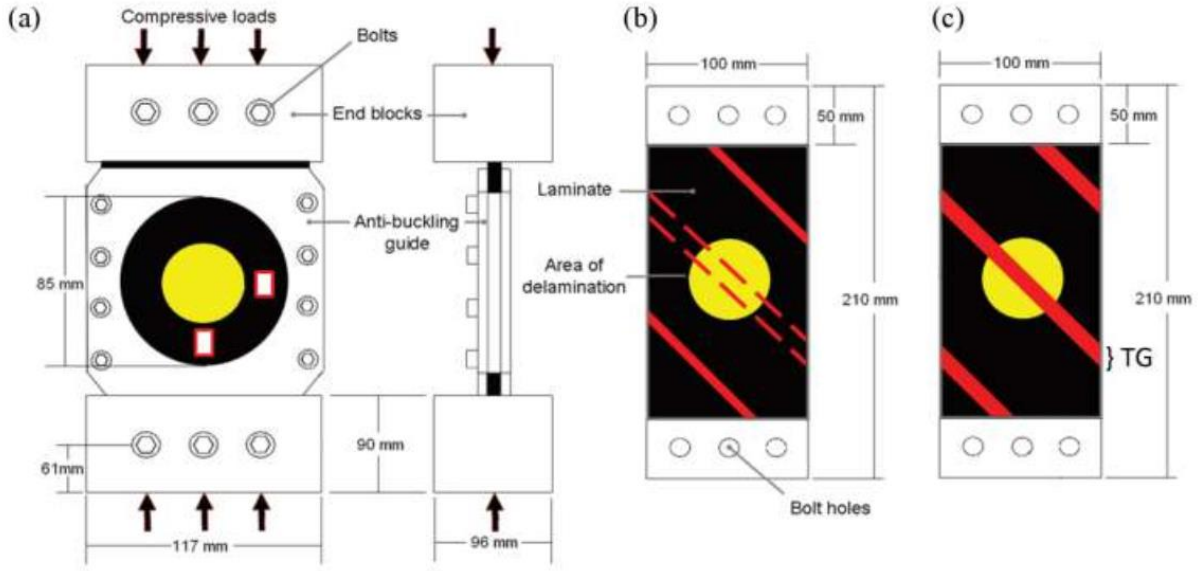

Figure 24: a = CAI test fixture with strain gauges highlighted in red; b = Coupons A; c = Coupons B showing areal positioning of tow gaps [37]

The test results show that position, width and depth of tow gaps have a significant effect on damage resistance. The visible damages in coupons A and B are depicted in Figure 25 (a) and (b). It is shown that the impact of a coupon directly over a tow gap, which is close to the non-impacted side (coupon B) produces a smaller projected delamination area than impacting a region with a tow gap near the impacted side (coupon A), as shown in the US-scan images of Figure 25 (c and d). The diameter of the projected delamination areas is highlighted as ϕ. Red areas indicate delaminations involved in 1st sub-laminate buckling event and blue areas delaminations in 2nd sub-laminate buckling event. The CAI tests results show that the presence of tow gaps near the non-impacted side can inhibit the sub-laminate buckling and the delamination growth, which is the most critical failure mode for CAI failure as shown in Figure 25 (e to h). That why the CAI strength of coupon B was 14% higher than the CAI strength of coupon A. Based on the author, the improved behavior of coupon B is because of the 3 mm built wide channel as a consequence of the consolidation of plies in the manufacturing process which is located directly under the impact site. It prevents two separate delaminations from coalescing during compression loading. Thus, he concluded that tow gaps may be beneficial for damage tolerance and it is noted that it may be possible to derive an optimal distribution of deliberate tow gaps for improved CAI strength**.** However, he recommends to investigate the effect of tow gaps in the vicinity of an impact rather than directly below it on damage resistance and damage tolerance.

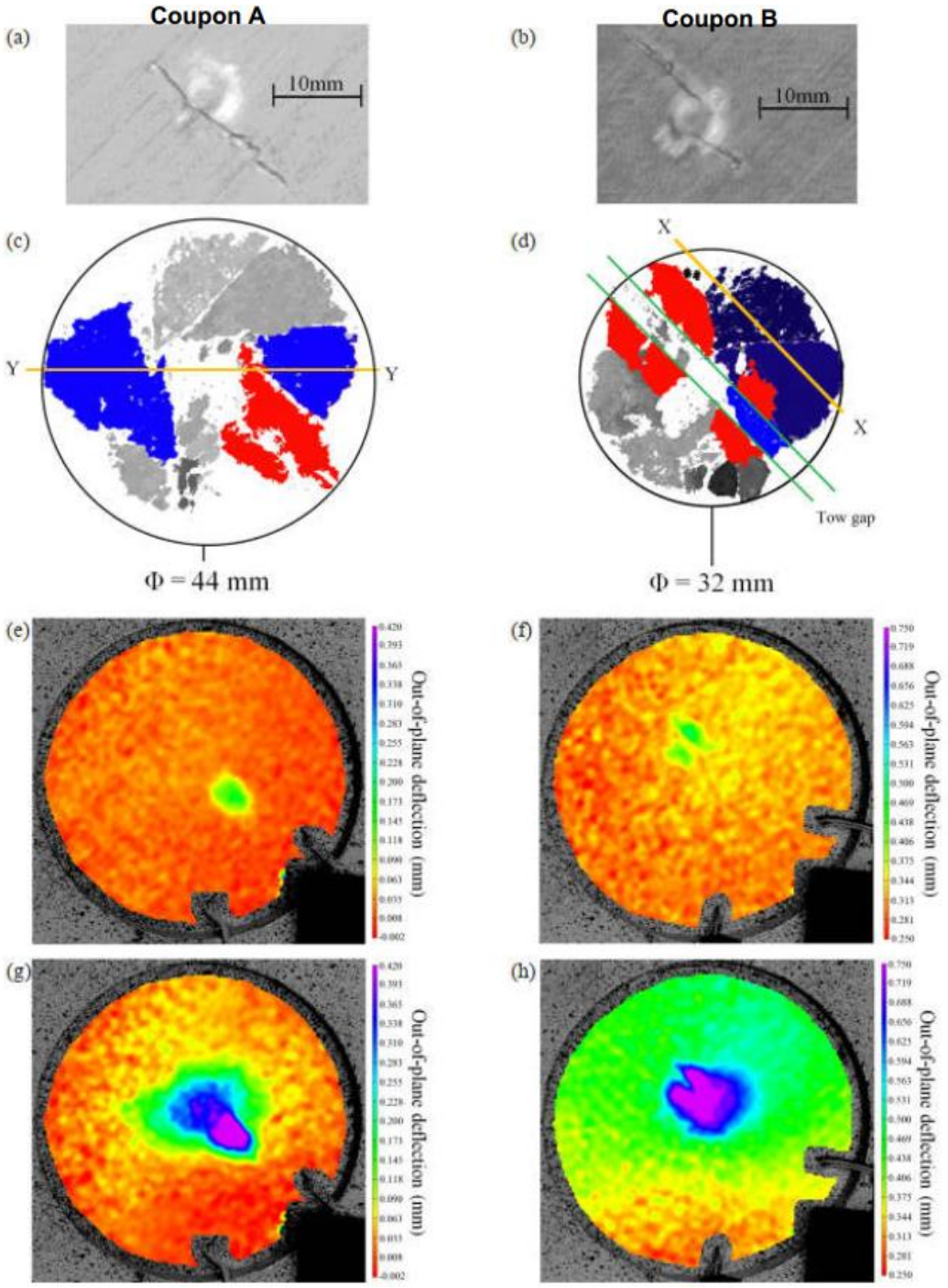

Figure 25: a and b = Visible damages - impact side. c and d = US-scan images - impact side. e and f = DIC images of fully formed 1st ply buckles. g and h = DIC images of multiple sub-laminate buckles immediately prior to propagation [37]

Falco [38] investigated experimentally the effect of tow gaps on the low velocity impact behavior and CAI in composite laminates. Two different configurations, with and without ply-staggering were manufactured via AFP as shown in Figure 26. These were compared with their baseline counterpart without defects. The baseline and defective specimens were made of AS4-8552 with a nominal laminate thickness of 4.32 mm. The effect of three different impact energies was investigated 15 J, 30 J and 45 J by means of a drop weight tower with a 16 mm diameter hemispherical impactor. The delamination areas were detected by means of

US-scan method. For each impact energy and for each configuration, two specimens with gap defects were tested. Additionally, two baseline specimens were not impacted to assess the non-impacted laminate strength. In case of the non-staggered gap specimens two impact positions were investigated. The first one was outside of the defect and the second was just inside of the fiber-free area as shown in Figure 27. This differentiation was not possible in case of the staggered gap specimens.

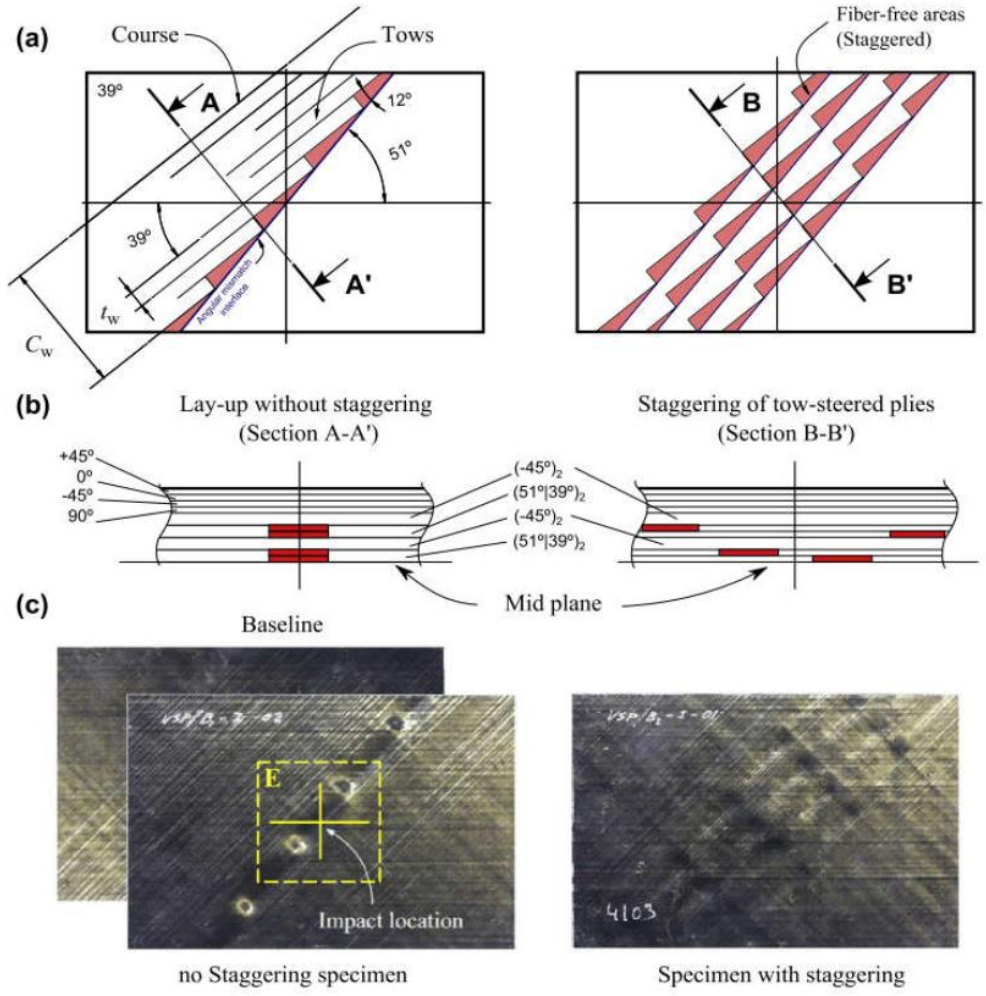

Figure 26: a = Specimen geometry: the discontinuity interface in the ply [51°/39°] and resin rich areas are represented. b = Layup for no staggered and staggered configurations. c = Tow-drop gap defects in specimens with and without staggering [38]

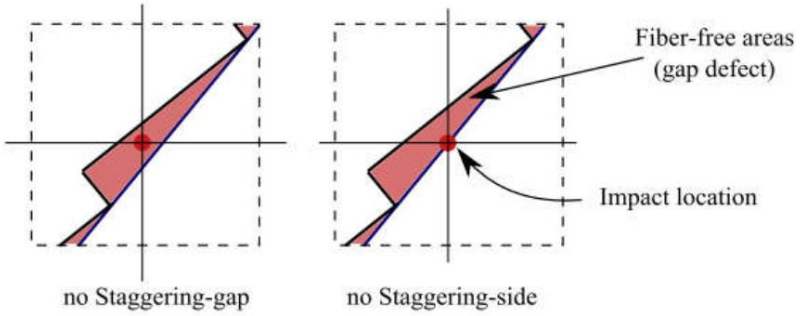

Figure 27: Impact positions in case of the no staggered gaps [38]

It was found out, that the compression strength reduction is driven by the impact itself rather than by the influence of manufacturing-induced defects. For high impact energy levels, the shape of the delamination areas is very similar to the baseline counterpart as is shown in Figure 28 and Figure 29. The author states, that the similarity in the shape of the delamination indicates that the effect of the gap defects is relevant only under small impact energy level. Further for larger impact energy levels, the damage mechanisms are not driven by manufacturing-induced defects. From Figure 28 it is obvious, that the extension of the delamination areas induced by 30 J and 40 J is close to the edges of the specimens and, therefore, do not exactly comply with a requirement of the conducted test standard. The longitudinal strain distributions of the baseline, staggered and no staggered gap specimens impacted at 15 J are depicted in Figure 30. It is observed, that the strain distributions of the staggered and no staggered gap specimens differ from the baseline specimen.

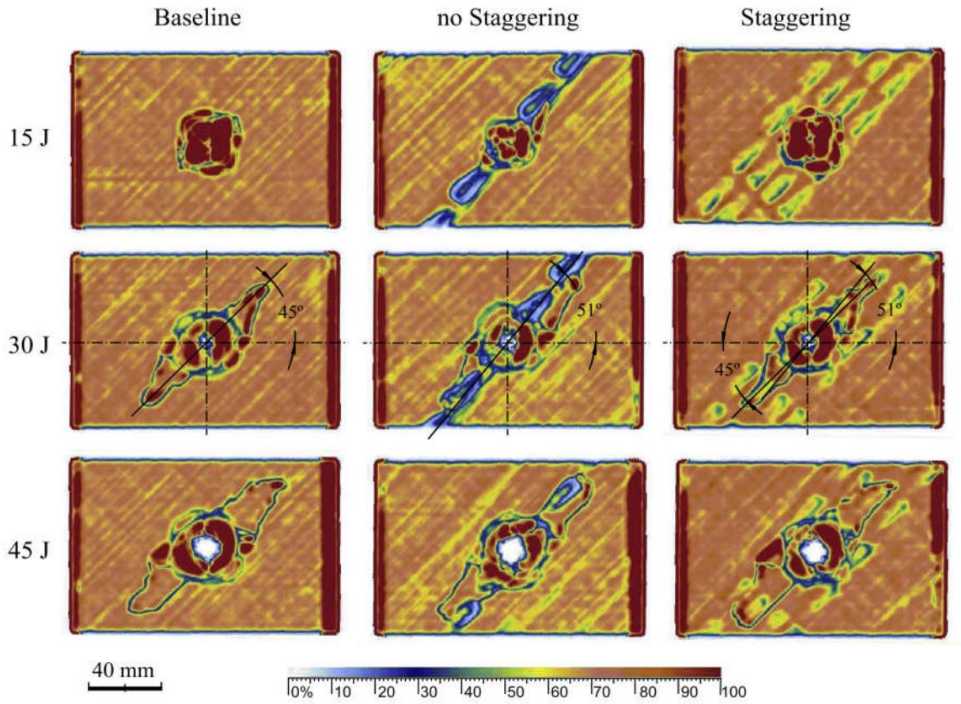

Figure 28: Delamination areas of the impacted specimens at different energy levels. The different colors identify the signal amplitude [38]

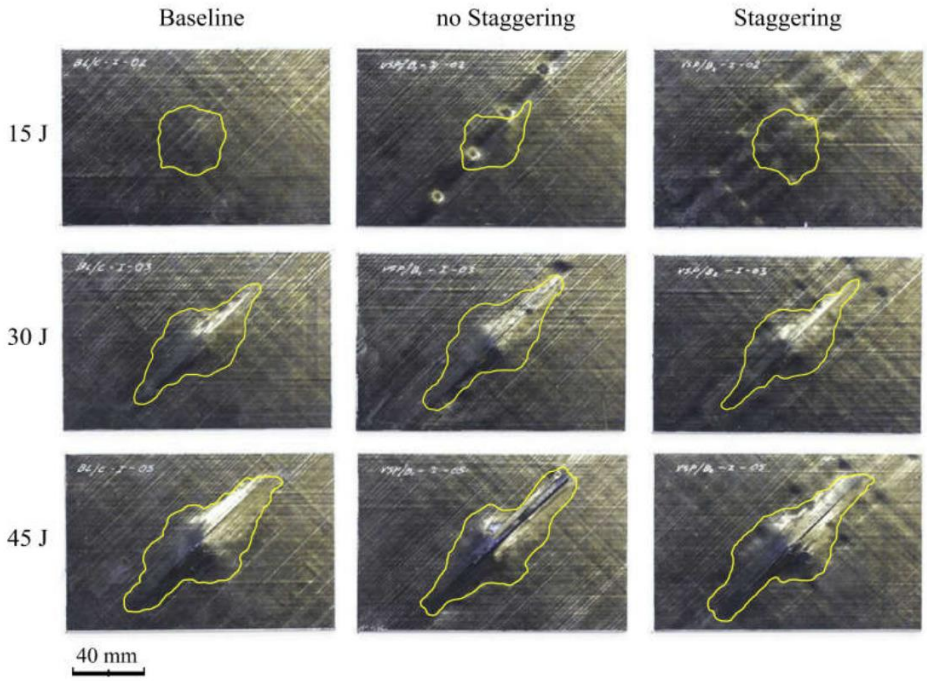

Figure 29: Delamination areas of the impacted specimens at different energy levels. Non-impacted side, [38]

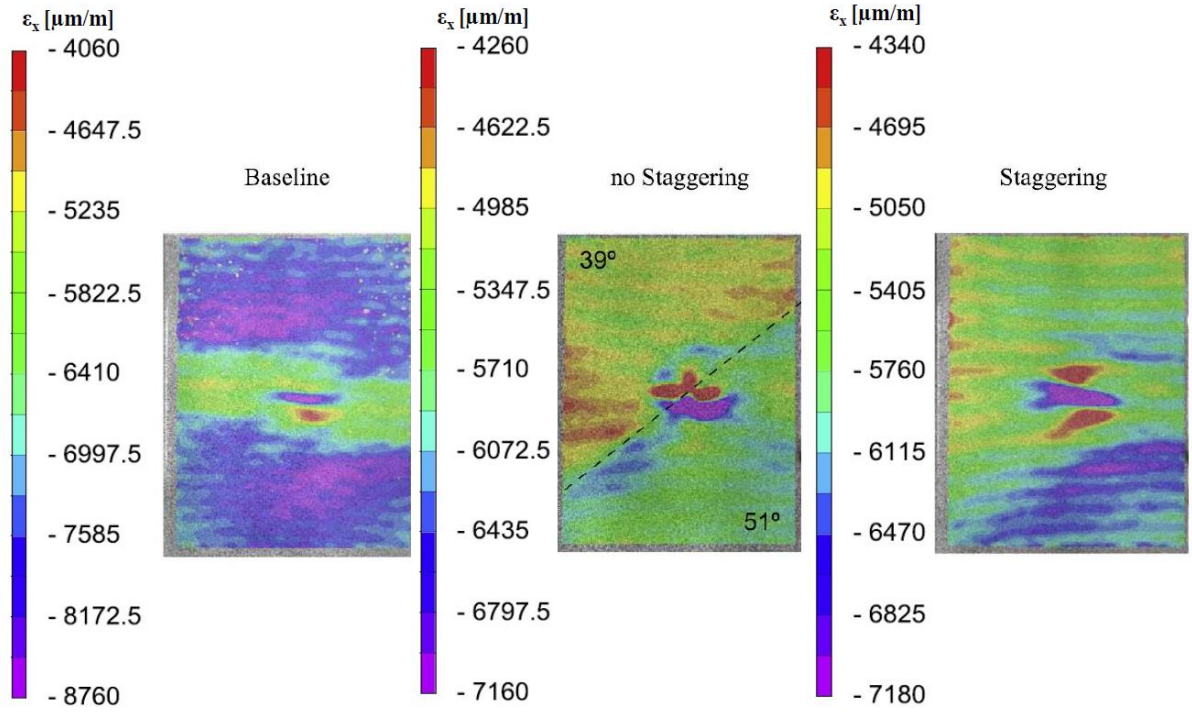

Figure 30: Longitudinal strain distribution of the specimens measured by DIC system: Baseline, no staggering and staggering at impact energy of 15 J and compression load value of 81.1 kN, 64.0 kN and 68.0 kN, respectively [38]

Ghayour [39] investigated the effect of periodically induced gaps on the impact response of composite structures. No CAI test was conducted. QI laminates made of HTS-977-2 with and without gaps were manufactured. The periodic gaps between the fiber courses were embedded in all layers of the laminates as shown in Figure 31. An average of 2.0 mm was chosen for the width of the periodic gaps between fiber courses, which generates 8 % of gap percentage in the whole laminate during the fiber placement. The specimens were impacted with different impact energies 5, 10 and 15 J with 16 mm hemispherical impactor.

The gap effect on the impact response was investigated by means of the US-scan method, micrographs and the impact data gained experimentally. It was found out, that gaps can change the shape of the projected delamination pattern and increase the delamination area up to 50 % as shown in Figure 32. Further, the delamination failure is initiated in the gap area. The delamination threshold load, which is identified as the first significant force drop in the load impact evolution, is affected by the gaps. It represents the initial value at which a significant change in the stiffness properties is detected. Its value is associated with the development of a first significant delamination. After this point, the response of the structure is affected by a large variety of damage mechanisms such as matrix cracking, interface debonding between fiber and matrix, delamination and fiber failure. It was observed, that the delamination threshold load varies with the impact energy level, in contrast, the baseline configuration shows no dependency from the impact energy level. It is assumed that the variation in the delamination threshold load is because the resin rich areas, which are a consequence of the gaps. These resin rich areas can accelerate the delamination initiation under impact loading.

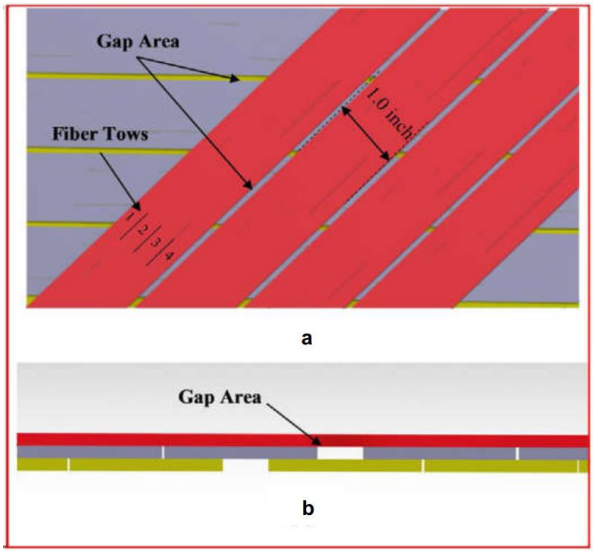

Figure 31: a = Top view of the laminate including the periodic gaps; b = Cross section view of the laminate [39]

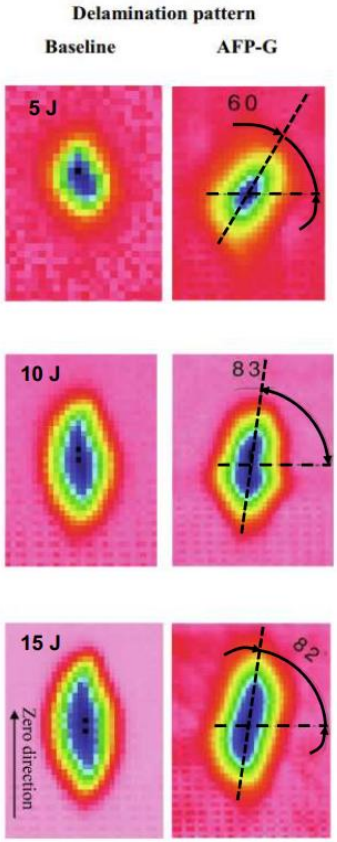

Figure 32: Projected delamination areas at different energy levels [39]

The reviewed literature confirms, that the interaction between waviness and impact is almost unexplored. Only few works [2], [37], [38] and [39] treat the effect of manufacturing defects on the damage tolerance behavior. Nevertheless, these works confirm that there is still a lack of knowledge in the interaction behavior. Thus, there is a need to understand this interaction, since damage tolerance of low velocity impacts is a key and a critical factor in the design of aircraft structures. Low velocity impact can be more relevant compared to high velocity impact, as it can induce a barely visible impact damage (BVID), which might reduce the compression residual strength significantly as described in Section 2.3.

2.5 Failure modes in wavy structures

There are different sources for inducing defects, which can be created during manufacturing, assembly and in-service as described in Section 2.1. The applied load in connection with the geometry of the structures is a further source for inducing defects in composite structures. Depending on the applied load direction relative to the fiber orientation, different failure modes can occur. The spatial stress state of an UD element is depicted in Figure 33 illustrating the inplane and out of plane stresses relative to the fiber direction based on [40]. The inplane stress σ_1 acts in fiber direction and is equivalent to $\sigma_\parallel$. The inplane stress σ_2 and out of plane stress σ_3 act perpendicular to the fiber orientation and are equivalent to $\sigma_\perp$. The interlaminar stress τ_{31} and inplane shear stress τ_{21} are equivalent in their effect to $\tau_{\perp\parallel}$. The shear stress τ_{32} is equivalent to $\tau_{\perp\perp}$.

Loading type effect on the evolution of failure modes

In case of an applied load acting parallel to the fiber direction a distinction has to be made between compression and tension load, since these lead to different failure modes. Tension load in fiber direction leads to a fiber fracture failure mode and compression load leads to a fiber kinking as shown in Figure 34 (a and b). In case of an applied load perpendicular to the fiber direction, a distinction has to be made between compression and tension, too. Both load cases cause matrix failure but with different fracture planes as shown in Figure 35. Matrix failure can be induced by shear stresses $\tau_{\perp\parallel}$ and $\tau_{\perp\perp}$ as shown in Figure 36, too. More details related to these stresses/load cases can be found in [40].

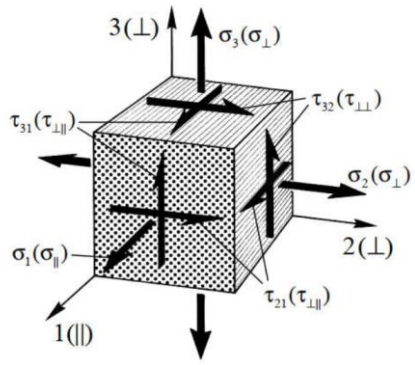

Figure 33: Spatial stress state of a UD element [40]

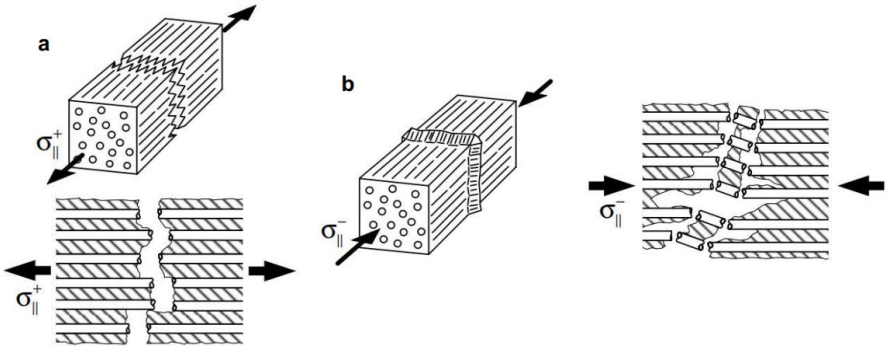

Figure 34: a = Schematic illustration fiber fracture induced by tension; b = Fiber kinking induced by compression parallel to fiber orientation [40]

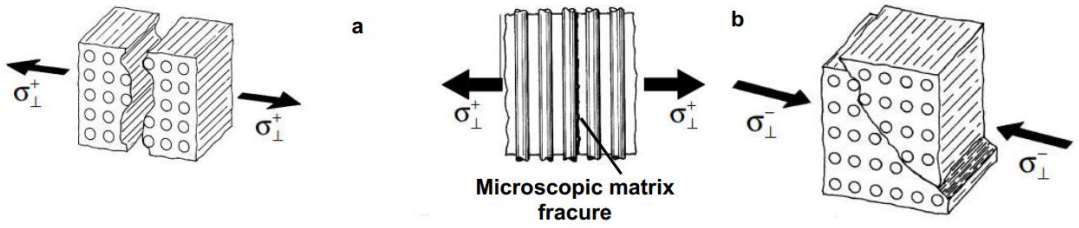

Figure 35: Schematic illustration matrix fracture induced by tension (a) and compression (b) perpendicular to the fiber direction [40]

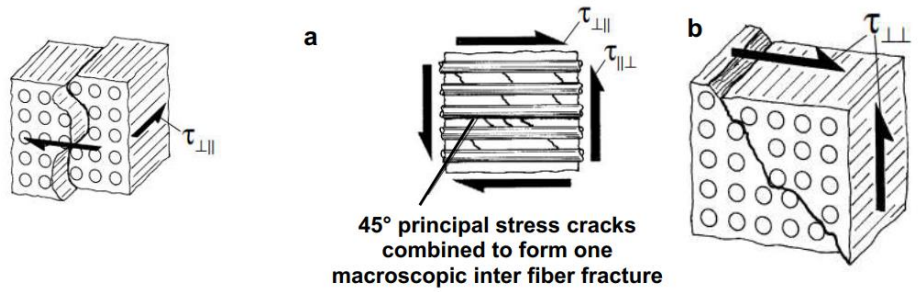

Figure 36: Schematic illustration of matrix fracture induced by shear stresses (a) $\tau_{\perp\parallel}$ and (b) $\tau_{\perp\perp}$ [40]

Another respected loading type in the design of composite structure is the low velocity impact. It is the main driving factor for the evolution of delamination, which represents a very critical failure mode. The evolution of single or multiple delamination can reduce the axial and bending stiffness of the structure initiating a local sub-laminate buckling or even in the worst case a global buckling leading to the collapse of structure. The impact loading is often accompanied by further damages as described in Section 2.3. The through thickness delamination distribution is a function of the impact energy. High impact energies cause delamination in almost each interface, which are increased in the non-impacted side building the well-known pine tree formation as shown in Figure 4 (b). Low impact energies result mostly in intralaminar and interlaminar matrix cracks, as shown in Figure 4 (a). Interlaminar matrix cracks are often the starting point for delamination, too.

Geometrical effect on the evolution of failure modes

Often only the interlaminar shear stresses are considered, although interlaminar normal stresses, if they occur as peel stresses, are usually more dangerous [40]. Peel stresses can be initiated due to the geometrical condition of the component such as curved structures. The loading of a curved structure in the opposite direction to the curvature leads to considerable interlaminar tension stresses and thus delamination as shown in Figure 37. In the worst case, the transverse force induced shear stresses and the interlaminar peel stresses are superimposed.

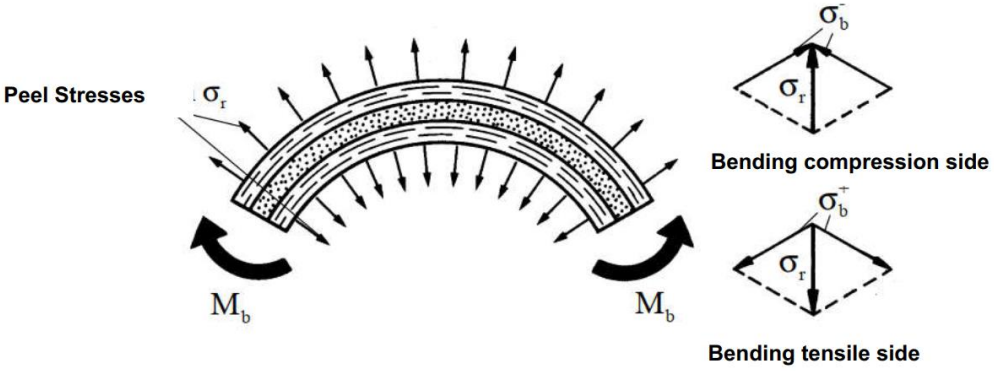

Figure 37: Evolution of interlaminar normal peel stresses in curved structure [40]

Ehrlich [36] confirmed by his experimental study the interaction effects between the geometry condition of the structure and the applied load as described in Section 2.4 and shown in Figure 38. He found out, that the curvature of the structure plays a crucial role on the damage tolerance. Even a slight curvature is sufficient to obtain a state of stress with a typical shell character. With a decreasing curvature radius, applied vertical loads are no longer transferred exclusively via transverse forces and moments, but rather via membrane forces. Convex structures generate local membrane compression loads and thus increase the interlaminar stresses during the impact. On the other hand, concave structures generate local membrane loads, which lead to a reduction in interlaminar stresses. In Figure 38 the effect of curved structures on the stiffness and membrane stresses in comparison to plane structures is illustrated. The vertical axis on the left represents the relative stiffness, which is the quotient of the maximal deflection in the plane plate (w_{max}^{Pl}) to maximal deflection in the curved plate (w_{max}) as a function of U which is the severity of the curvature. The vertical axis on the right represents the relative membrane stress, which is the quotient of the maximal membrane stress in the curved plate ($\sigma_{x,\,max}^{mem}$) to maximal bending stress in the plane plate ($\sigma_{x,\,max}^{B}$). The relative symmetrical stiffness curve indicates, that the curvature increases the stiffness of the structure regardless its orientation. The curve of the relative membrane stress is antimetric revealing that the membrane stresses are increased with the curvature. Convex loaded plates generate compression stresses and concave loaded plates generate tension stresses. Consequently, the orientation of the curvature plays a crucial role. These findings shown in Figure 38 are based on calculation using the Kirchhoff plate theory, for more details refer to [36].

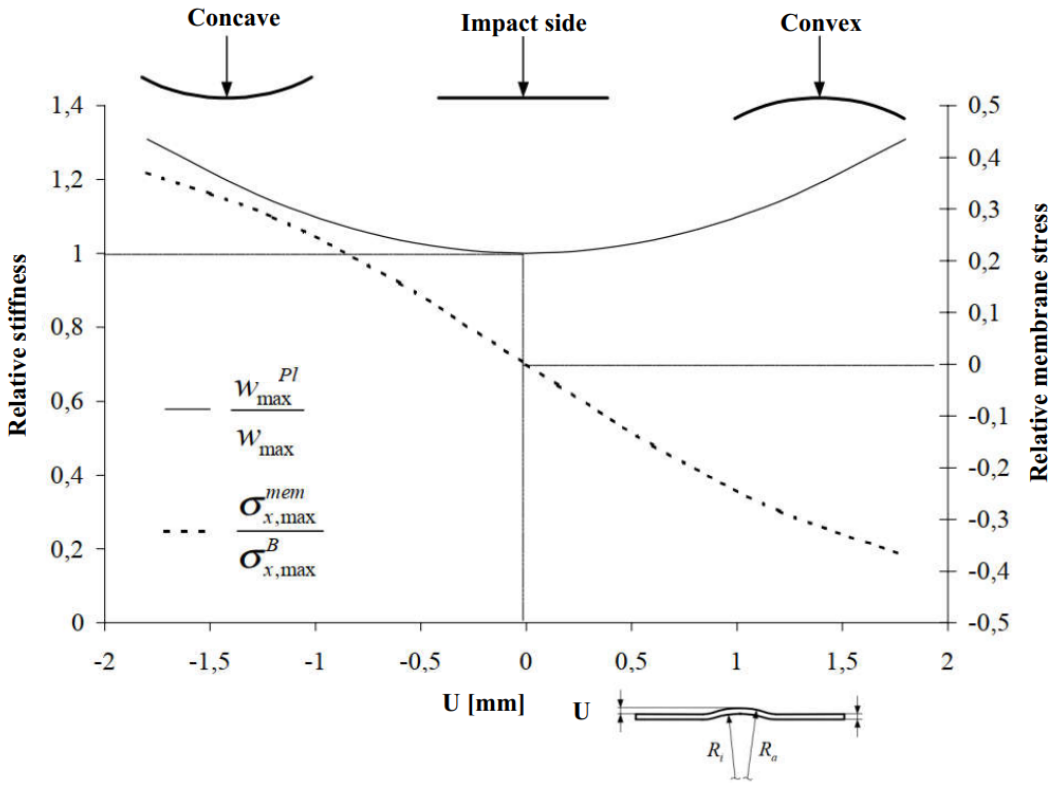

Figure 38: Geometry dependence of the relative stiffness and the relative membrane stress of slightly curved plate [36]

Roos [41] derived new models for the calculation of the interlaminar normal stress (ILNS), which is induced due to the geometry condition of the structure, namely singly and doubly curved thickwalled laminates. The models are based on the CLT. It is stated, that high ILNS occur in thick-walled curved laminates due to external loads such as normal force and bending moment. To validate the model results thick curved specimens as showen in Figure 39 were fabricated. The thickness (t), amplitude (h) and length (l) are 8 mm, 20 mm, and 80 mm, respectively. The cross ply specimens were loaded by inplane compression loading and the UD specimens by inplane tension loading, respectively. It was found, that tension loading causes high positive ILNS in region III as shown in Figure 39 leading to a delamination failure mode. The ILNS distribution of an UD specimen is depicted in Figure 40. The failure in the cross ply specimens under compression loading started with a matrix failure as shown in Figure 41, which passed over into delamination. The failure evolution in the cross ply laminate is comparable to the failure evolution occurred in the QI laminate investigated by Mukhopadhyay [10] as shown in Figure 16. In the compression case, the failure mode was initiated by ILSS. Critical ILNS and ILSS are predicted in region III and II, respectively.

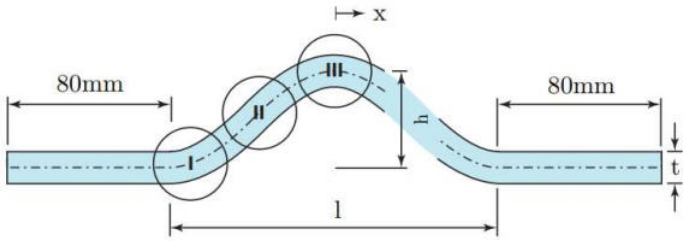

Figure 39: Geometry of the singly curved specimen [41]

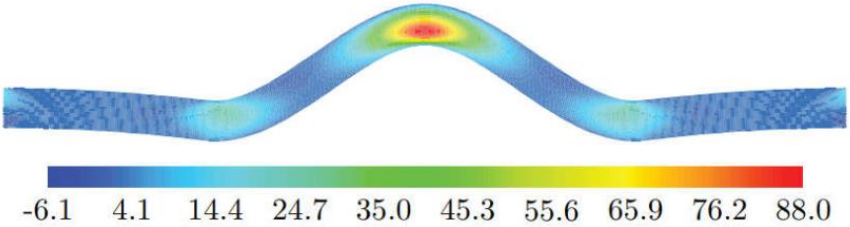

Figure 40: Interlaminar normal stresses distribution induced by tension loading in UD specimen [41]

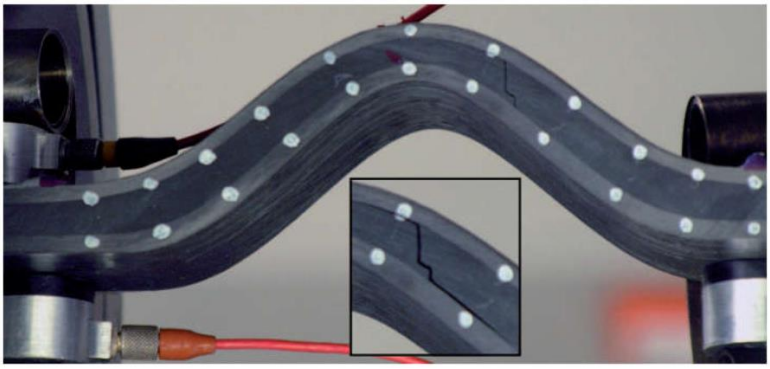

Figure 41: Interlaminar shear stresses failure mode by compression loading in cross ply laminate [41]

Thus, in general it can be stated, that the evolution of different failure modes depends mainly on the applied load and the geometrical condition of the structure in addition to further influencing paramters such as material properties, enviromental condition etc.. This thesis focuses on failure modes initiated by inplane compression loading and low velocity impact event. The compression failure mode of composite structures is sensitive to the properties of the matrix and the degree of imperfection induced by the presence of manufacturing, assembly and in-service defects.

Failure mechanisms of UD laminate under compression loading

According to Altmann and Manikarnika [12], [42] failure modes observed in UD laminates subjected to inplane compression loading are; elastic microbuckling, plastic microbuckling, fiber crushing, matrix splitting, buckle delamination and shear band formation as shown in Figure 42. The cause for the elastic microbuckling failure mode is a global elastic instability

of the fibers. Plastic microbuckling represents a localized instability of the fibers. Fiber crushing is defined as the failure of the fiber themselves at microscopic level. Matrix splitting is defined as the development of matrix cracks parallel to axial direction due to the low matrix toughness. Buckle delamination is defined as the separation of the laminate into sub-laminate with a low thickness and base laminate with higher thickness due to the presence of delamination. As a consequence, the sub-laminate tends to buckle at a lower buckling load. Shear band formation represents a ductile failure of the matrix, which happens when the fiber volume fraction is so low, so that the applied loading cannot be carried by the fibers. Based on [12] it is expected, that similar failure mechanisms occur in composite structures affected by waviness.

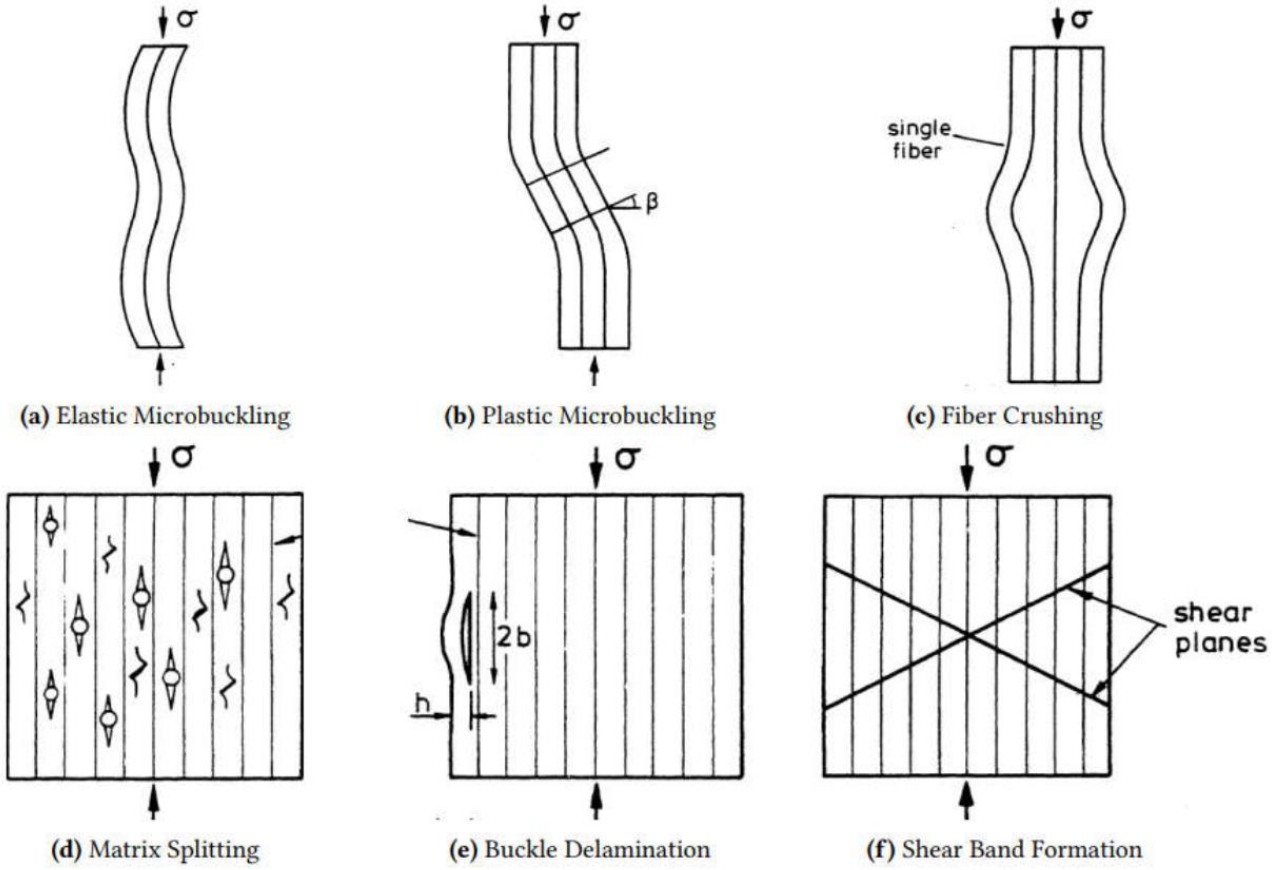

Figure 42: Failure mechanism under compression loading [42]

Failure mechanisms of wavy structure under compression loading

Out of plane ply waviness induces a 3D stress field due to the change in the geometrical shape of the ply as shown in Figure 43. The resulting stresses are a combination of interlaminar normal and shear stresses. Components subjected to compression loading undergo interlaminar normal stress known as peel stresses in combination with interlaminar shear stresses. The interlaminar peel stress initiates delamination between the adjusted plies and the matrix is additionally stressed by the induced interlaminar shear stresses. The consequence of compression loading is an increase in the waviness severity (Θ, A/L respectively). In contrast, tension loading tries to straighten the fibers and the developed interlaminar normal stress supports the connection between the adjusted plies as shown in Figure 44.

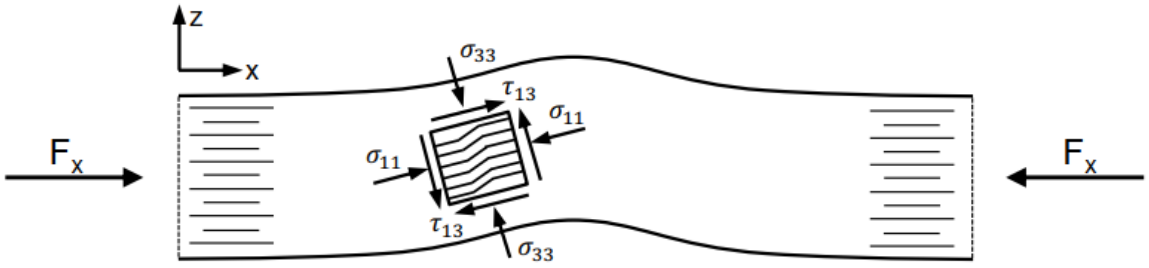

Figure 43: stress state in wavy ply [12]

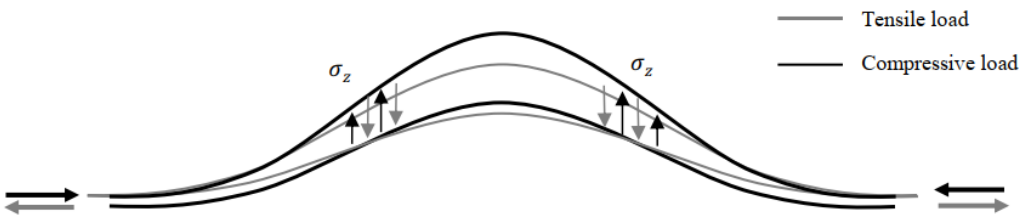

Figure 44: Induced OoP stress in wavy ply subjected to compression and tension loading [12]

The reviewed literature in [12] states, that fiber kinking is the initial failure mode in thick wavy laminates, which is followed by delamination. The source for fiber kinking is plastic microbuckling, refer to Figure 42. Fiber kinking represents an inplane or out of plane rotation of the fibers from the nominal inplane fiber orientation. Further, fiber kinking is described as a localized shear deformation of the matrix, which is accompanied by fiber fracture. Therefore, the matrix mechanical properties play a crucial role under compression loading. It is expected that fiber kinking occurs at the maximum inclination of wavy composite due the high shear stress field in this region.

2.6 Sub-laminate buckling behavior of delaminated structures

In [23] Abrate, it is stated, that low velocity impact damages are initiated by matrix cracks leading to delaminations at ply interfaces. These delaminations are introduced only at interfaces between plies with different orientations. If two adjacent plies have the same orientation, no delamination will be created. The major axis of the delamination is oriented in the direction of the fibers in the lower ply at that interface.

Further, the through thickness delamination distribution depends on the thickness of the laminate. In thick laminates, matrix cracks are first generated in the first ply due to the high localized contact stresses induced by the impact event. The delamination distribution in this case represents a pine tree pattern as shown in Figure 45 (a). In thin laminates, bending stress in the bottom side of the laminate generates matrix cracks in the lowest ply, which induces a pattern of further matrix cracks and delaminations leading to a reversed pine tree as shown in Figure 45 (b).

The reason why delaminations are introduced, is related to the orthotropic elastic behavior of each ply. Under impact loading, each ply tends to deform in a particular way, so that interlaminar normal and shear stresses in the interfaces force the layup behaving as one plate. When these interlaminar stresses become too large, delaminations are introduced [23].

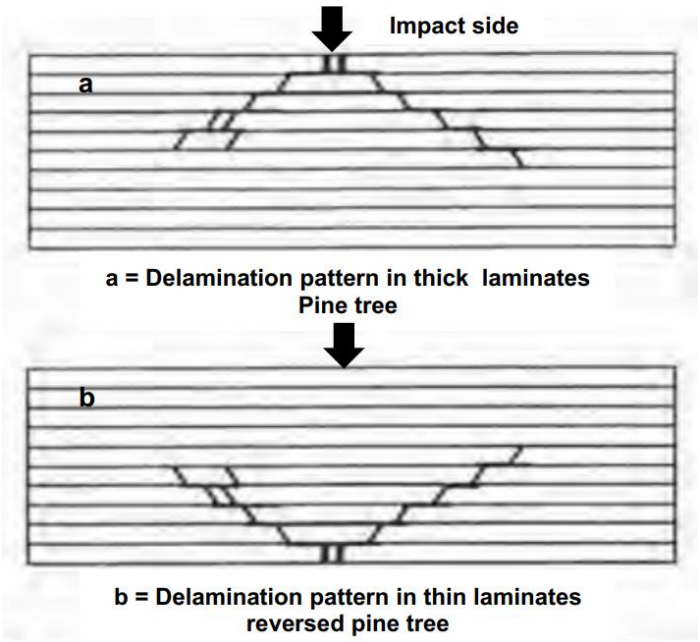

Figure 45: a = Through thickness delamination pattern in thick laminate; b = Pattern in thin laminate [23]

Impact induced delaminations are particularly dangerous in case of components that are at risk of buckling. Buckling is a sudden change in the geometry of the structure due to an applied load, when a certain critical limit of the load is achieved. There is always a risk of buckling when membrane compression, shear or combination of both loadings occur. Due to the separation of the layers, the bending stiffness of the laminate has been drastically reduced, so that premature buckling of the laminate with subsequent catastrophic collapse is the result.

There are three types of buckling modes as shown in Figure 46; local, global and mixed mode buckling. Local buckling mode has received considerable attention. In this case the delamination is located near to the outer surface, so that the structure is divided into two parts, sub-laminate and base laminate as schematically shown in Figure 46 (a) and Figure 20. Usually the base laminate can have further delaminations. However, the sub-laminate buckles firstly, while the rest of the laminate remains straight. In case of global mode buckling, a short delamination is located near to the midplane of the laminate. Its effect on the stability behavior of the laminate is small, so that the entire laminate buckles as if undamaged as shown in Figure 46 (b). In case of mixed mode buckling, the overall stiffness of the laminate is reduced and the remaining portions are no longer symmetrical, due to the existing delaminations. The thinner portion buckles under local buckling mode, meanwhile the thicker one buckles under global buckling mode, as shown in Figure 46 (c).

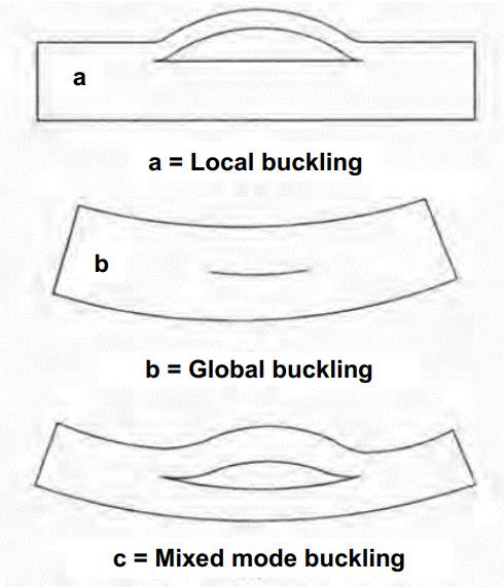

Figure 46: Buckling mode types: a = Local buckling, b = Global buckling, c = Mixed mode buckling [23]

2.7 Neutral axis position and its effect on the evolution of eccentric load

The design of midplane symmetrical laminates, in which the midplane is the neutral plane is always advantageous due to the following reasons as described by Schürmann [40]:

- The midplane of the laminate represents the general neutral plane.
- The membrane and the shell problem can be treated separately, if the midplane of the laminate is chosen as the reference plane for the stiffness matrix. In this case, the elements of the coupling matrix become zero leading to a reduction in the calculation effort.
- Consequently, normal or shear fluxes only cause inplane deformations without curvatures or twists. Moment fluxes do not cause any expansional or shear deformation, but only curvatures and twists.
- The general neutral plane is at the same time the neutral plane under bending around the x, y axes and under twisting.
- There is no distortion due to thermal or residual stresses.

From a structural mechanical point of view, it is advantageous if the neutral plane/axis of the laminate and the load axis coincide, as otherwise additional bending moments can be induced. Accordingly, it plays an essential role in the evolution of the different failure modes. In case of stability, an external compression loading can generate with respect to the neutral axis a bending moment that counteracts the buckling deformation but also supports the buckling. The position of the neutral axis can be shifted for instance in case of asymmetric laminate, geometrical change in the structure or the presence of defects such as delamination, waviness, overlaps, gaps, foreign objects or resin rich areas. In such cases is advantageous to now the

new neutral axis position to estimate the effect of the induced eccentric load on the deformation behavior and consequently on the failure mode evolution and final failure.

2.8 Summary and conclusions

Based on the reviewed works related to OoP waviness, the following findings and conclusions are summarized:

- The majority of the literature reviewed focus on the effect of A/L ratio on the strength response in UD and cross ply laminates either with one to several distributed affected 0°-ply/ plies or uniform waviness. Only few works [10], [13] and [21] treat the OoP waviness effect in multilayered laminates. Nevertheless, there is a need to understand the dependency between the waviness angle and stepwise increased number of affected 0°-plies in more complex laminates such as QI laminate or multilayered laminates with high number of 0°-plies (0° > 40 %). Such laminates are more relevant for the industrial applications.
- OoP waviness induces a 3D stress state in material subjected to uniaxial loading. Interlaminar shear (τ_{13}) and interlaminar normal (σ_3) stresses are induced due to the geometry of the waviness, which can be superimposed with the applied axial loading– affecting the failure load as well as the failure mode.
- Regardless the waviness morphology (A, B and C) and distributions within the laminate, the interlaminar stresses seem to be driving the failure initiation under compression loading as summarized in Table 2. The cause for the initiation of the interlaminar stresses can be traced back to the curvature of the structure as described in [41], consequently, the curvature induced by the waviness.
- Beside the induced interlaminar stresses due to the geometry of the wavy ply, the waviness morphology itself such as morphology B or C can contribute an additional bending moment as shown in the strain distribution of Figure 17 and in the experimental investigation [2] and [13]. The development of a bending moment is related to the displacement of the neutral axis.
- The interlaminar stresses are the cause for the compression strength reduction, which is decreased as the waviness angle and the number of affected 0°-plies are increased. Adams [7], Duangmuan [9], Thor [13] and Al-Kathemi [2] observed experimentally the dependency of the increased number of affected 0°-plies with the reduction in the compression strength.
- The position of the 0°-plies affected by waviness plays a crucial role on the failure behavior. Depending on it, an out of plane bending due to the localized non-symmetry in the laminate can be induced, refer to Adams [7]. That why the majority of the researchers fabricate waviness at laminate midplane or close to it.
- As shown by Thor [13], the failure mode evolution depends on the waviness parameters namely the waviness angle and the thickness of the structure. In case of the tested specimens with big waviness angle, the failure mechanism was dominated by

the bending moment, which initiated delamination as major first failure. The final failure was mainly fiber fracture. In case of the tested specimens with small waviness angle, the failure mechanism was determined by material failure, which was pronounced by fiber kicking followed by delamination.

Ref.	Lam.	Morph.	t [mm]	ILNS (σ_3) Pos.	ILSS (τ_{13}) pos.	Failure mode	Load type
[15]	Cross ply	A - central	3 plies	At Θ_{Max}	See Figure 8	ILSS	Figure 8
[7]	Cross ply	A - distributed	2.3 - 4.1	Vicinity of Θ_{Max}		ILSS → Delamination	Figure 9
[5]	UD	A - Graded	9		At Θ_{Max}	ILSS → Delamination → local buckling → Collapse	Figure 10
[9]	Cross ply	A - distributed	1.78 - 10.9	Above wavy 0°-ply at vicinity of Θ_{Max}	At Θ_{Max}	First failure delamination due to ILSS	Figure 12
[10], **[21]**	QI	A - central	6	Above wavy 0°-ply at vicinity of Θ_{Max}		Matrix failure → delamination → fiber kinking	Figure 16
[12]	UD	C	8.1	At Θ_{Max}		Collapse due to fiber kinking	Figure 14 - Figure 15
[13]	QI	C	5	Failure mode depends on Θ & morphology		Big Θ = failure by bending moment; Small Θ = Material failure → fiber kinking	Figure 17
[41]	Cross ply	C	8		Region II refer to Figure 39	Matrix crack → delamination	Figure 39

Table 2: Overview of the positions of interlaminar stresses in wavy specimens with different morphology, thickness, layup under compression loading

Based on the reviewed works related to impact and CAI as well as the few works related to the interaction between impact and manufacturing-induced defects, the following findings and conclusions are summarized:

- The curvature of the structure plays a crucial role on the damage resistance of the structure, refer to [36]. Consequently, a geometrical change due to presence of defects can influence the damage resistance.
- The impact side relative to the curvature orientation plays a crucial role on the damage resistance of the structure, too, refer to [36].
- The presence of manufacturing defects has influence on the position of the neutral axis which can significantly affect the deformation and consequently the failure behavior of the structure, refer to [2].
- The impact side relative to the position of the defect and its geometry have a significant effect on damage resistance and thus on the damage tolerance, refer to [37].
- The CAI strength reduction is driven by the impact event itself rather than by manufacturing-induced defects, refer to [2] and [38].
- An adequate impact energy level in dependence of the manufacturing defect parameters has to be chosen, to enable a better damage visualization, refer to [2] and [38].
- There is an increase in the delamination areas and a change in the delamination shape due to the presence of manufacturing defects, refer to [2] and [39].
- The impact event itself induces a 3D stress state and interlaminar stresses which may cause delaminations which are mainly followed by a sub-laminate buckling.
- The CAI strength is decreased as the impact damages increase.

3 Scope and outlines of the thesis

This chapter comprises the research of the thesis. The research and working hypotheses as well as the scope of the thesis are presented in Section 3.1. Subsequently, Section 3.2 contains the outline of each chapter and a summary of its respective contents.

3.1 Scope

Waviness as well as impact damages are very common industrial defects, which lead individually to a serious reduction in the strength – in particular compressive strength - and stiffness, and are therefore respected during design. In addition, waviness and low velocity impact damages are often difficult to detect, therefore it is advantageous, if the design of composite structures would be as tolerant against such defects as possible. Both fields were separately analyzed in detail analytically, numerically and experimentally.

Nevertheless, the interaction between waviness and impact damages is almost unexplored. Only few works [37], [38] and [39] treat the effect of manufacturing defects, namely gaps effect on the impact resistance and the compression strength after impact. Al-Kathemi [2] treats the effect of OoP waviness on the impact resistance and the compression strength after impact. These works confirm that there is still a lack of knowledge in the interaction between manufacturing-induced defects and damage tolerance behavior. In the aircraft sector, the worst case must be covered including the interaction effect between waviness and impact damages to satisfy damage tolerance requirements. This leads to conservative design requirements and tight tolerances in production. Therefore, this thesis focuses on the interaction effect between OoP waviness and low velocity impact damages.

In the view of these points, there is a need to understand this interaction, to derive a simplified methodology for assessing their interaction effect on the strength capacity as well as to derive a such kind of distinction catalog related to the waviness morphology in connection with impact side and further influencing parameter to reduce conservatism in the design.

Consequently, the research hypothesis is as follow:
It is possible to demonstrate physical interaction effects of out of plane waviness and impact damages of fiber composite structures by experimental approaches.

Additionally, the following working hypotheses are formulated to investigate experimentally the research hypothesis:

1) It is possible to design a systematic experimental campaign, which covers distinct cases (Chapter 4);
    a) by categorizing the waviness morphology in convex, concave and flat geometry
    b) with regards to the impact side relative to the orientation of the waviness morphology
    c) with regards to the impact position relative to the waviness position and waviness severity
    d) by considering the number of affected 0°-plies in dependence on the waviness angle

e) by considering that the damage tolerance strain allowable is affected by the presence of waviness.

f) by considering the thickness in dependence on the number of affected 0°-plies and waviness angle

2) Assess the main influencing factors of waviness defects, impact and the effect of their combinations on the residual strength of fiber composite plates based on experiments (Chapter 5).

3) It is possible to derive a simplified physical interaction relation of out of plane waviness and impact (Chapter 5).

4) It is possible to verify the results by other experimental results (Chapter 6).

3.2 Outline of the thesis

The current thesis consists of seven chapters:

- **Chapter 1 Introduction:** highlights the motivation and focuses of the thesis.
- **Chapter 2 State-of-the-art:** provides a brief description of damages which occur in composite structures during manufacturing, assembly and in-service. It reviews different investigations related to waviness effect on the stiffness, strength capacity and the non-linear behavior due to the presence of waviness, the impact effect on the damage resistance and damage tolerance behavior as well as the interaction effect between manufacturing-induced defects and impact damages. Further, the evolution of different failure modes in dependence on the loading direction and the geometry of the structure is described. Finally, the role of the neutral axis on the failure mode initiation is outlined briefly.
- **Chapter 3 Scope and outlines of the thesis:** includes the scope, the research and working hypotheses as well as the outline of the thesis.
- **Chapter 4 Planning and experimental investigations:** describes firstly the background for the planning process of the conducted compression and compression after impact tests with and without artificially induced OoP waviness. Additionally, the specimen's geometry, material used, layup, the waviness fabrication method, the measurement methods used as well as the test fixture and mechanical testing method are outlined.
- **Chapter 5 Experimental results and discussion:** in the first section, suitable knock down factors (KDFs) are defined. These KDFs are derived experimentally, which cover the waviness effect on the compression strength of an undamaged structures, the impact effect without waviness as well as the interaction effect between both defects on the compression strength after impact. The second section includes all results and discussion related to the plain strength compression (PSC) tests. The third section contains all results and discussion related to the conducted CAI tests. Finally, a

comparison between the PSC and CAI test is performed and the related findings are highlighted.

- **Chapter 6 Experimental verification:** In this chapter the available works from the literature related to the interaction between manufacturing-induced defects as well as the interaction effect between curved structure and low velocity impact are put in the context of this work to verify the experimental findings of this thesis.
- **Chapter 7 Final remarks:** In this chapter the main conclusions, a critical assessment of the identified interaction relations as well as an outlook related to the future works are presented.

4 Planning and experimental investigations

As shown in the state-of-the-art, there is still a lack of knowledge in the interaction behavior between manufacturing-induced defects and damage tolerance. In particular the interaction behavior between OoP waviness and low velocity impact damages is still unexplored. Therefore, the objective of this experimental investigation is to provide a physical understanding of the interaction between the above-mentioned defects by identifying the critical parameters and their effects separately and in interaction for representative layup of industrial applications on the compressive strength. Consequently, plain strength compression (PSC), impact and compression after impact (CAI) specimens with and without OoP waviness were fabricated.

The PSC test is an experimental method to determine the compression strength of undamaged composite structures. The CAI test is an experimental method to determine the damage resistance and damage tolerance of an impacted structure. The process is divided into three steps: The first step represents the impacting process of the CAI specimen with a specific set of impact parameters (impact velocity, impactor weight, impactor diameter, etc.). The second step represents the US-scan inspection to identify the damage resistance characteristics (delamination projected area, dent depth, visible impact damages, etc.). Finally, the CAI test is conducted to determine the compression strength after impact.

Within the PSC testing the effect of the waviness morphology and different waviness angles (Θ) in dependence on number of affected 0°-plies ratio ($\alpha_{0°}$), total number of affected plies ratio (α) as well as the thickness are investigated on the strength and deformation behavior, in order to derive the pure waviness effect. Ratios $\alpha_{0°}$ and α are defined in Equations (1) and (2). Adams [7] and Duangmuan [9] introduced the ratio $\alpha_{0°}$ called as “wave fraction” in their investigations to study the effect of affected 0°-plies on the compression strength reduction in cross ply laminates.

$$\alpha_{0°} = \text{Number of all wavy 0°-plies} / \text{Total number of 0°-plies in laminate} \quad (1)$$

$$\alpha = \text{Number of all wavy plies} / \text{Total number of plies in laminate} \quad (2)$$

The objective of the CAI testing without waviness is to identify the pure impact energy effect on the strength reduction and deformation behavior by means of the detected delamination shape, size and through thickness distribution. These damage characteristics, which represent the reference data are the fundamental to investigate how the waviness parameters (Θ, $\alpha_{0°}$, α) change the damage resistance of the structure and thus the damage tolerance behavior.

The objective of the CAI testing with waviness and impact is the investigation of the interaction behavior between these damages, quantifying the change in the damage characteristics due to the waviness presence in comparison to the CAI without waviness, identifying the damage main driver for the strength reduction and deformation behavior, as well as the critical waviness parameters. Based on the reviewed literature without [2], the

following influencing parameters shown in Table 3 are considered as relevant influencing parameters.

Influencing factors	Load cases		
	PSC	CAI	Interaction
Energy level		✓	✓
Impact side relative to defect position			✓ (Gaps)
Defect dimension and position within the laminate	✓		✓ (Gaps)
Waviness morphology	✓	✓	✓
Waviness angle (Θ)	✓	×	×
No. of affected 0°-plies (α_0)	✓	×	×
No. of total affected plies (α)	✓		✓
Thickness	✓	✓	×
Investigated = ✓		Not investigated = ×	

Table 3: Relevant influencing factors from literature

4.1 Planning

For the design of the test campaign, the findings gained from the literature are considered. These form the basis for defining a specific test matrix, which covers critical cases and relevant parameters. Since most of the experimentally investigated laminates with waviness are either UD or cross ply laminates, it was decided to choose a QI laminate, which is more representative for the industrial applications.

Selection of the waviness morphology

Ehrlich [36] showed in his experimental investigation, that the impact of curved specimens with convex shape caused greater damage than the concave and flat ones. The damage in this context is related to the size of the projected delamination area and the through the thickness delamination distribution. The projected delamination area of the flat specimens was between the concave and convex one as shown in Figure 23. Based on that, it was decided to select a waviness morphology B with a convex shape. On the one hand morphology B enables the investigation of different number of affected 0°-plies and total number of affected plies, on the other hand it enables the consideration of geometrical affects induced by the waviness morphology. Further, morphology B is not investigated by other authors in the literature, yet, although it represents a relevant case for the industrial application as described in Section 2.2.

Selection of the impact side relative to waviness morphology and position

The interaction effect between the curvature of the structure and the applied load on the failure evolution was demonstrated experimentally by Ehrlich [36] as described in Section 2.4. Schürmann [40] uses structural-mechanical relations to clarify this dependency as described in Section 2.5. Both works point out that the application of a load against the curvature of the structure induces interlaminar stresses which provoke failure. Consequently, a waviness morphology with a convex shape can be considered as more critical than a waviness morphology with concave shape or even flat outer surface. Additionally, Rhead [37] showed in his experimental investigation described in Section 2.4, that impacting a coupon directly over a tow gap, which is close to the impacted side, is more critical than impacting a coupon with a gap close to the non-impacted side. In the view of these points it is reasonable to consider the waviness side as the impact side.

The role of affected 0°-plies in dependence on relevant layup

The majority of the investigated waviness cases in the literature ([7], [9] and [15]) treats cases with 100 % affected 0°-plies, located wavy 0°-ply in laminate midplane or several distributed wavy 0°-plies around the laminate midplane in cross ply and UD laminates as described in Section 2.2 and summarized in Table 4. It is found that the compression strength reduction depends on the ratio of the affected 0°-plies. However, the literature lacks investigations related to this effect in relevant laminates for the industrial applications. Consequently, it was decided to increase the number of affected 0°-plies stepwise in a QI laminate to investigate their effect on the compression reduction and also to find out, whether the range described by Duangmuan [9] is available in a QI laminate, too.

Selection of the waviness angle

As described in Section 2.2, Thor [13] found that in case of wave 1 (= 15°, refer to Table 4), the failure is determined by the bending moment, which is superimposed with the axial global loading. In case of wave 2 (= 7°, refer to Table 4), the contribution of the bending moment is less in the superposition of the loading resulting in material failure. Therefore, it was decided to investigate the effect of different waviness angles 5°, 10° and 15° in dependence on different number of affected 0°-plies, different total number of affected plies as well as different thicknesses on the failure behavior.

Reference	Lam.	Morph.	Waviness formation	t [mm]	Θ [°]	α_{0° [%]	KDF [-]
[5]	Cross ply	A	Central	9.0	7	20	0.77
			Graded	9.0	7	100	0.69
	UD		Uniform	19.0	15	100	0.18
[9]	Cross ply	A	Distributed	5.3	13	20	0.81
				4.3		50	0.62
				5.3		60	0.53
[10]	QI	A	Central	6.0	10 & 12	33	0.66
[13]	QI	C	Uniform	5.1	7	100	0.68
	QI			5.1	15		0.35
	UD			2.1	7		0.50
	UD			2.1	15		0.25

Table 4: Investigated waviness morphologies from literature in dependence of layup types, waviness parameters, thickness and related KDFs

4.2 Geometry, material, layup and curing

The geometry of the PSC and CAI specimens are according to Airbus standards [43] and [28]. Schematic sketches of the PSC and CAI specimens are depicted in Figure 47. The specimens were fabricated with and without waviness using IM7-8552 UD. The specimens without waviness, designated as “clean” serve as reference to estimate the waviness effect for investigated load cases. Two thicknesses were planned for the PSC specimens 4 mm and 8 mm. The 4 mm clean specimens have flat outer surfaces and a QI layup consisting of 32 plies, $[[45/-45/90/45/0/-45/90/0]_2]_s$. The 8 mm clean specimens have a QI layup consisting of 64 plies, $[45/-45/90/45/0/-45/90/0]_4]_s$. The layup sequence in both thicknesses is the same to ensure the comparability of the results. The specimens with waviness have the same layup (32 plies/ 64 plies) but with additional inserts to induce the waviness. The insert itself represents a group of stacked 90°-strips/plies, which are placed on top of each other as exemplified by the detailed geometric representation for the insert with the waviness angle of 5° in Figure 48. In case of the 4 mm specimens, the inserts were placed at three different positions throughout thickness in order to cover different total number of affected plies and number of affected 0°-plies as shown in Figure 48. In case of the 8 mm specimens, the inserts were only placed at one position through the laminate thickness, so that, only one total number of affected plies and one number of affected 0°-plies are investigated. In this work only one fixed material type, waviness morphology and impact side are investigated.

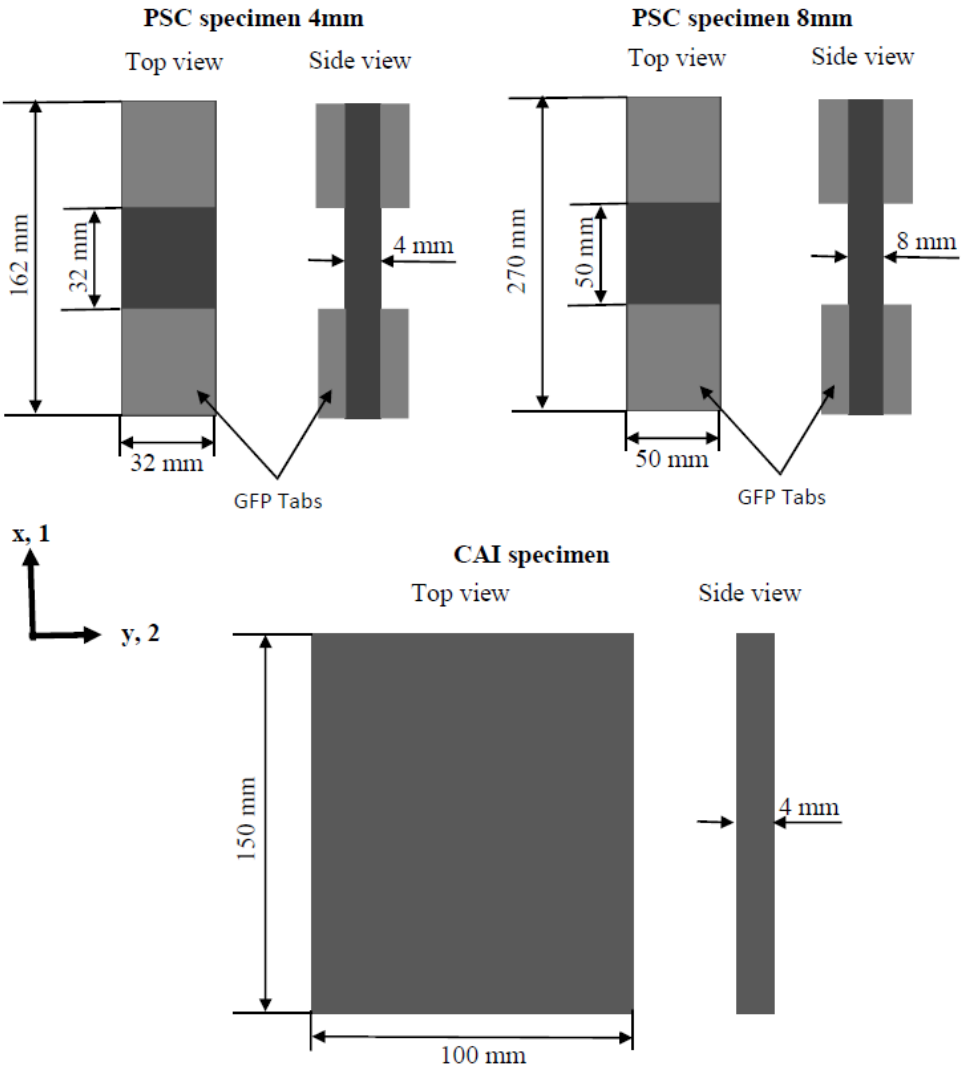

Figure 47: Schematic sketches of the PSC specimens (4mm and 8mm) with tabs from glass fiber reinforced plastic (GFP) and CAI specimen

Hsiao [5], Adams [7], Duangmuan [9] and Mukhopadhyay [21] used the insert technique to induce isolated and distributed OoP waviness in and around the laminate midplane (Morphology A). But this technique does not meet the above-mentioned objectives of covering further morphology with different Θ in dependence on different α_{0° and α ratios as shown in Figure 48. Therefore, preliminary manufacturing trials with different insert geometries were conducted to ensure the target parameters Θ, α and α_{0°. For this purpose, the following principles were experimentally investigated: a) tubed shaped prepreg strips with different diameters, b) stacked strips in form of rectangular, and c) rhombus and trapezoid with a defined geometry. After curing, micrographs were done to proof reliability of the target parameters. The micrographs showed that inserts with trapezoid geometry provided consistence Θ, α and α_{0° as shown in Figure 49. By means of different insert geometry different waviness angles were achieved. The positioning of the inserts inside the specimens induced a local increase in the thickness as is shown in Figure 49 as well as a local change in the stacking sequence. Thus, the upper surface of the wavy specimens is curved having a

sinusoidal shape, and the lower surface is flat, so that Morphology B is realized. The curing cycle of all specimens was performed according to Hexcel Product Data Sheet [44].

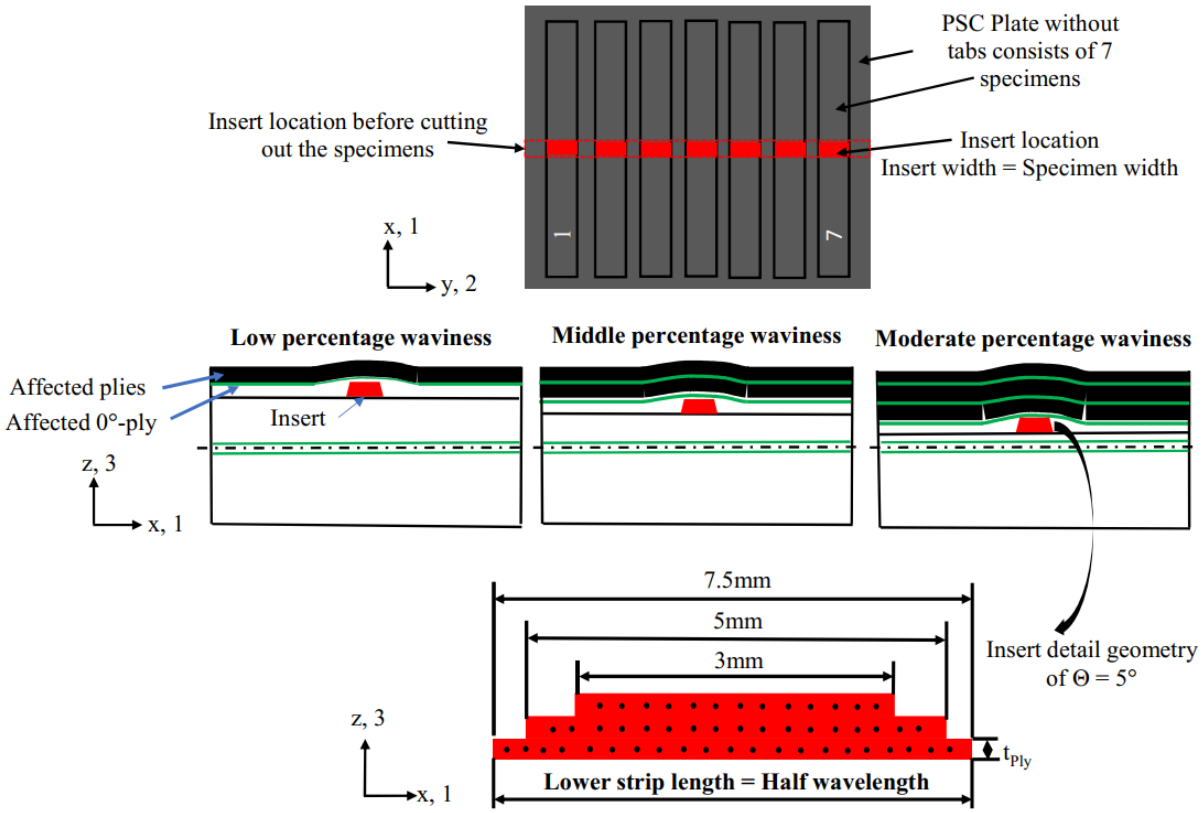

Figure 48: Morphology B, insert position in x-z & x-y planes and insert detail geometry for the configurations with waviness angle Θ = 5° [2]

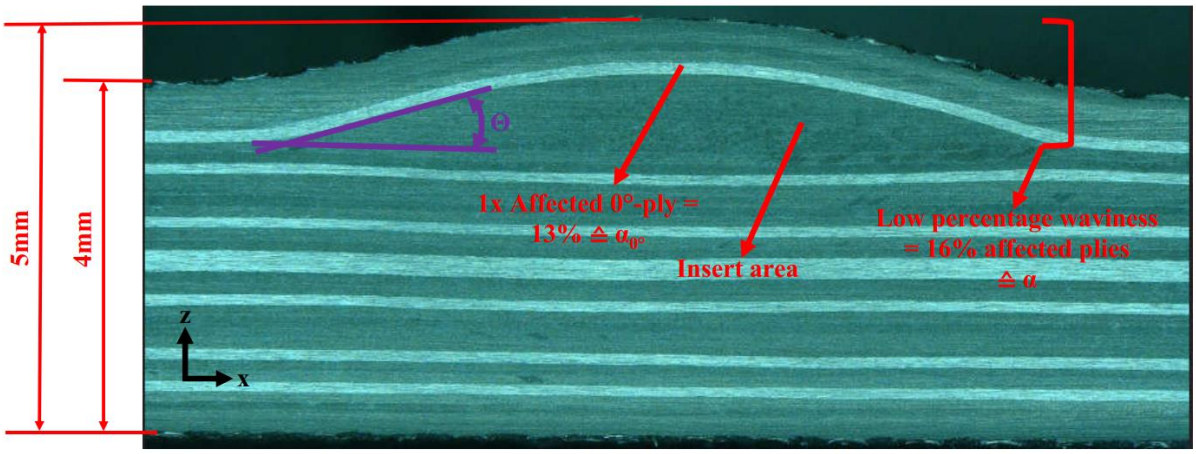

Figure 49 : Definition of waviness angle, affected plies ratio (α) and affected 0°-plies ratio ($\alpha_{0°}$) [2]

4.3 Waviness fabrication method

There is no standard for waviness fabrication, that why preliminary manufacturing trials with different insert geometries were conducted, as described in the previous section. Up to three different waviness angles (Θ) 5°, 10° and 15° in dependence on different number of affected 0°-plies ratio ($\alpha_{0°}$) and total number of affected plies ratio (α) were fabricated for the investigated PSC and CAI load cases. Table 5 contains Θ, $\alpha_{0°}$ and α for each configuration. In Figure 49, Θ, $\alpha_{0°}$ and α are depicted using the example of low waviness configuration. Θ is the included angle between the wavy plies and a horizontal parallel to the 0° direction. All plies above the insert area are affected by waviness, meanwhile the plies below the insert are not affected by waviness.

Load case	Waviness classification	Θ [°]	No. of total wavy plies	No. of wavy 0°-plies	α [%]	$\alpha_{0°}$ [%]
PSC 4mm	Low	5, 15	5	1	16	13
	Middle	5, 10, 15	8	2	25	25
	Moderate	5, 15	13	3	41	38
PSC 8mm	Low	5, 10, 15	8	2	13	13
CAI 4mm	Low	5, 10, 15	5	1	16	13
	Moderate	5,10, 15	13	3	41	38

Table 5: Waviness parameters classification. Each 4 mm layup consists of 32 plies = (0°, 45°, -45°, 90° => each angle in sum 8 plies) in addition to the insert. 8 mm layup consists of 64 plies = (0°, 45°, -45°, 90° => each angle in sum 16 plies) in addition to the insert

Depending on the magnitude of Θ the trapezoid inserts vary in the number of the stacked strips/plies and thus in their thicknesses. The thickness of each strip is equal to the ply thickness. The strip length (x-axis) of each insert is varying in the thickness direction, to ensure sinusoidal waviness. The lower strip length corresponds to half wavelength and is oriented in the 0°-ply direction, so that the waviness is aligned in the mean loading direction.

The inserts are located in the middle of the corresponding plates perpendicular to the x-axis as is shown in Figure 48 exemplarily for the PSC plate. The x-axis is the length direction of specimens. After curing, the specimens were cut out. The entire width of each specimen is affected by the OoP waviness as shown in Figure 48. The number of affected plies was achieved by placing the insert at certain positions in laminate thickness direction as is shown in Figure 48, so that always the 0°-plies and all plies above the insert were affected by the waviness.

All CAI and PSC wavy specimens were sanded manually and the waviness angle was measured as shown in Figure 49 by means of Keyence microscope. The waviness angles of the PSC wavy configurations were measured from each side. In Figure 50 the average waviness angle and the corresponding deviation for each configuration are depicted. In case of the CAI configurations, the waviness angle was measured only from one side. The average waviness angle and the corresponding deviation for each configuration are summarized in

Figure 51. Later in Section 5.2, it is shown, that the strong deviation in the waviness angle has negligible effect on the corresponding failure load deviations.

The technique of placing the inserts with trapezoid geometry inside the laminates enabled that the target parameters Θ, α and $\alpha_{0°}$ were achieved. Therefore, it can be stated, that the waviness manufacturing process was successful and is repeatable. By this technique artificially induced waviness covers industrial cases, in which the OoP waviness is induced by overlaps or inadvertently inserted foreign objects during the layup process.

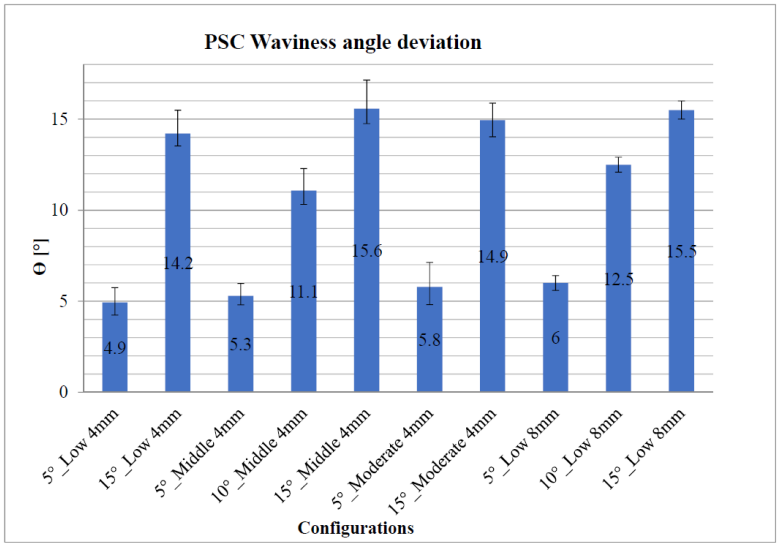

Figure 50: PSC waviness angle for the 4mm and 8mm configurations

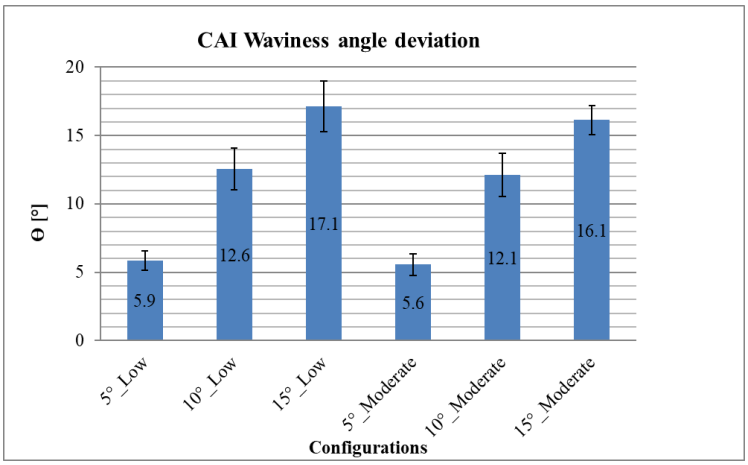

Figure 51: CAI waviness angle [2]

4.4 Test set ups and mechanical tests

There are no standard test methods for wavy specimens, nevertheless the Airbus test standards [43] and [28] are involved to derive the waviness effect on the compression strength. The impact tests were conducted in a Zwick drop tower system of type HIT 600 with a 2 kg – 16 mm diameter impactor as shown in Figure 52 (a). The CAI specimen was fixed by means of the clamping device shown in (b). The free impact area is 75 mm x 125 mm.
The CAI testing was conducted by means of a testing machine of type “Zwick 1484” with a testing speed of 0.5 mm/min using a CAI device as shown in Figure 53 (a). The applied compression load is indicated by means of the red arrow. All CAI specimens are fixed in the CAI device as shown in Figure 53 (a) by means of the anti-buckling rails and the upper and lower clamping areas. The standard anti-buckling rails are straight, therefore, due to the morphology of the wavy specimens, a modification of the anti-buckling rails was required as shown in Figure 53 (b). The Anti-buckling rails were manufactured with a cutout for the out of plane waviness to ensure adequate clamping of the CAI specimen in the CAI device as shown in Figure 53 (a). Numerical pretest simulations as well as experimental verification tests showed that this slight modification is not affecting CAI measurement accuracy compared with the standard anti-buckling rails.

The 4 mm PSC test was also conducted by means of a testing machine of type “Zwick 1484” with a load capacity of 200 kN and a testing speed of 0.5 mm/min, too as shown in Figure 54. The figure on the left represents the testing machine without specimen and the right one with the PSC specimen. The specimens are clamped as shown in Figure 54 (a) and the applied compression load is indicated by means of the red arrow in (b). Due to the increased load capacity in the 8 mm specimens, the compression testing was conducted using an Instron testing machine with a load capacity of 500 kN and a testing speed of 0.5 mm/min as shown in Figure 55.

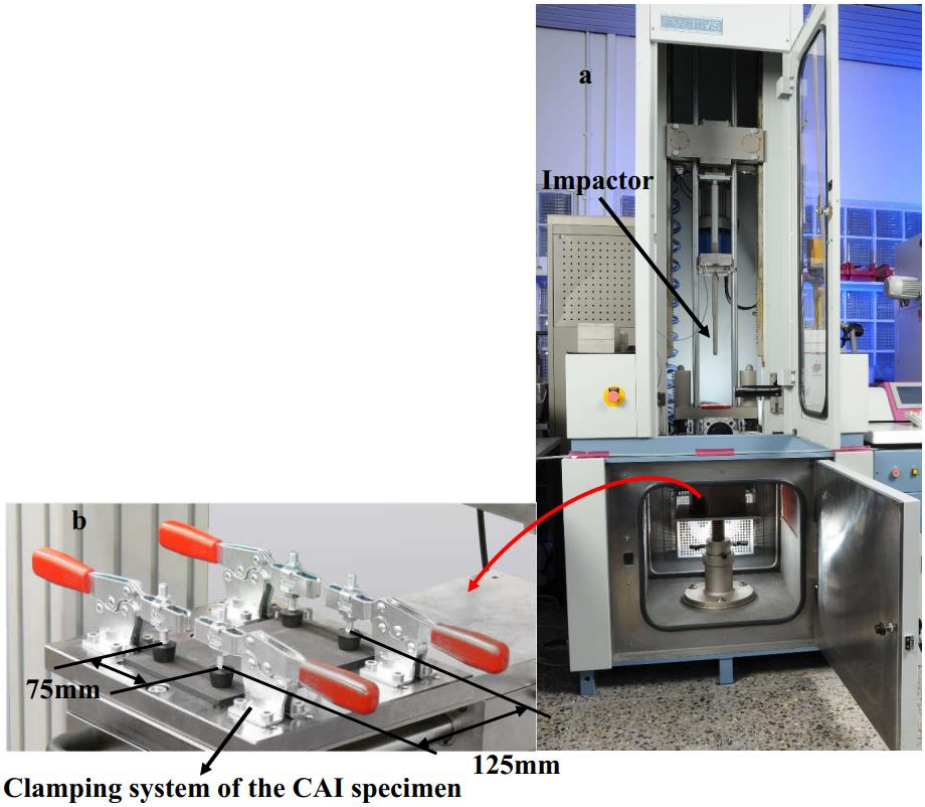

Figure 52: a = Impact tower Zwick HIT 600, b =Schematic illustration of the CAI clamping system [2]

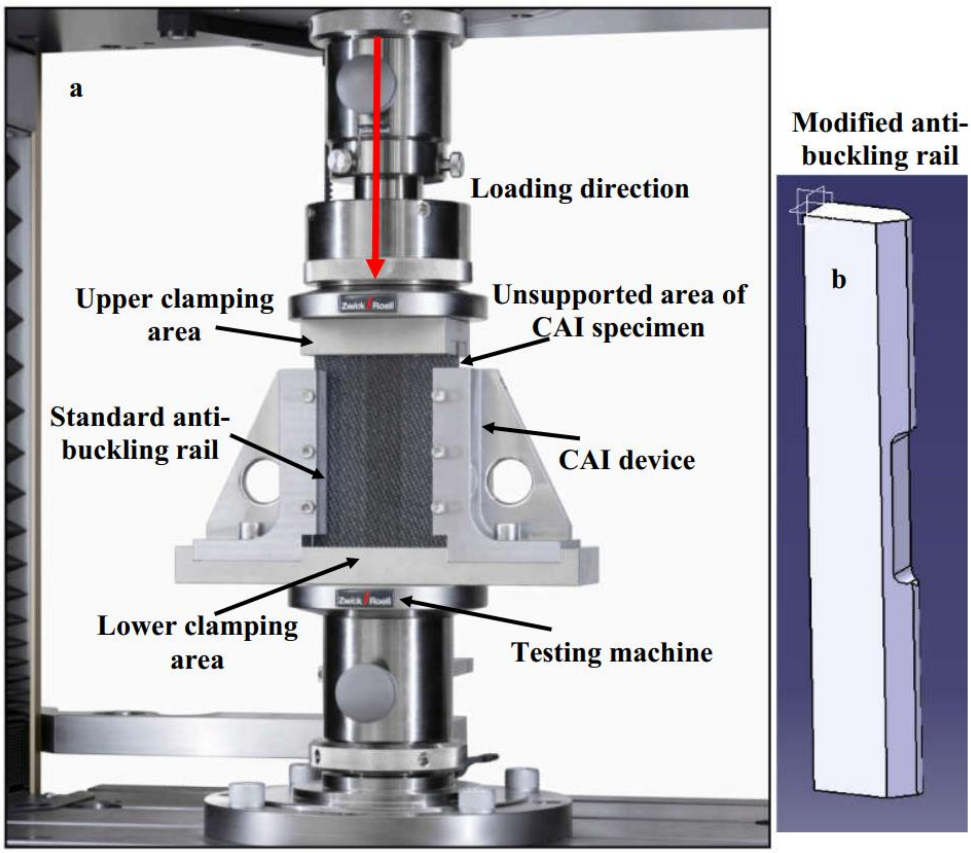

Figure 53: a = Schematic illustrations of Zwick testing machine and CAI device, b = Schematic illustration of the modified anti-buckling rail [2]

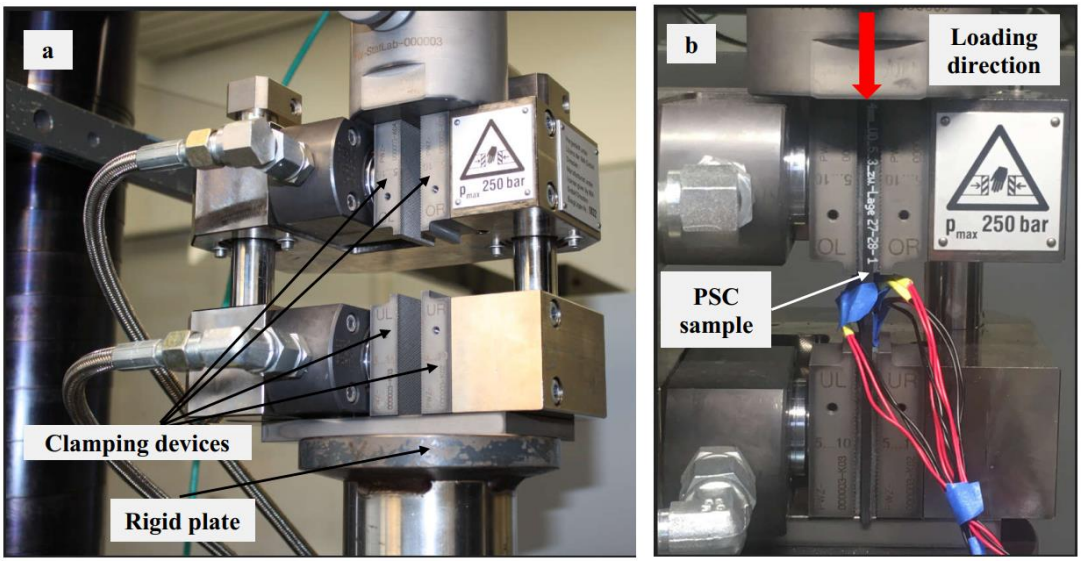

Figure 54: a = PSC Zwick testing machine without specimen; b = PSC testing machine with specimen [2]

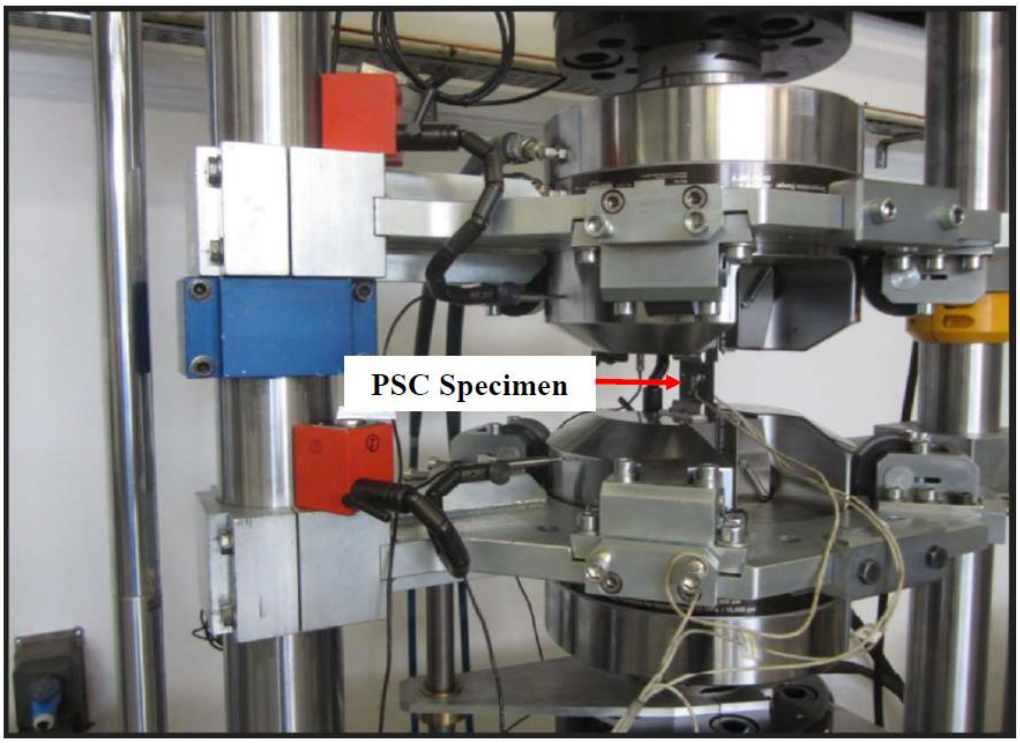

Figure 55: Instron – F16 testing machine for the 8 mm specimens

4.5 Test matrix overview

Seven CAI and eight PSC configurations were fabricated and tested. In Table 6, the CAI configurations, impact energy and the target waviness parameters are listed. Five specimens of the clean configuration were impacted with 15 J and the remaining two specimens with 25 J and 35 J. The impact took place in the middle of each specimen as shown in Figure 56. In Table 7 the PSC configurations and target parameters are depicted.

CAI configurations

Waviness classification	Θ [°]	No. specimens	Impact [J]	α [%]	α_{0° [%]
Clean	-	5	15	-	-
	-	1	25	-	-
	-	1	35	-	-
Low	5	7	15	16	13
	10	7	15	16	13
	15	7	15	16	13
Moderate	5	7	15	41	38
	10	7	15	41	38
	15	7	15	41	38

Table 6: CAI configurations [2]

PSC 4 mm and 8 mm configurations

Waviness classification	Θ [°]	No. specimens	α [%]	α_{0° [%]
Clean 4 mm	-	7	-	-
Low 4 mm	5	7	16	13
	15	7	16	13
Middle 4mm	5	7	25	25
	10	7	25	25
	15	7	25	25
Moderate 4 mm	5	7	41	38
	15	7	41	38
Clean 8 mm	-	7	-	-
Low 8 mm	5	7	13	13
	10	7	13	13
	15	7	13	13

Table 7: PSC configurations

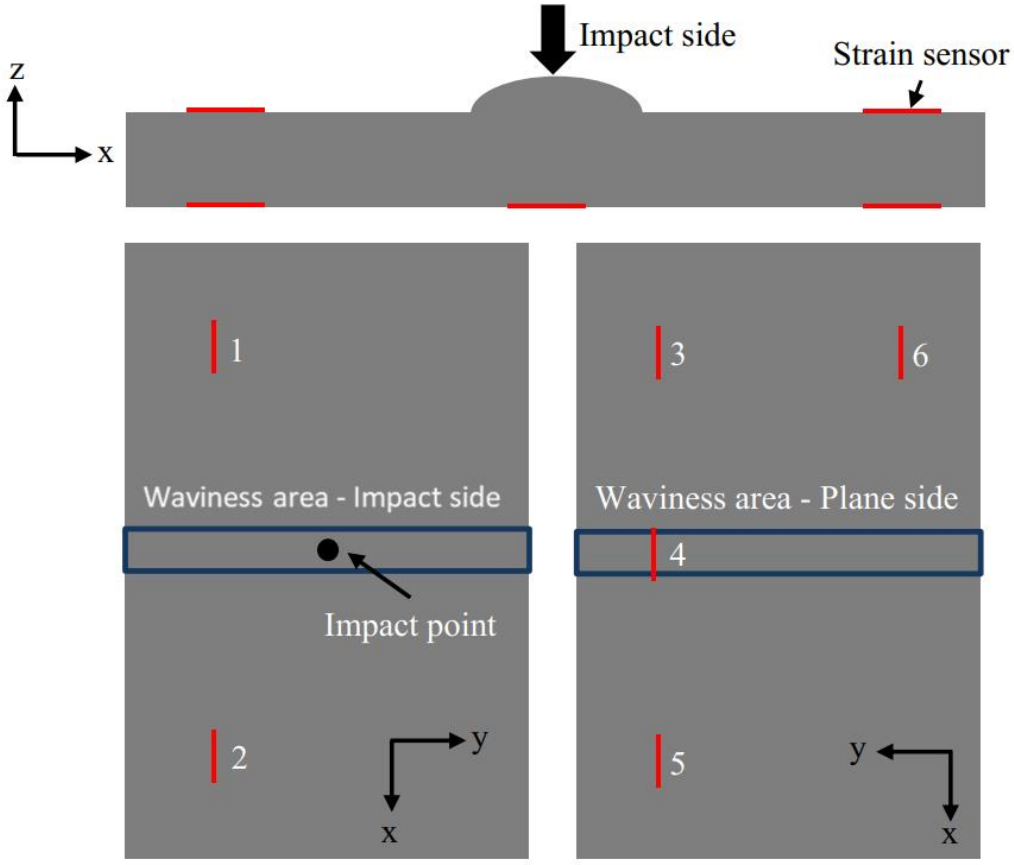

Figure 56: CAI strain gauges positions and impact side [2]

4.6 Measurement instruments

25 CAI specimens of 49 were provided with six strain gauges as shown in Figure 56. The strains of these strain gauges are used to derive the average membrane strains for each configuration (cf. Section 5.4.2) and to prove the stability behavior of the specimens. Additionally, 14 specimens were inspected with a Digital Image Correlation system (DIC system) which is a common camera-based technique for non-contact measurement of inplane and out of plane deformation. The remaining specimens were without measurement instruments. In this work, the DIC system is used to investigate the out of plane deformation, the inplane strain distribution of the specimens as well as for comparison purpose with the gained strains from the strain gauges. By doing this switch between the strain gauges and the DIC system, it was possible to get detail insights in the mechanical behavior of the tested specimens. The projected delamination areas of the impacted CAI specimens and the through the thickness distribution of the delaminations are determined by means of US-scan experimental method.

Each PSC specimen was provided with two strain gauges as shown in Figure 57. Based on [45] applied strain gauges on curved surface can lead to an error in the measured strains. The smaller the radius of curvature (r) and the greater the distance between the measuring grid of the strain gauge and the component surface (h), the stronger the effect. Therefore, the curvature radius of some specimens from different PSC configurations were measured to

estimate the error in the measured strains. In Figure 57 the curvature radius is depicted. Based on [46] the error (Δε) in the measured strain (ε) can be estimated according to the formula below:

$$\Delta\varepsilon = (h/r * \varepsilon) * 100 \quad (3)$$

This formula is valid for bended symmetrical structure. The distance h is considered to be 0.1 mm, refer to [46]. The wavy specimens are not symmetrical and are loaded in addition to the compression load by a local bending moment as it is described in Section 5.2. Nevertheless, this formula provides at least the order of magnitude of the error in the measured strains on the wavy side. In Table 8 the curvature radius and the corresponding error of some specimens are presented. It shows that the error in the measured strain is negligible.

Classification	θ [°]	r [mm]	ε_{Wavy} [με]	Δε [%]
Low	5	50	11727	0.0023
	15	23	5027	0.0022
Middle	5	32	9340	0.0030
	10	30	5856	0.0020
	15	26	3952	0.0015
Moderate	5	27	7440	0.0028
	15	23	3401	0.0015

Table 8: PSC curvature radius and errors (Δε); For all calculations h = 0.1mm is considered [2]

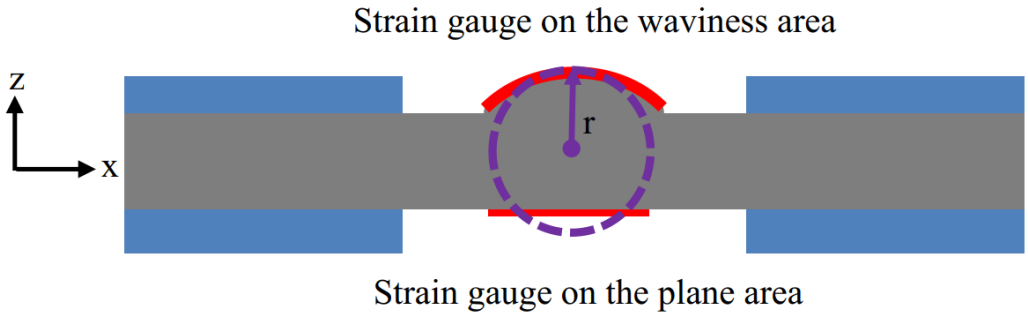

Figure 57: Strain gauges (red), curvature radius (violet) [2]

5 Experimental results and discussion

In this chapter the experimental results related to the plain strength compression, compression after impact as well as the derived KDFs are presented and discussed.

5.1 Knock Down Factors (KDFs) derivation

As described in [2], in order to evaluate the influence of pure impact, pure waviness and their combination on strength, four different KDFs are derived, refer to Table 9. $KDF_{Wav,\ PSC}$ describes the pure waviness effect on the compression strength derived from PSC test (refer to Section 5.2). The other KDFs are related to the effect of impact, waviness, and their interaction effect on compression strength derived from the CAI test (refer to Section 5.4).

KDF	Formula	Remark
Pure waviness effect (PSC) (refer to Section 5.2)	$KDF_{Wav,\ PSC} = FL_{Wav} / FL_{Clean,\ PSC}$	• FL_{Wav} is the average failure load of the wavy PSC specimens • $FL_{Clean,\ PSC}$ is the average failure load without waviness.
Pure impact effect (CAI) (refer to Section 5.4.2)	$KDF_{Imp,\ CAI} = FL_{Imp}/FL_{No\ Defect}$	• FL_{Imp} is the average failure load of the impacted specimens without waviness. • $FL_{No\ Defect}$ is the average failure load derived from the PSC clean configuration ($FL_{Clean,\ PSC}$) and is considered as the failure load at 0J (refer to Equation 4).
Pure waviness effect (CAI) (refer to Section 5.4.2)	$KDF_{Wav,\ CAI} = FL_{Imp,Wav}/FL_{Imp}$	• $FL_{Imp,\ Wav}$ is the average failure load of the impacted wavy specimens.
Interaction effect (CAI) (refer to Section 5.4.2)	$KDF_{Interaction,\ CAI} = FL_{Imp,Wav} / FL_{No\ Defect}$	• $FL_{Imp,\ Wav}$ is the average failure load of the impacted wavy specimens.

Table 9: Four types of KDFs derived from PSC and CAI tests [2]

It is challenging to experimentally determine failure load at small impact levels ($FL_{No\ Defect}$). Experimental works [27], [30] and [47] showed that the failure load determination of a CAI specimen without impact and even at small impact energy like 1.6 J leads to an invalid failure mode in the unsupported area of the CAI specimen between the upper clamping area and the anti-buckling rails as shown in Figure 58. In Figure 53 the unsupported area of the CAI specimen is depicted. A failure mode is declared as valid when it occurs in the center of the CAI specimens. Starting with the well-known problem of invalid failure mode, Sanchez [48]

developed three different CAI devices as shown in Figure 59 (a - c). CAI device (a) is similar to those of the aeronautical groups SACMA, NASA, Boeing or Airbus. CAI device (b) is provided with anti-buckling plate with window instead of the anti-buckling rails. The anti-buckling plates of the CAI device (c) were modified by splitting them into two parts, an upper and a lower plate as shown in the 3D view, too. Using the CAI devices (a – b) lead to similar invalid failure modes as shown in Figure 58 and as reported in [27], [30] and [47]. In contrast, the CAI device (c) leads to a valid failure mode in the center of the specimen. Therefore, it was decided to renounce the testing without impact and use $FL_{No\ Defect}$ as equivalent failure load at 0 J derived from PSC measurements to quantify the pure impact and interaction effect on the compression strength:

$$FL_{No\ Defect} = FL_{Clean,\ PSC} * Width_{CAI} / Width_{PSC} \quad (4)$$

The distinction in the derived KDFs helps to identify the critical parameters for each load case separately and in interaction. The different KDFs are important means to have a better understanding of the interaction behavior and to answer the following questions:

1. What is the effect of the waviness parameters (Θ, $\alpha_{0°}$, α) within the two load cases?
2. What is mainly driving the strength reduction Θ, $\alpha_{0°}$, α or even Θ in dependence on ratios $\alpha_{0°}$ and α?
3. What is the effect of the waviness in particular Θ on the delamination shape, size and distribution as a function of ratios $\alpha_{0°}$ and α?

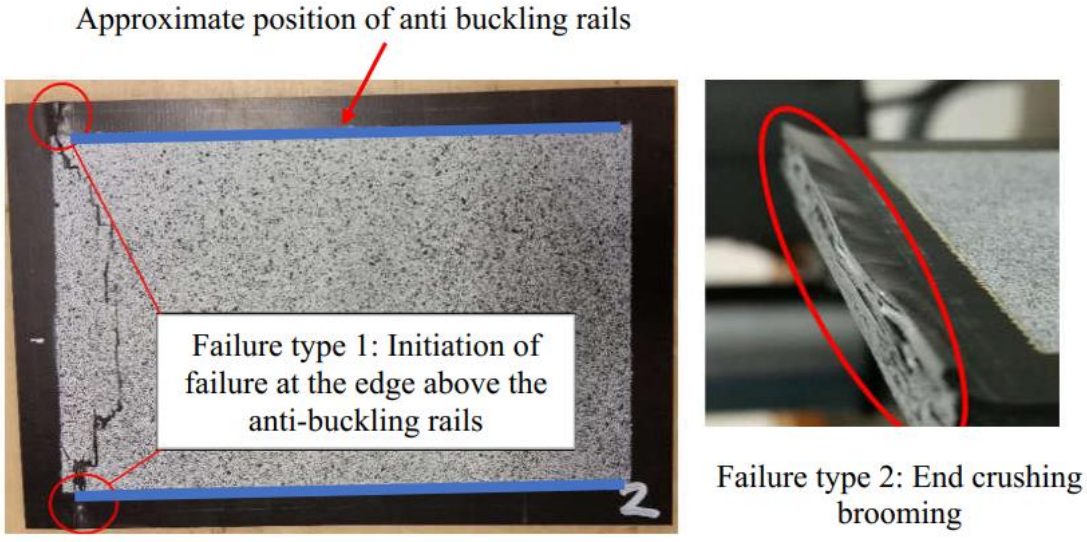

Figure 58: Invalid CAI failure modes in the unsupported area of non-impacted CAI specimen [2]

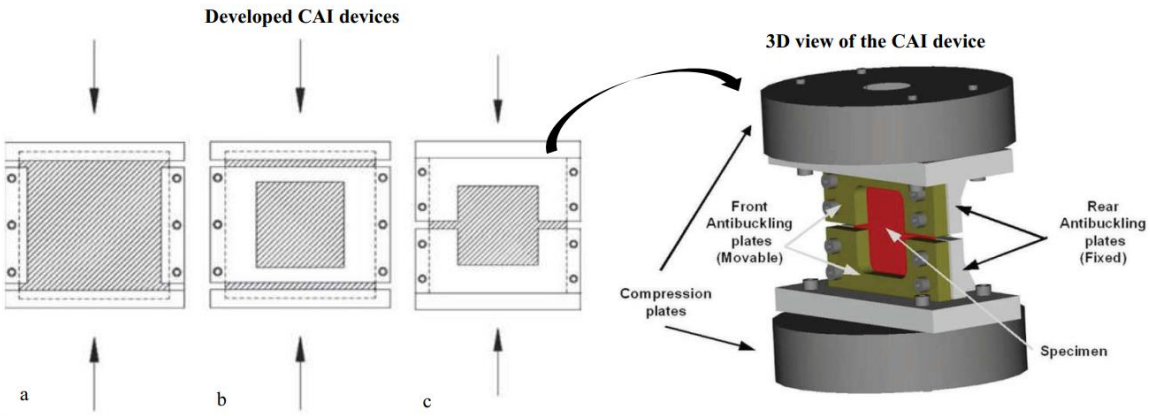

Figure 59: Developed CAI devices by Sanchez [48]

5.2 PSC experimental results

5.2.1 PSC results with 4 mm thickness

The load displacement curves of selected representative specimens of each configuration are depicted in Figure 60. From these results, it is evident, that the failure for all configurations was sudden and catastrophic. In the following, the compression sign "-" of failure loads and strains is omitted.

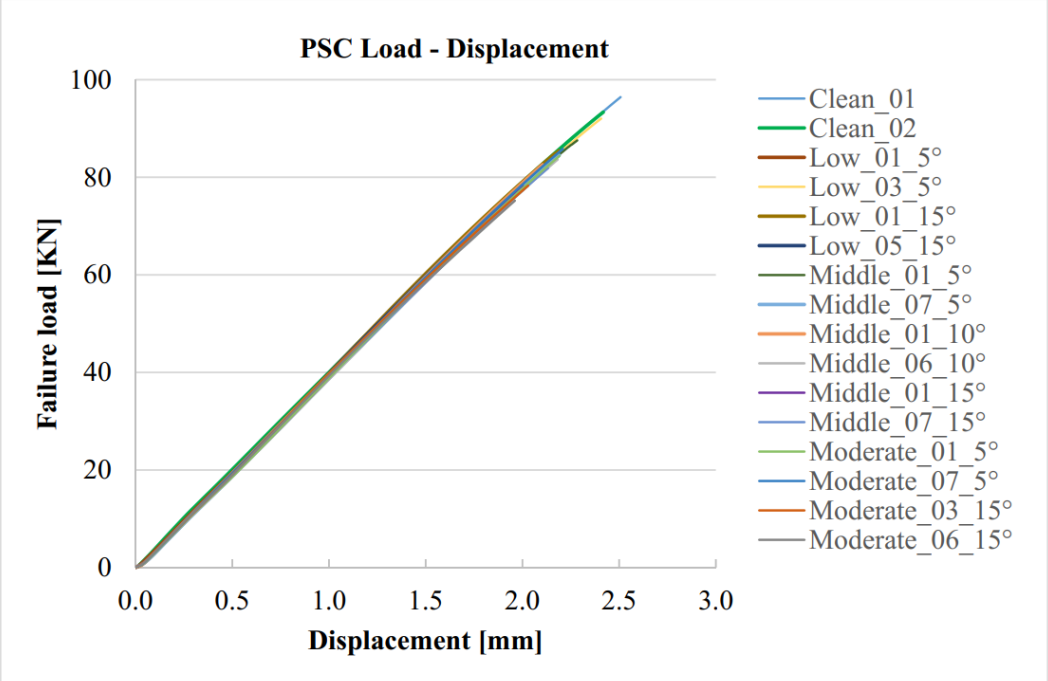

Figure 60: PSC load displacement curves of selected representative specimens of each configuration [2]

The average failure loads (FL) of each configuration with the corresponding deviations in the failure loads and waviness angles (Θ) as well as the KDFs, which are calculated according to Table 9 are summarized in Figure 61. The difference between both figures (a) and (b) is only in the visualization. Figure 61 (a) shows the absolute values and (b) shows the KDFs, which

are normalized by the average failure load of the clean configuration. The KDFs visualization represents a common practice in the industry. It is found that the failure load of each configuration scatters by maximum 3 % despite the large waviness angles deviation reported in Section 4.3. However, within the individual configurations, the failure load decreases, when Θ, the number of affected 0°-plies ratio ($\alpha_{0°}$) and total number of affected plies ratio (α) increase. Further, for the low and middle configurations the failure loads are in same range. Whereas the failure load reduction in the moderate configurations is clearly more distinctive. It is reduced by 12 % at 5° and 20 % at 15°.

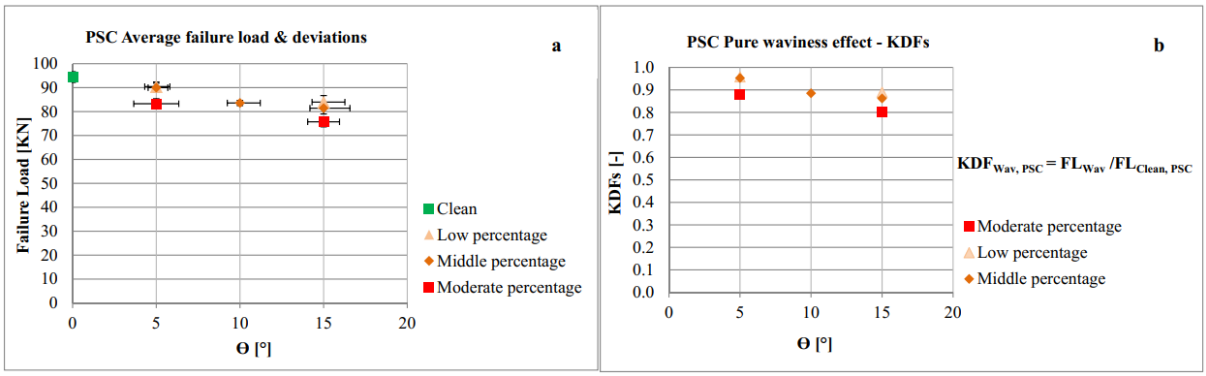

Figure 61: a = PSC failure loads; b = Waviness effect KDFs (b) of 4 mm configurations [2]

In the following the average membrane strains, the membrane strains at flat and wavy sides, as well as the derived bending strains for each configuration are introduced. The interest behind their presentations is to investigate the morphology effect on the mechanical behavior with regards to the strain distribution and deformation behavior of the wavy configurations in comparison to the clean one. The effect of the waviness morphology is discussed in Section 5.3. The formulas used for their calculations are based on [45]. ε_{Flat} and ε_{Wavy} are the measured strains at the locations shown in Figure 57.

For symmetrical cross section, the average membrane ($\varepsilon_{Membrane}$) and average bending ($\varepsilon_{Bending}$) strains of the clean configuration are calculated by means of the measured strains ($\varepsilon_{Flat,1}$; $\varepsilon_{Flat,2}$):

$$\varepsilon_{Membrane,sym} = 1/2\,(\varepsilon_{Flat,1}+\varepsilon_{Flat,2}) \quad (5)$$

$$\varepsilon_{Bending,sym} = \pm 1/2\,(\varepsilon_{Flat,1}-\varepsilon_{Flat,2}) \quad (6)$$

The average membrane and average bending strains of the wavy configurations are calculated according to the formulas below considering asymmetrical cross section:

$$\varepsilon_{Membrane,asym} = \varepsilon_{Flat} + c^{*}\,(\varepsilon_{Wavy} - \varepsilon_{Flat})/t^{*} \quad (7)$$

c = Cross section centroid highlighted in Figure 66
t* = the increased thickness due to the waviness

Bending strain on the flat side:

$$\varepsilon_{Bending,flat} = \varepsilon_{Flat} - \varepsilon_{Membrane,asym} \quad (8)$$

Bending strain on the wavy side:

$$\varepsilon_{Bending,wavy} = \varepsilon_{Wavy} - \varepsilon_{Membrane,asym} \quad (9)$$

The respective average failure membrane strains for each configuration are depicted in Figure 62 to Figure 64. It is found that the deviation in the failure membrane strains of each configuration goes up to a maximum of 5 %. Within the individual configurations, the tendency of the average failure membrane strains is comparable to the observed tendency for the failure loads. Nevertheless, the membrane strains are very close to each other. Further, the failure strain level on the wavy side is smaller than the strain level on the flat side. It is decreased with increased Θ and ratio α_{0° as is shown in Figure 64. The discrepancy between the strain level on the flat and wavy side indicates, that there is a local bending moment in addition to the compression loading. The corresponding bending strains for each configuration are depicted in Figure 65. These are increased, when Θ and ratio α_{0° are increased. The moderate configurations show the major increase in the bending strain. Based on the strain distribution the bending moment sense of rotation is derived as shown in Figure 66. This indicates, that the wavy side is under tensile preload and the flat side under compression preload.

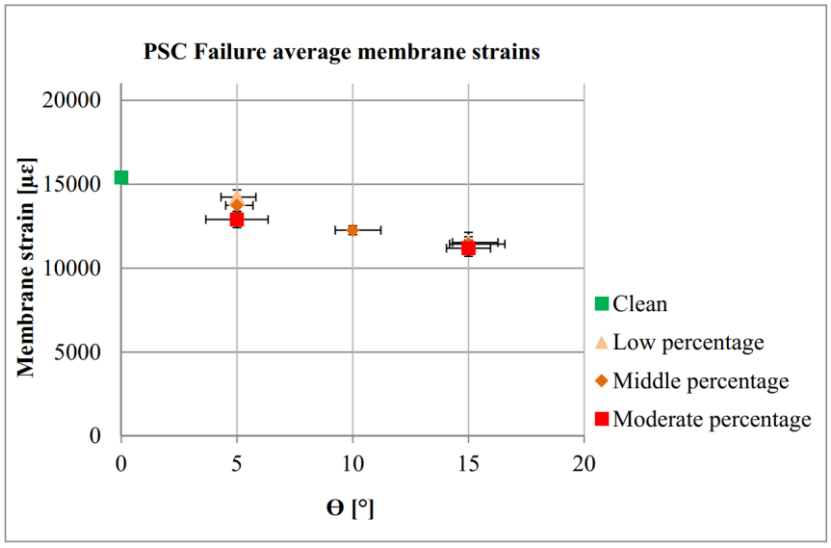

Figure 62: PSC failure membrane strains of 4 mm configurations [2]

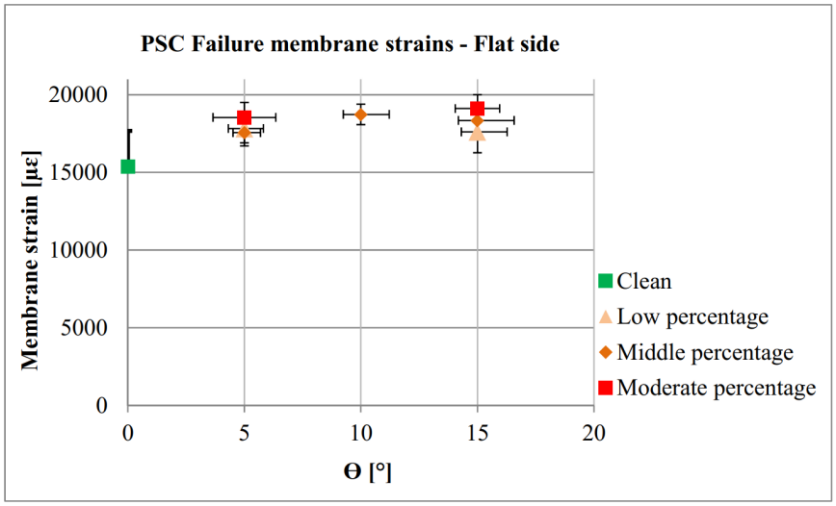

Figure 63: PSC failure membrane strains of 4 mm configurations - Flat side [2]

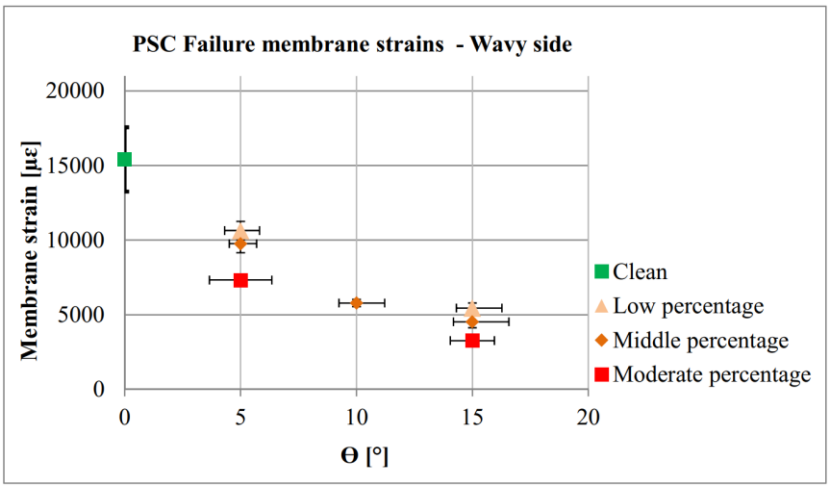

Figure 64: PSC failure membrane strains of 4 mm configurations - Wavy side [2]

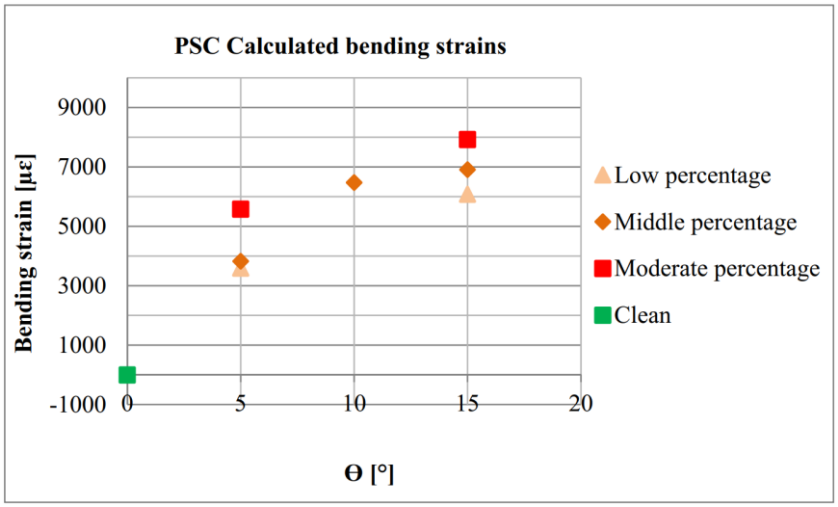

Figure 65: PSC bending strains of 4 mm configurations [2]

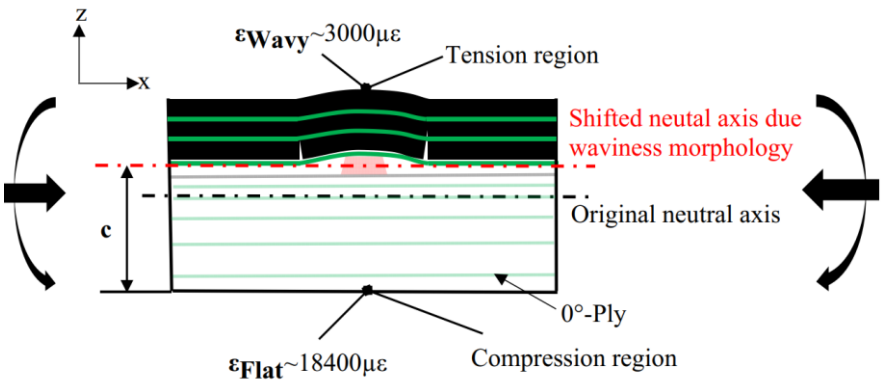

Figure 66:Bending moment sense of rotation [2]

5.2.2 PSC results with 8 mm thickness

The load displacement curves of selected representative specimens of the low waviness configurations are depicted in Figure 67. Like the 4 mm configurations, the failure for all configurations was sudden and catastrophic.

It is found that the failure load of each configuration scatters by maximum 3 % despite the shown waviness angles deviation in Figure 50. Within the individual configurations, the failure load decreases, when Θ is increased as shown in Figure 68. The strength reduction of the low configuration with 5° is almost marginal. The low configuration with 15° shows a maximum strength reduction of 5 %. Thus, it can be stated, that the strength reduction due to the waviness in the investigated configurations is negligible.

The respective average failure membrane strains and the failure membrane strains on the flat and wavy sides as well as the average bending strain for each configuration are depicted in Figure 69 (a - d). These strains are derived according to the formulas described in Section 5.2.1. It is found that the deviation in the failure membrane strains of each configuration goes up to a maximum of 8 %, except for the strain at the flat side of the low configuration with 15°, which goes up to 12 %. The observations related to the 4 mm specimens described in Section 5.2.1 are observed in case of the 8 mm specimens, too. These are the effect of the waviness morphology on the strain distribution as well as the dependency between the waviness angle and bending strain.

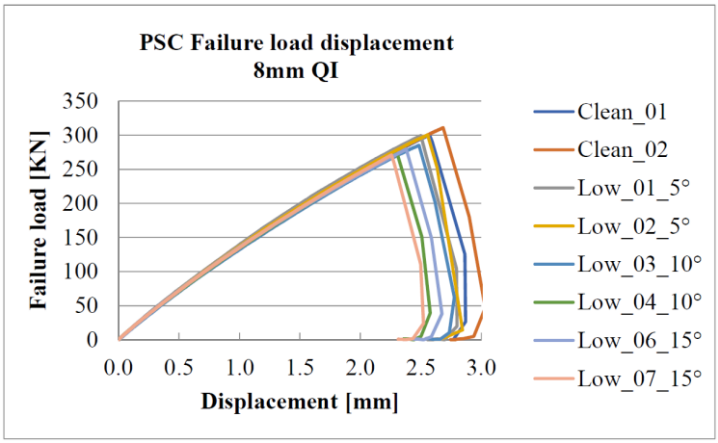

Figure 67: Load displacement curves of selected representative specimens of each configuration – 8 mm

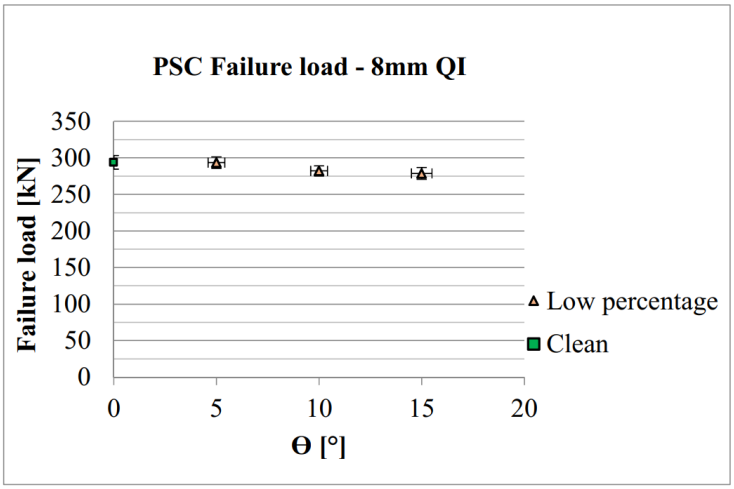

Figure 68: PSC Clean and low configurations failure loads – 8 mm

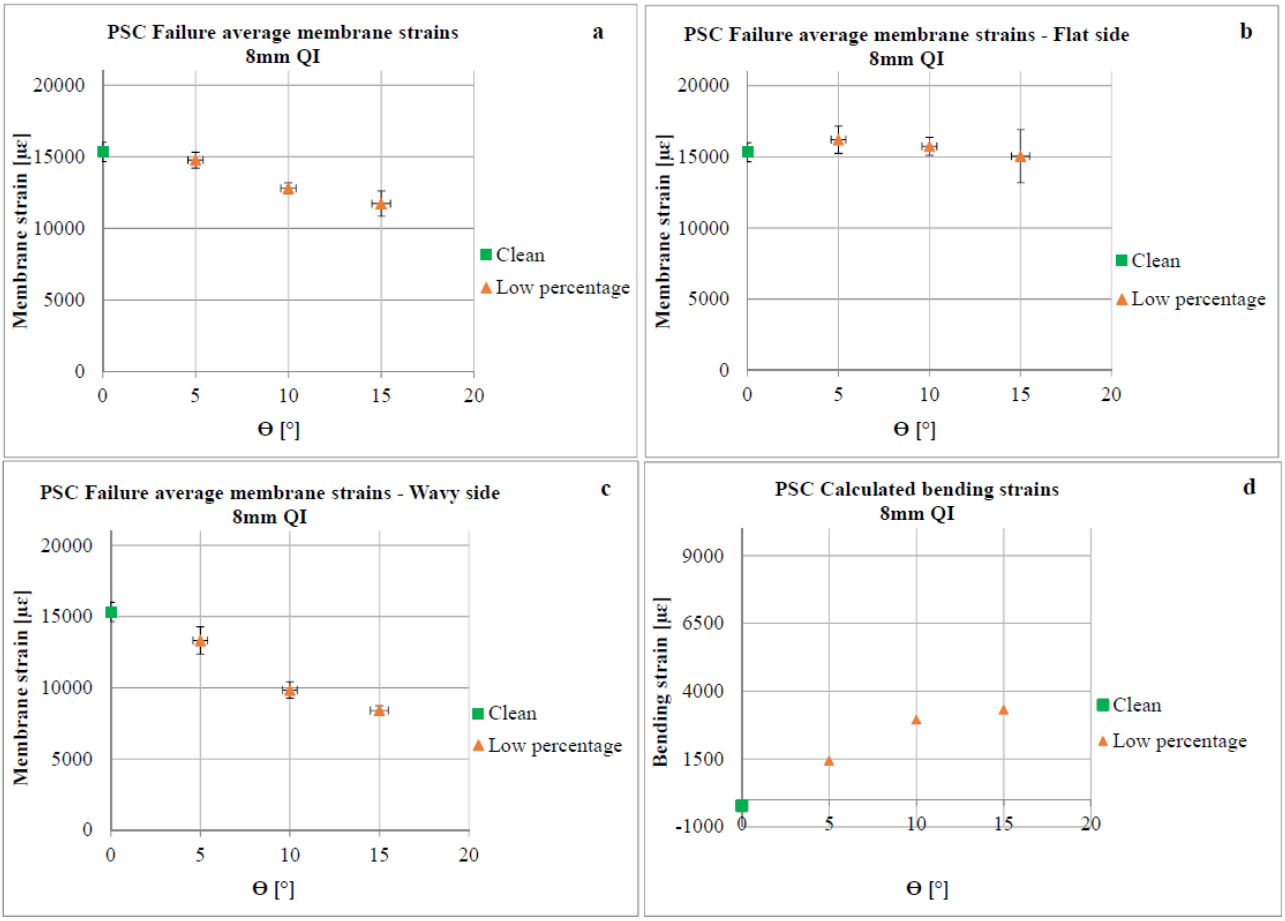

Figure 69: a = PSC Average failure membrane strains; b = Average failure membrane strains on flat side; c = Average failure membrane strains on wavy side; d = Average bending strains – 8 mm

5.3 PSC discussion

The test results confirm the general trend [5], [6], [10] and [21], that the compression strength decreases when Θ and α increase. Assuming an error free waviness angle measurement determination, it is concluded, that the large scatter in Θ and the low scatter in the failure loads indicate that Θ alone is not the main driver for the reduction. Based on the load reduction in the moderate waviness configurations, especially at 5° in comparison to the low and middle configurations, it is concluded, that this reduction is mainly attributed to the increased number of affected 0°-plies ratio ($\alpha_{0°}$). The total number of affected plies ratio (α) is not the driving cause for the reduction, since α ratio in the middle configurations (α = 25 %) is higher than the low configurations (α = 16 %). Nevertheless, both configurations provide similar failure loads as shown in Figure 61. There is a range in which the number of affected 0°-plies is increased, but the decrease in strength remains unchanged, as experimentally demonstrated by Duangmuan [9]. This would be clarifying, why the failure loads of the low and middle configurations are in same range as described in the following.

The dependency of the strength reduction from $\alpha_{0°}$ ratio was observed by Duangmuan [9] and other authors mentioned before, too. He investigated this effect in cross ply laminates with

different thicknesses and different waviness formations by holding the waviness angle constant. Two examples of the investigated waviness formations are schematically illustrated in Figure 70. The upper one is with one affected 0°-ply and two affected 90°-plies. In this case, the total number of affected plies is three (0°-ply + 2 times 90°-plies). The lower one is with three affected 0°-plies and four affected 90°-plies. The total number of affected plies is seven. It was found that the compression strength reduction is mainly related to the increased ratio α_{0°, the waviness in 90°-plies is negligible. In addition, there is a certain range, in which ratio α_{0° is increased, but the reduction in the strength is almost the same as shown in Table 10. Further, it was found, that the interlaminar normal and shear stresses are increased with increased number of wavy 0°-plies as shown in Figure 71. Within each configuration the interlaminar shear stress is increased with increased ratio α_{0°. In contrast, the normal interlaminar stresses are almost in the same order of magnitude up to a certain ratio α_{0°, and then decrease with increasing ratio α_{0°.

The chosen configurations by Duangmuan [9], which are based on cross ply laminates, can significantly distinguish the role of ratios α_{0° and α, since the 90°-plies under such loading conditions are generally not involved of carrying the load. That is why he introduced only the ratio α_{0° as significant influencing factor. The current investigated laminate configurations are more complex. Nevertheless, the 90°-plies are not involved of carrying the load, too. It is understandable, that the ±45°-plies can be involved of carrying the load on a small percentage basis. Nevertheless, the 0°-plies remain the main actors for resisting and carrying the applied load. However, for better and more precise understanding of the role of ratios α_{0° and α, further experimental investigations would be needed. A possible experimental investigation, based on the current morphology and layup, would be to position the insert between the second and third ply, so that only the first ±45°-plies are affected by waviness. By doing this, the role of an affected 45°-ply on the strength reduction could be better understood. Further experimental investigations with further increased α_{0° would be recommendable.

In summary, despite different layups, the current investigation shows comparable trends to those obtained by Duangmuan [9]. Thus, it is reasonable to assume, that the findings regarding the interlaminar stresses can be transferred to the current investigation.

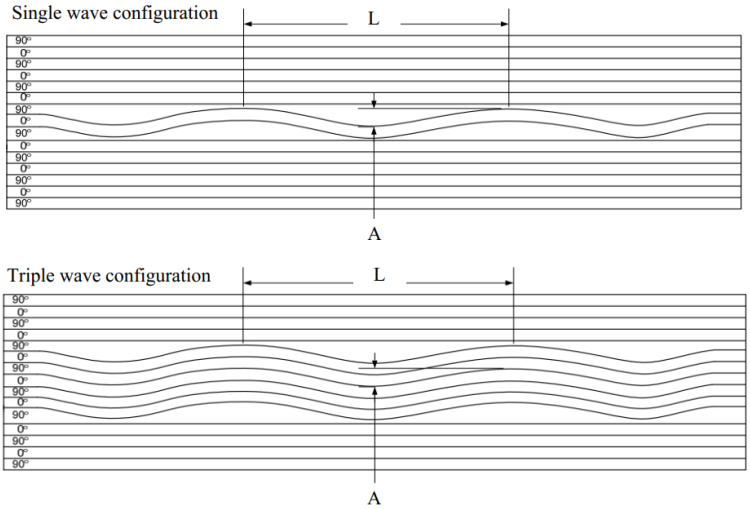

Figure 70: Single and triple waviness formation in a cross ply laminate [9]

t [mm]	Total no. of 0° plies	No. of wavy 0° plies	Total no. of 90° plies	α_{0° [%]	Θ [°]	KDF [-]
2.79	5	1	6	20	13	0.82
2.79	5	3	6	60	13	0.61
3.81	7	1	8	14	13	0.88
3.81	7	3	8	43	13	0.64
3.81	7	5	8	71	13	0.61

Table 10: Investigated single and triple waviness configuration with different ratios α_{0° [9]

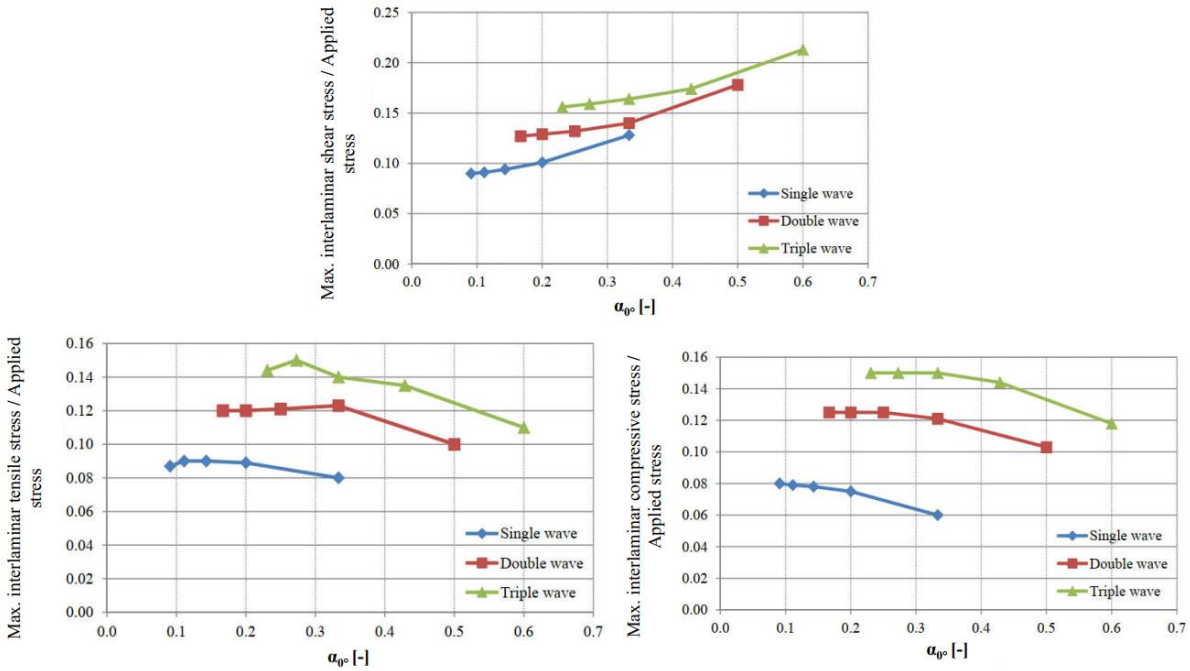

Figure 71: Induced interlaminar normal and shear stresses due to waviness divided by the applied stress for different waviness formations [9]

Morphology effect on strength reduction

The waviness morphology affects the neutral axis position, as is shown in Figure 66. The displacement of the neutral axis causes a local bending moment which is superimposed with the axial global loading as described in Section 2.7. The induced bending moment greatly influences the strain distribution as is shown in Figure 63 to Figure 64. The bending strains are increased, when Θ and α_{0° are increased. The moderate configurations show the major increase in the bending strain. This clarifies, why the reduction in the failure loads is higher than the low and middle configurations. The increase in the bending strain is an indication for the neutral axis displacement. Thus, the waviness morphology is a key parameter for affecting the deformation behavior. The change in the deformation behavior affects the loading state, the strains distribution and thus the failure mode as experimentally demonstrated by Thor [13].

In summary, it is not only the magnitude of the waviness angle Θ, which is relevant for the reduction. It is the interplay between waviness morphology, waviness angle (Θ) and number

of affected 0°-plies ($\alpha_{0°}$), which ultimately lead to a significant reduction in the compressive strength.

Thickness effect on the strength reduction

To investigate the interplay between the thickness, waviness angle and number of affected 0°-plies on strength reduction, 8 mm thick specimens with and without waviness were fabricated. To ensure comparability, the stacking sequence of the 4 mm specimens was redoubled as described in Section 4.2. The inserts in the different 8 mm low waviness configurations (5°, 10° and 15°) were at comparable position in the laminate through the thickness as the wavy 4 mm low configurations, so that a 13 % number of affected plies ratio was achieved as shown in Table 7.

A comparison between the pure waviness KDFs of the 4 mm and 8 mm low waviness configurations is illustrated in Figure 72. The evaluation of these results indicate that the thickness increase has a beneficial effect on the KDFs. The largest detected reduction in the 8 mm low configuration with 15° goes up to a maximum of 5 %. In contrast, the reduction in the 4 mm low waviness configuration with 15° geos up to 11 %, which represents a significant reduction in comparison to the reduction in 8 mm configuration. It is assumed that the improvement in the KDFs is not only due to the thickness but also to the increased number of 0° plies. This assumption is reasonable, because the remaining healthy 0°-plies compensate the loss in load bearing capacity due to the waviness.

Further, although the KDFs are decreased with increased waviness angle, nevertheless, these are very close to each other, especially in case of the low waviness configurations with 10° and 15° (10° → 0.96 and 15° → 0.95). These results lead to the conclusion that it is not only the waviness angle that is decisive for the reduction, but also the thickness in addition to influencing factors identified in case of the 4 mm configurations.

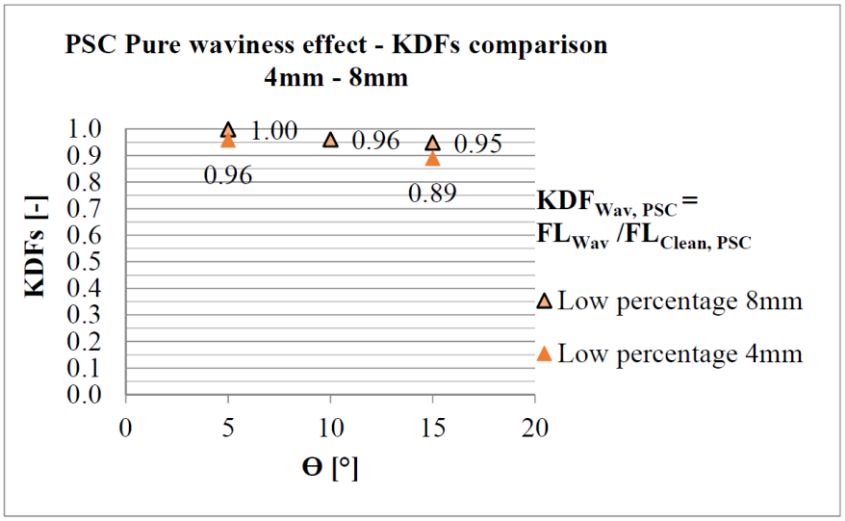

Figure 72: Pure waviness KDFs comparison between 4 mm and 8 mm low waviness configurations

5.4 Impact and CAI experimental results

5.4.1 Impact test results

Selection of an appropriate impact energy

To enable the investigation of the waviness effect on the damage tolerance behavior, three samples of the clean configuration were impacted with different impact energies to choose the appropriate one; 15 J, 25 J and 35 J. The delamination shape, size of the projected delamination area and the through thickness delamination distribution of these samples are shown in Figure 73 (Top view). The corresponding distribution in length and width direction are shown in Figure 74 (Cross section views). The largest delamination areas caused by 15 J are detected in the depth of 2.9 - 3.5 mm, measured from the impact side. The largest delamination areas caused by 25 J and 35 J are detected in the depth 2.5 - 3 mm. The through thickness delamination distribution provides the typical pine tree formation in length and width specimen direction, which is highlighted by the dashed lines as shown in Figure 74. There is delamination in almost each interface. The delamination shape of the impacted sample with 15 J is circular and spreads symmetrically with regards to the specimen geometry. The delamination shape of the impacted sample with 25 J is no more circular and has an asymmetrical spread. The third sample additionally showed a complete penetration of the material and the bottom 45°-ply was partly detached. Based on the damage morphology caused by 25 J and 35 J in comparison to the 15 J, it was decided to use 15 J as an impact energy for the clean and wavy configurations. The damage morphology indicates that 25 J and 35 J are very high for the investigated thickness.

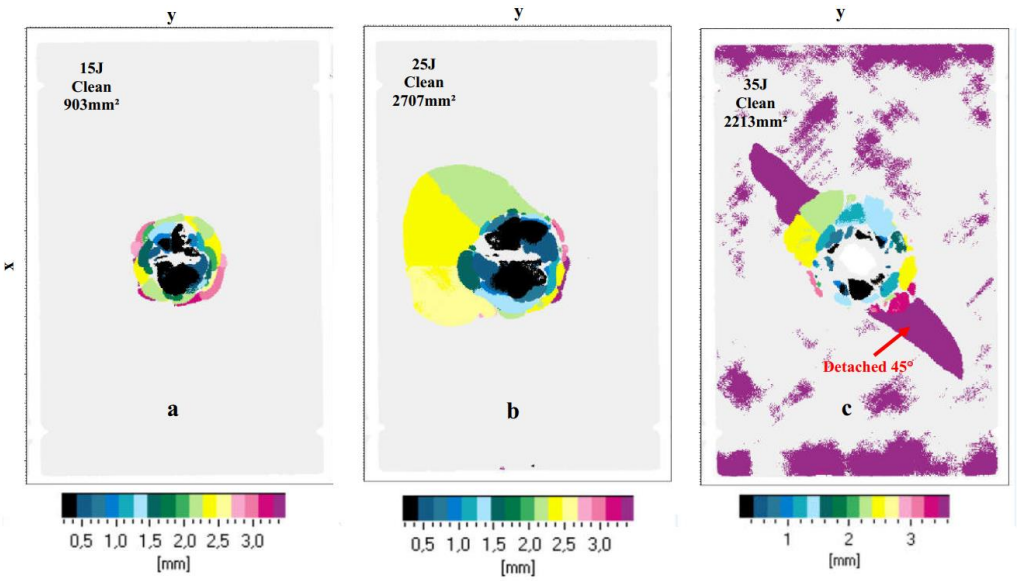

Figure 73: Top view of the delamination distribution & shape - clean (a = 15 J, b = 25 J, c = 35 J) [2]

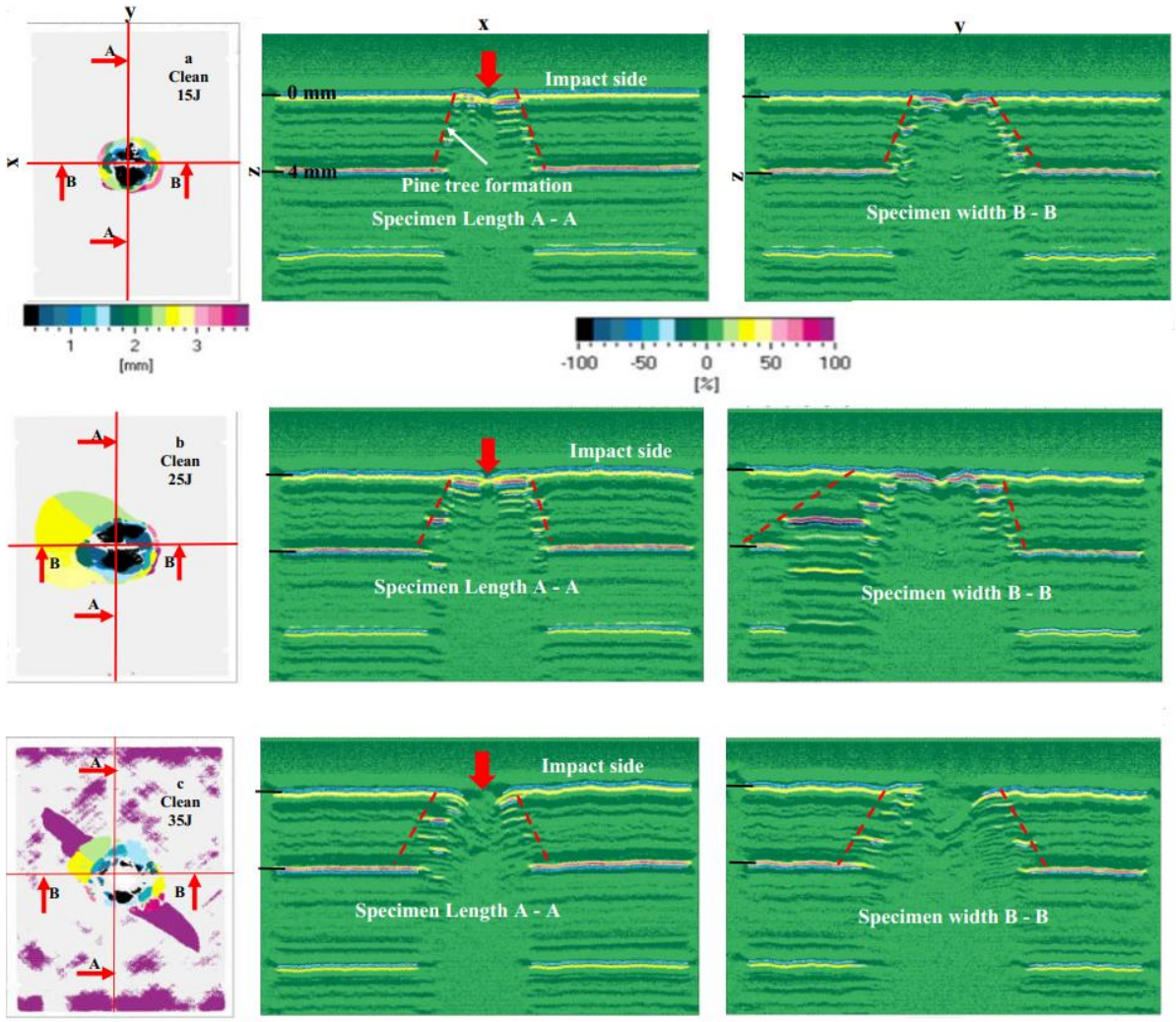

Figure 74: Top and cross section views of the delamination distribution within the laminate thickness - Clean (a = 15 J, b = 25 J, c = 35 J) [2]

Damage characteristics

The dent depth of all tested configurations was directly measured after the impact process as shown in Figure 75. Unfortunately, the dent depth measurement in case of the wavy configurations, was not considered reliable enough, due to the curvature of the waviness. The comparison with clean configuration is not expedient. So, it was decided to neglect the dent depth completely in the evaluation. Nevertheless, the average dent depth of all configurations tested with 15 J as well as the two specimens tested with 25 J, 35 J, respectively, are depicted in Figure 76. Regarding the damage status of the surfaces after impact, most of the specimens had barely visible dent in the impact location. On the non-impacted side, no damage was observed. Except for the specimen impacted with 35 J, as described before. Its damage is characterized as visible impact damage (VID) on both sides.

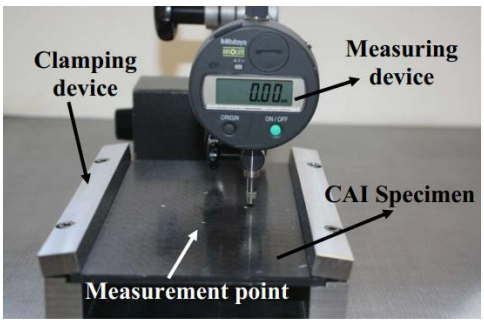

Figure 75: Device for determining the dent depth [2]

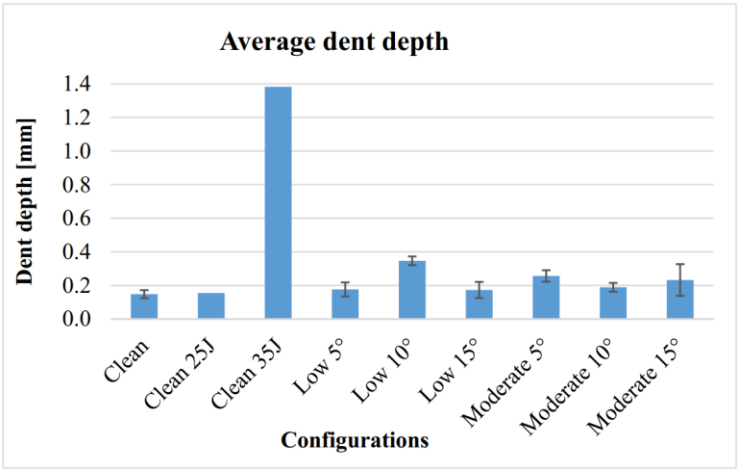

Figure 76: Dent depth of all tested configurations measured after impact directly [2]

Impact force – Time history

The Impact force – Time curves of some representative samples from the clean configuration impacted with 15 J, 25 J and 35 J are depicted in Figure 77. Additionally, the location of significant force drop is highlighted, too. It is observed that the significant force drop of the three shown samples which are impacted with different impact energies, is in the same range. Samples of the low and moderate configurations in comparison to samples of the clean configuration impacted with 15 J are illustrated in Figure 78 and Figure 79. As can be seen, the curves of the wavy and clean configurations are comparable. The first significant force drop of the clean and wavy configurations, highlighted by means of the green arrow, is almost in the same range. In contrast, the maximum impact force (black arrow) of the moderate configurations is a maximum of 12 % lower compared to clean configuration.

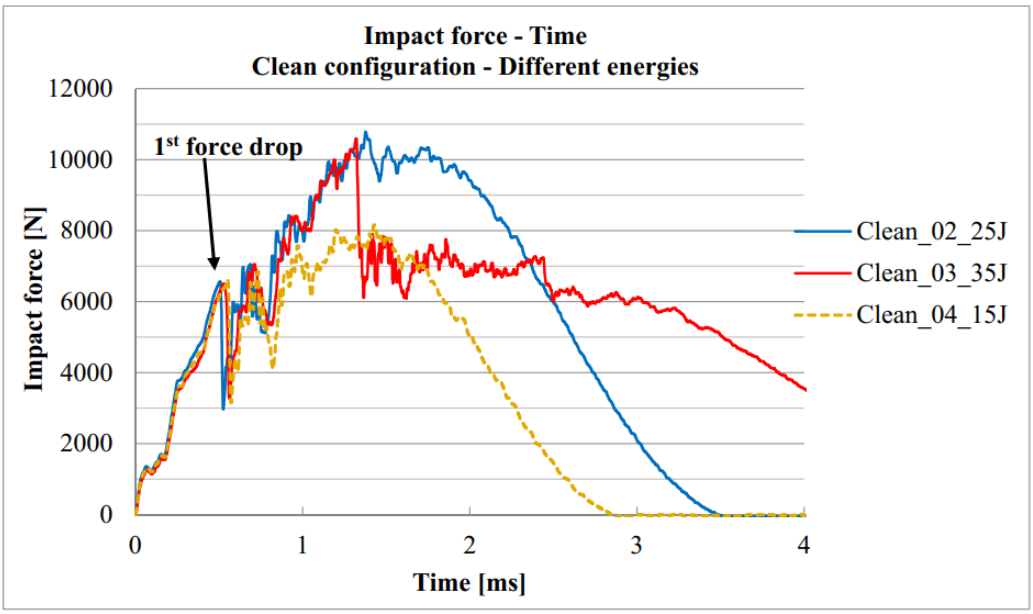

Figure 77: Impact force – Time history of some representative samples of the clean configuration impacted with different impact energies [2]

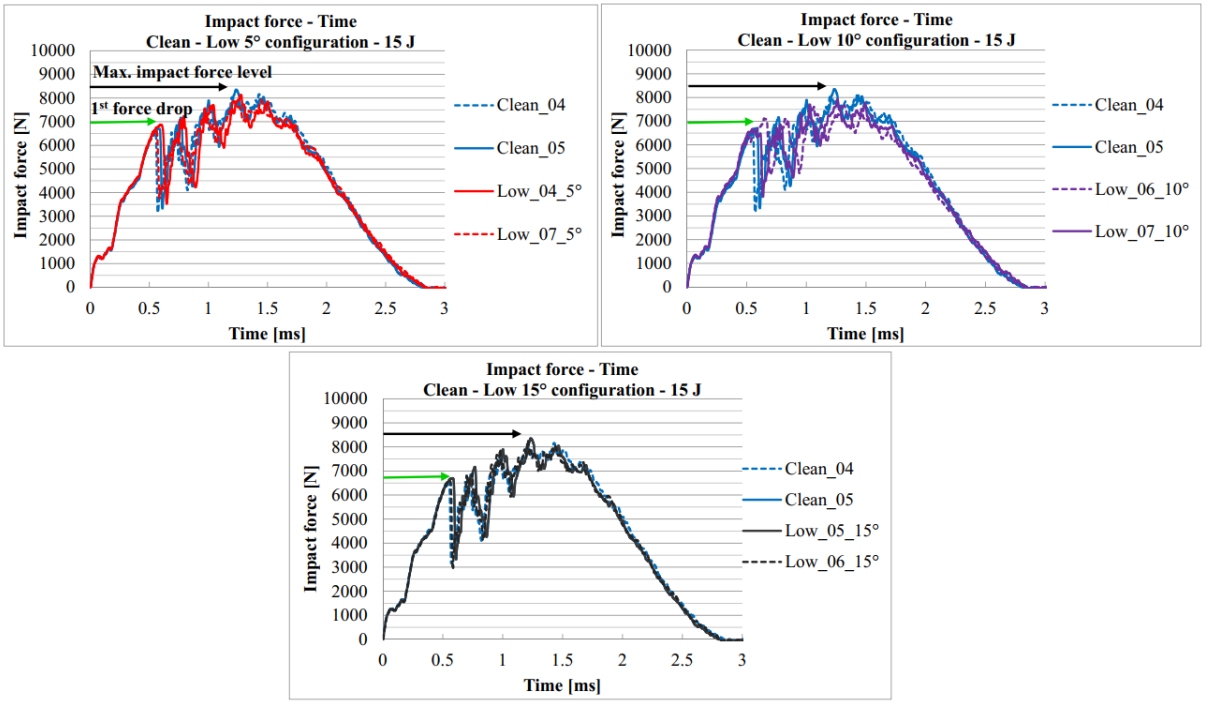

Figure 78: Impact force – Time history of selected representative samples of the clean and low configurations impacted with 15 J [2]

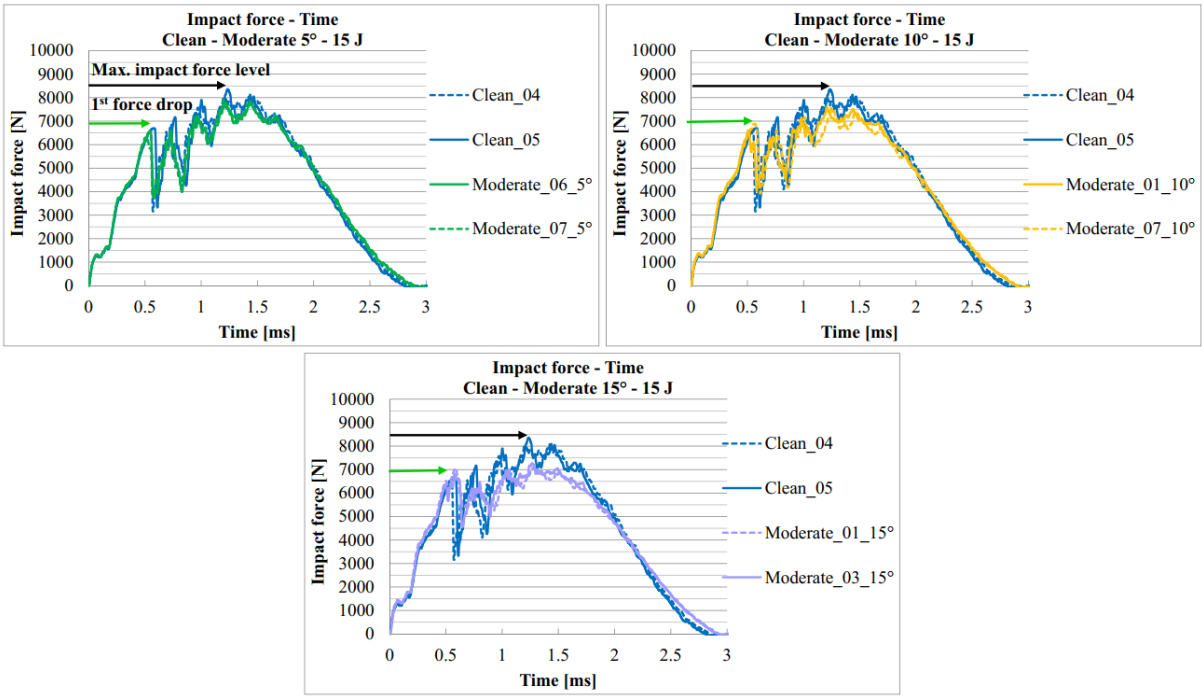

Figure 79: Impact force – Time history of selected representative samples of the clean and moderate configurations impacted with 15 J [2]

Delamination areas

The clean configuration was examined only from the impacted side. All wavy configurations were examined from both sides. The average size of the projected delamination areas of all configurations is depicted in Figure 80. It is obvious, that the average delamination size of the clean configuration is in the same range as for 5° waviness configurations. The delamination sizes of the moderate configurations with 10° and 15° are in same range but are clearly larger than the clean and low configurations. The delamination shape of the impacted and non-impacted sides of the low and moderate configurations are depicted in Figure 81 to Figure 84. To exhibit the effect of waviness angle and number of affected plies on the delamination shape and size, the data related to the clean configuration are illustrated.

The delamination shape of the low and clean configurations is circular and symmetrical with regard to the specimen edges. Nevertheless, few specimens of the low configurations show irregularities. These are related to the delamination propagation along the inserts, which are visible in the configurations at 10° and 15°. In contrast, the delamination shape of the moderate configurations with 10° and 15° is no longer circular, more irregularities and asymmetry as well as delamination propagation along the insert get more visible.

Figure 85 illustrates the through thickness delamination distribution of representative specimens from the clean, low and moderate configurations. It is observed, that there are delaminations in almost each interface. The low and moderate configurations show a modified pine tree in specimen width direction in comparison to the clean configuration, which is highlighted by the dashed lines. The pine tree formation is reconstructed by means of the through thickness delamination distribution images from impacted and non- impacted side

(Low: b_1 - b_2; Moderate c_1 – c_2). I.e. there is a significant change in the delamination distribution immediately in the waviness region.

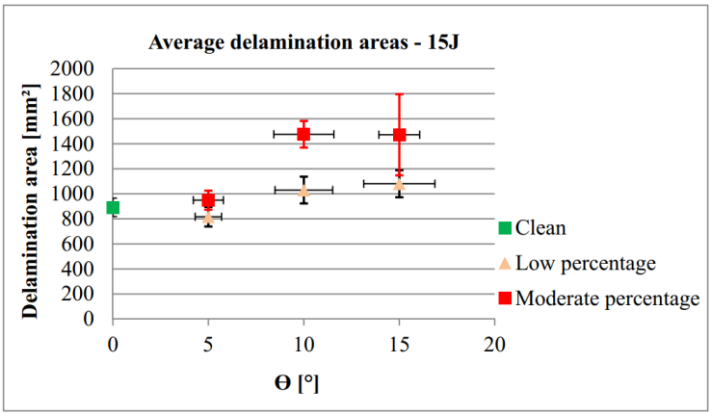

Figure 80: Size of the projected delamination areas - All configurations [2]

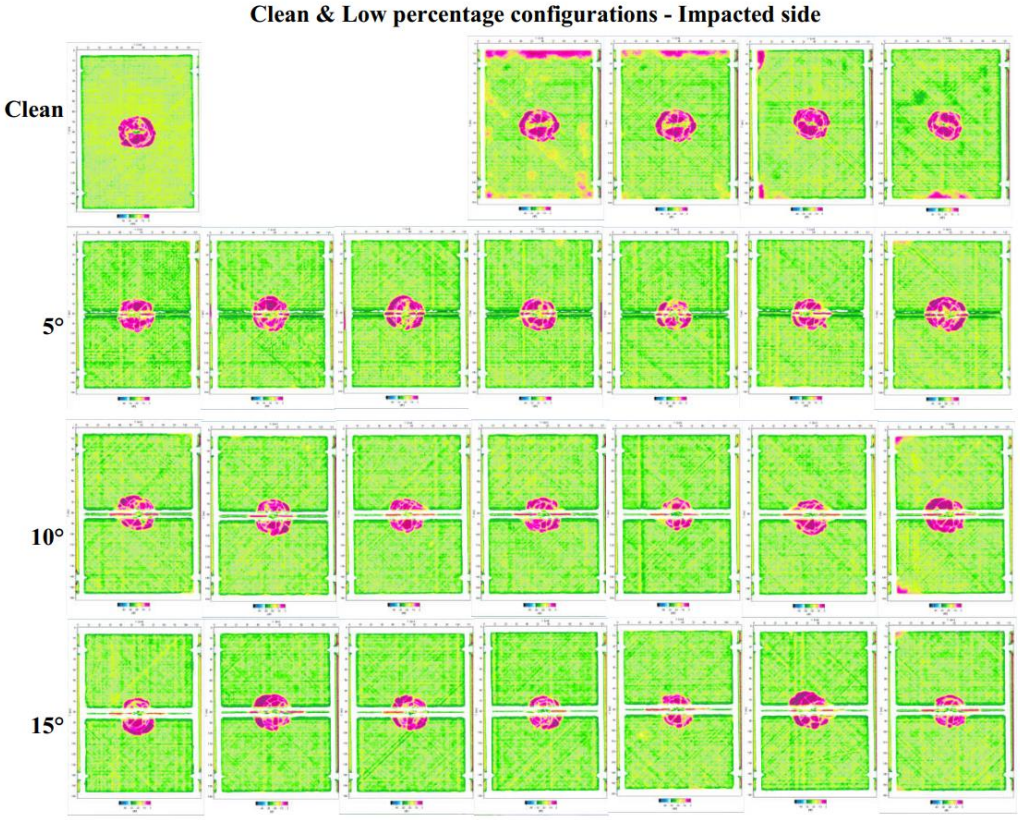

Figure 81: Delamination shape 15J - Low configurations, each configuration from one plate - Impacted side [2]

Figure 82: Delamination shape 15J - Low configurations, each configuration from one plate – Non-impacted side [2]

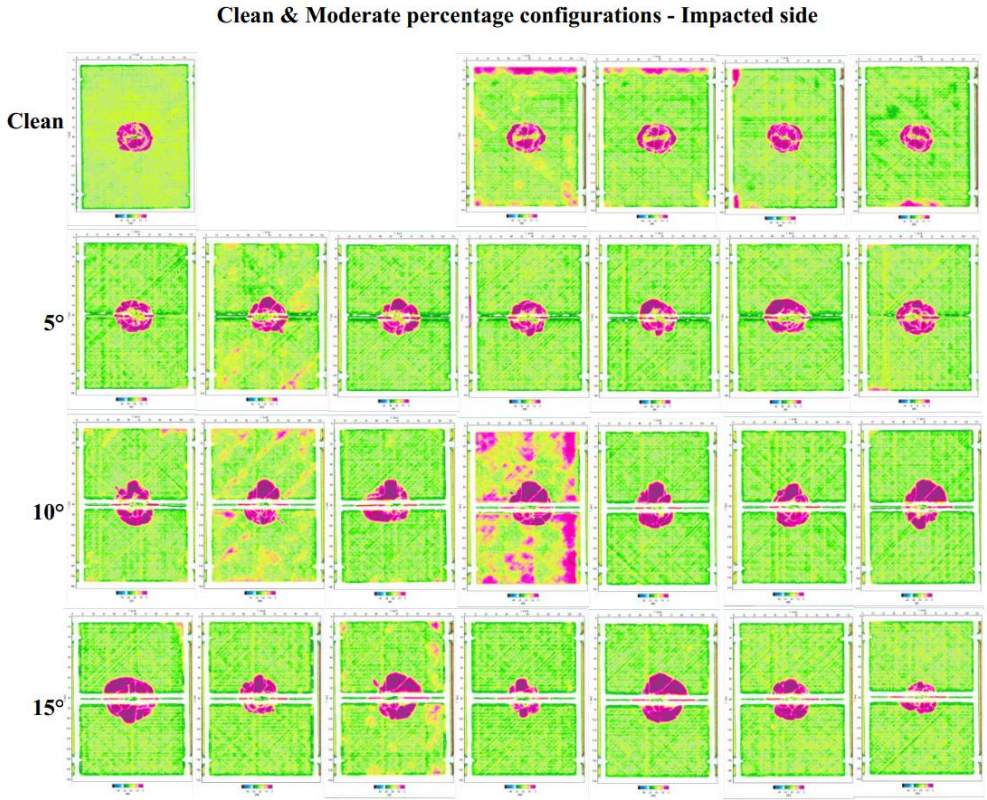

Figure 83: Delamination shape 15 J - Moderate configurations, each configuration from one plate Impacted side [2]

Figure 84: Delamination shape 15 J - Moderate configurations, each configuration from one plate – Non-impacted side [2]

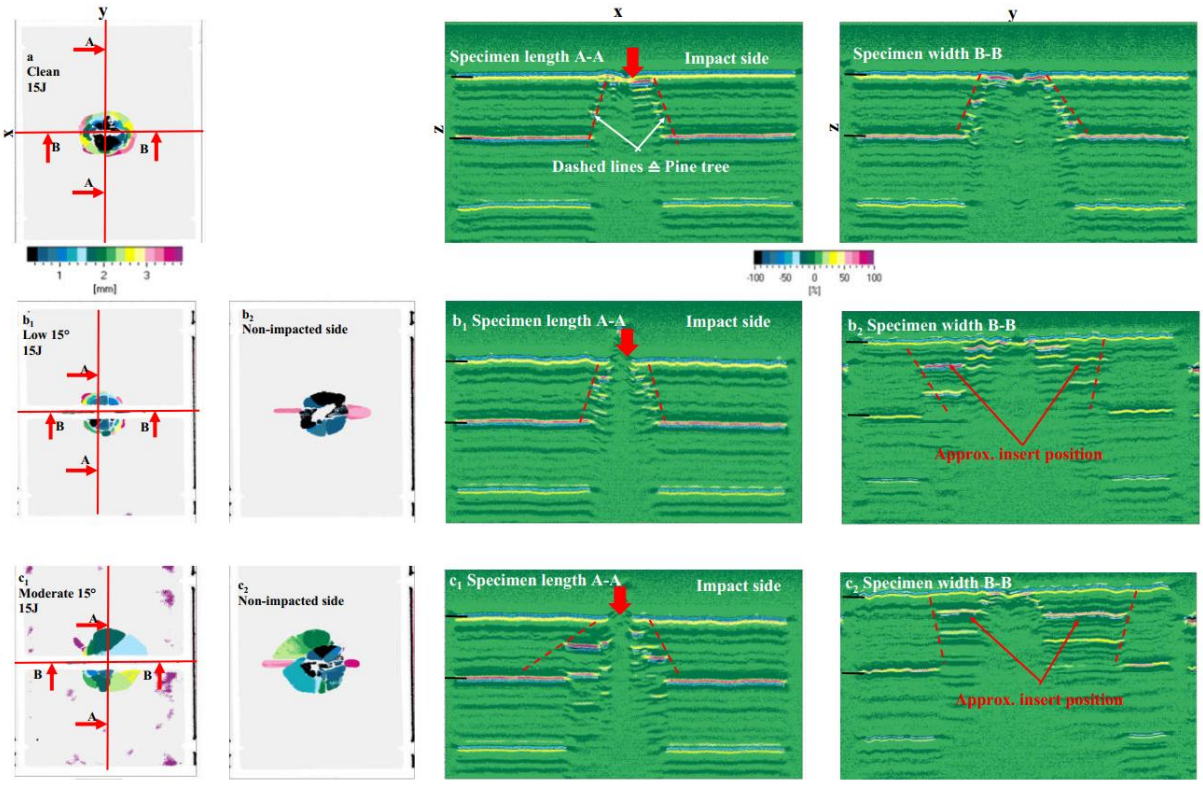

Figure 85: Top view and cross sections view of the delamination distribution within the laminate thickness 15 J, a = Clean, b1 = Low 15° impact side, b2 = Low 15° non-impacted side, c1 = Moderate 15° impact side, c2 = Moderate 15° non-impacted side [2]

5.4.2 CAI test results

The Failure load – Displacement curves of selected samples of the clean configuration impacted with different impact energies (15 J, 25 J and 35 J) are illustrated in Figure 86 (a). In (b) representative samples of all configurations impacted with 15 J are depicted. The failure for all configurations was sudden and catastrophic.

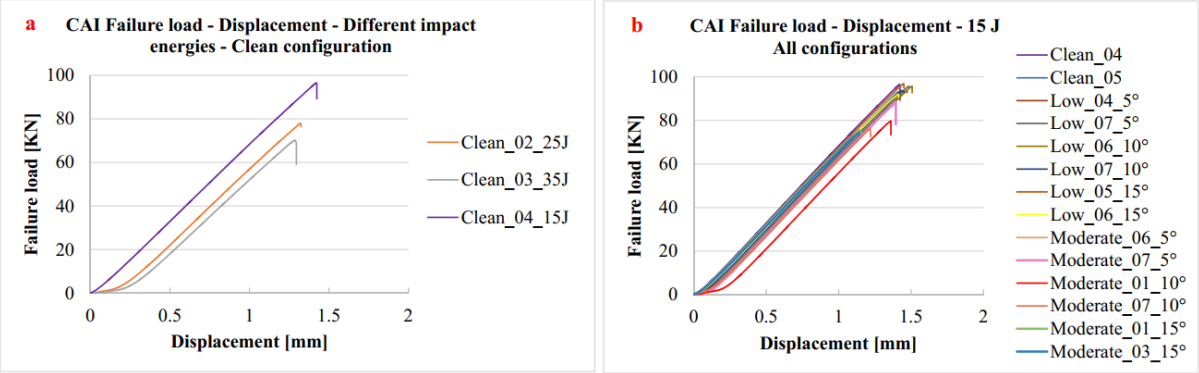

Figure 86: CAI failure load - displacement of the clean configuration impacted with different impact energies and the wavy configurations impacted with 15 J [2]

The average failure loads (FL) of the configuration without waviness are illustrated in dependence on the impact energy in Figure 87 (a). It provides the generally relation known from the literature [23] that the CAI strength decreases with increasing impact energy. The depicted failure load without impact is derived from the PSC failure load without waviness according to Equation (4). The compression strength reduction due to the impact itself is about 66 % at 15 J and about 76 % at 35 J.

The average failure loads of the clean and wavy configurations are depicted in dependence on Θ in Figure 87 (b). The deviation in the failure loads of all tested configurations goes up to a maximum of 5 %. Two important tendency are obvious: The failure load reduction in the low configurations is not significant and the dependency from Θ is negligible. The moderate configurations show significant reduction in the failure load and is depending on Θ.

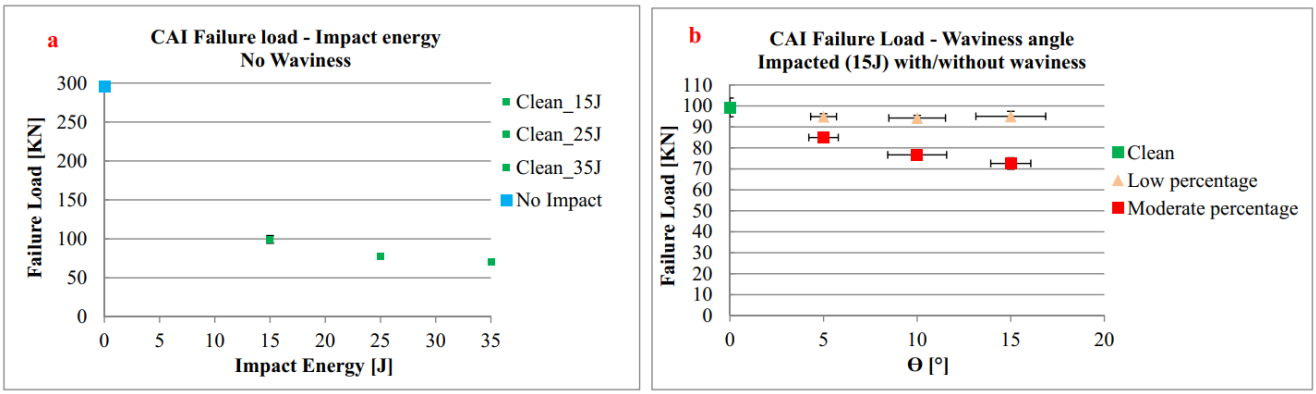

Figure 87: a = Failure load of the clean configuration in dependence on different impact energies; b = Failure load of the clean and wavy configurations impacted with 15 J in dependence on the waviness angle (Θ) [2]

Figure 88 (a) contains the average failure membrane strains without waviness as function of the impact energy at failure load. Additionally, the non-impacted failure membrane strain at 0 J is illustrated which is calculated analytically considering the CAI plate as an equivalent spring system. The non-impacted failure membrane strain, spring stiffness (K) and the specimen's length change (Δl) are calculated according to Equations 10 to 12. The plate E-Modulus was calculated according to the classical laminate theory. Its calculation was necessary, since no CAI test without impact was conducted. The objective of its illustration is to emphasize the dominant effect of the impact itself on the structure response. This figure provides the general known trend, that the membrane strain is decreased, when the impact energy is increased. The strain level at 15 J is approx. 3 times lower than the calculated strain at 0 J.

$$K = E * A/l_0 \quad (10)$$

$$\Delta l = FL_{No\ Defect}/K \quad (11)$$

$$\varepsilon = \Delta l/l_0 \quad (12)$$

K = spring stiffness, E = Plate E-Modulus, A = Cross section,
Δl = specimen's length change, l_0 = Specimen's initial length

The average failure membrane strains at failure load of the clean and wavy configurations impacted with 15 J as a function of the waviness angle (Θ) is shown in Figure 88 (b). The membrane strains of the low and moderate configurations show in spite of the big deviation in the Θ, assuming an error free waviness angle measurement determination, low deviation in their strain level. The same above mentioned two trends regarding the dependency from Θ are observed, too.

The membrane strain and out of plane deformation distributions at the failure load of some representative specimens from the clean as well as from the low and moderate configurations measured with DIC system are shown in Figure 89 and Figure 90. A cut parallel to the x-axis in the middle of the samples through the delamination region is made to visualize the out of plane deformations as illustrated in Figure 91. The objective is to exhibit the waviness effect on the inplane strain and out of plane deformation distribution in comparison to the clean configuration. This also allows conclusions to be drawn about the stability behavior of the wavy configurations compared to the clean configuration. The low and moderate configurations have tension strains in the waviness region in comparison to the clean configuration. Additionally, their out of plane deformations point in the opposite direction compared to the clean configuration. The tension strains in the waviness region together with the out of plane deformation shown in Figure 90 and Figure 91 is an indication for a modified sub-buckling mode in comparison to the clean configuration.

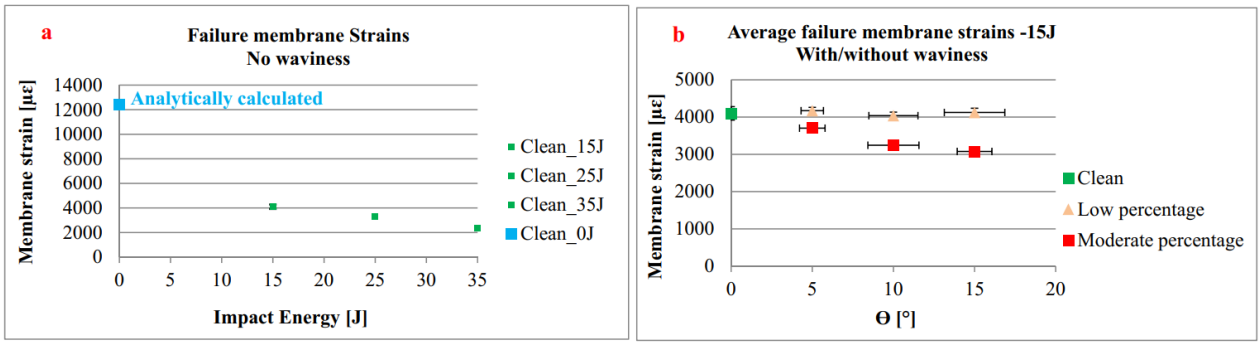

Figure 88: a = Failure membrane strains of the clean configuration in dependence on different impact energies; b = Failure membrane strains of the clean and wavy configurations impacted with 15 J in dependence on the waviness angle (Θ) [2]

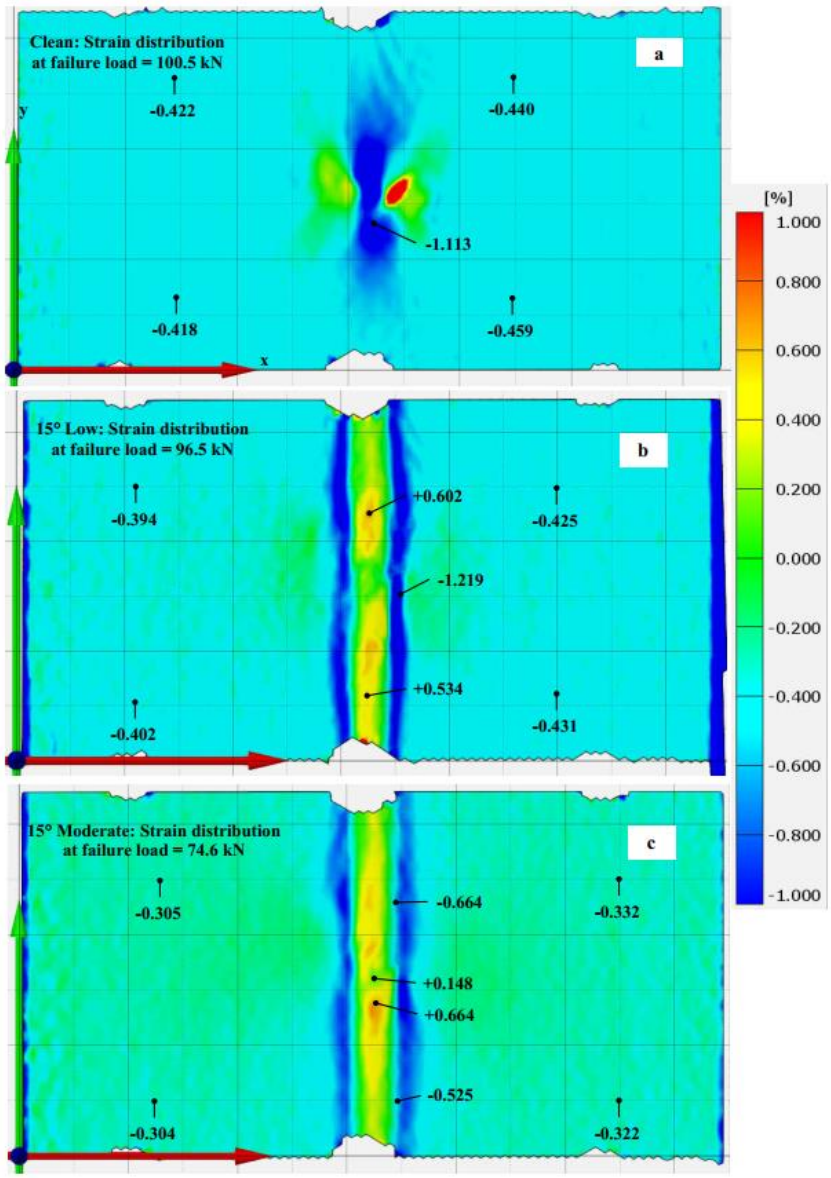

Figure 89: CAI Failure inplane membrane strains distribution at failure load, a = Clean, b = Low 15°, c = Moderate 15° [2]

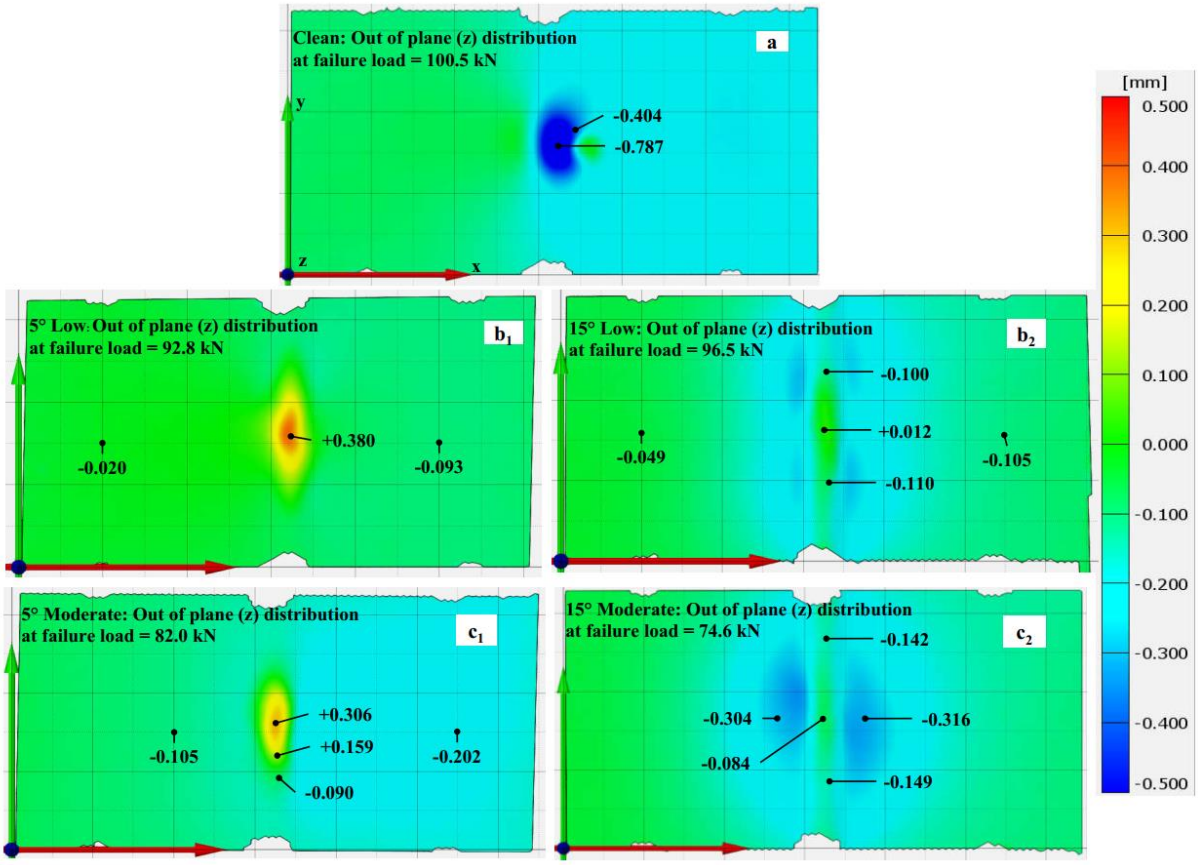

Figure 90: CAI z-Deformation distribution at failure load, a = Clean, b_1 = Low 5°, b_2 = Low 15°, c_1 = Moderate 5°, c_2 = Moderate 15° [2]

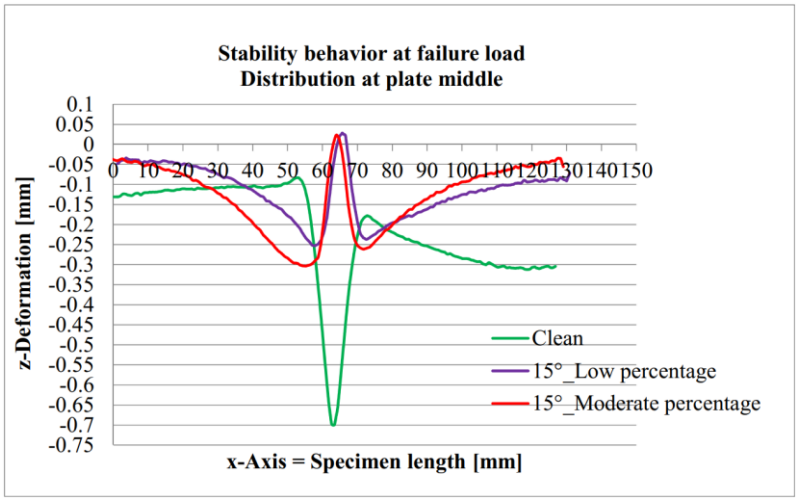

Figure 91: CAI sub buckling behavior illustrated by the out of plane deformation (z) at failure load of a cut parallel to the x-axis in the middle of the specimen through the delamination region [2]

5.4.3 Impact and CAI discussion

It is observed that impact itself is the main driver for the strength reduction and waviness can lead to an additional reduction as shown in Figure 87 (b), if certain conditions are present. These are related to the waviness morphology, impact side relative to the waviness orientation and position as well as number of affected 0°-plies in dependence on the waviness angle. The non-destructive ultrasonic results show, that waviness affects the shape, size of the delamination and the through thickness delamination distribution (pine tree) as shown in Figure 85.

Relation between impact side and shape of the defect

The impact side relative to waviness morphology is an influencing factor. The current investigated waviness morphology represents a convex shape as shown in Figure 92 (a). Ehrlich [36] impacted concave and convex specimens with different cambers (U) defined in Figure 92 (c). The projected delamination area in dependence of U is depicted in Figure 23. He found that the impact side relative to the curvature orientation of the structure plays a crucial role on the damage resistance. The loading of a curved structure in the opposite direction to the curvature orientation leads to considerable interlaminar peel and shear stresses as described in Section 2.5. Convex structures generate local membrane compressive stresses and thus increase the interlaminar stress during the impact. In contrast, specimens with a concave shape generate local membrane tension stresses, which lead to a reduction in interlaminar stresses. This clarifies, why his convex specimens shown in Figure 92 (c) had much larger damage than plane ones. In contrast, the concave specimens shown in Figure 92 (d) compared to plane ones were more tolerant against damage. His findings related to the convex specimens correlate well with the investigated wavy configurations with regards to the increase of the projected delamination areas in comparison to the flat configuration as well as with the dependency from the camber. Thus, it is reasonable to conclude, that the impact side relative to waviness orientation (convex or concave orientation) is an influencing factor, which affects the damage resistance of the structure and consequently the compression strength.

Relation between impact side and the through the thickness delamination distribution

It is assumed that the through the thickness delamination distribution can influence the stability behavior and consequently the residual strength. Based on Abrate [23], the delamination areas of a flat sample are increased in non-impacted side direction, building a pine tree formation. Despite the existing curvature of the cases examined by Ehrlich [36], the delamination areas are increased in non-impacted side direction, building a pine tree as shown schematically in Figure 92 (c and d), too. Although, only one impacted side relative to the waviness was investigated as shown schematically in Figure 92 (a), it is assumed, that impacting the flat side of the wavy sample causes a reversed pine tree in comparison to the investigated cases as shown in (b), i.e. the delamination areas are increased in waviness direction, non-impacted side, respectively. The verification of this assumption would be valuable due to the connection between the stability behavior and the residual strength of the structure. This assumption also covers the consideration of the defect position relative to the impact side**.** As reported in Section 2.4, Rhead [37] found that the impact of a coupon directly

over a tow gap (Coupon B), which is close to the non-impacted side, produces a smaller damage area in comparison to impacting a tow gap near the impacted side (Coupon A) as shown in Figure 25. Consequently, the CAI residual strength of coupon B was about 14% higher than coupon A. Unfortunately, no information regarding the through thickness delamination distribution was given.

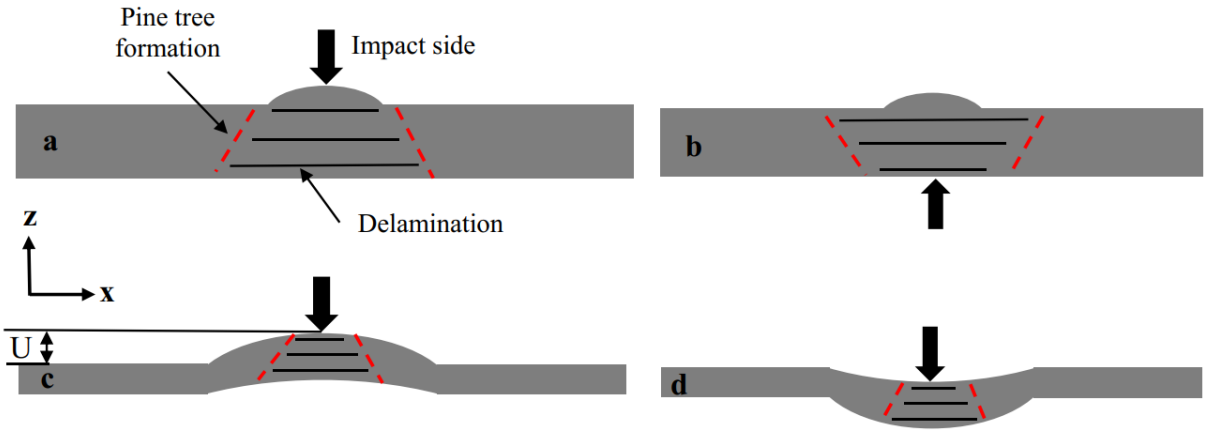

Figure 92: Schematic illustration of waviness morphologies and their through the thickness delamination distributions (Pine tree) in dependence on the impact side [2]

Stability behavior of impacted structures

Experimental studies [29], [37], [49] showed, that the failure of composite structures in CAI load case is generally governed by the local buckling of delaminated areas. The out of plane deformation curves of the clean and wavy configurations shown in Figure 91 together with the inplane strains shown in Figure 89 indicate that local sub-buckling occurred in the wavy configurations. That is why the failure membrane strains, failure loads and finally the KDFs show the two observed tendencies. The low configurations show negligible dependency from the waviness angle and an insignificant reduction in the strength. In contrast, the moderate configurations are dependent from the waviness angle with stronger strength reduction. Further, the local buckling load is dependent from the affected 0°-plies and the corresponding stiffness in the delaminated sub-laminate which is affected by waviness, too. I.e. this region is severely weakened by the waviness and impact damages.

In case of the low configurations only one 0°-ply is affected by waviness and the sub-laminate thickness is approx. equal to the total number of affected plies (5 plies*0.125 mm). In case of moderate configurations three 0°-plies are affected by waviness and the sub-laminate thickness is approx. equal to the total number of affected plies (13 plies*0.125 mm). Due to the local sub-buckling, it is expected, that load redistribution occurred. When the affected 0°-plies are in a small range (low configurations), their load portion is carried out by the remaining healthy 0°-plies and the waviness angle doesn't matter. But from a certain increased number of affected 0°-plies (moderate configurations ~ 40% affected 0°-plies), the remaining 0°-plies have to carry out their own load portion and in addition the load portion of the affected 0°-plies. Additionally, the effect of the waviness angle becomes significant from a certain number of affected 0°-plies due to the associated decrease in the stiffness. This is the

reason why the moderate configurations failed at lower load level in comparison to the low configurations.

Based on the low deviation in the failure loads and strong scatter in the waviness angles (assuming correct waviness measurement), it can be stated, that waviness angle alone is not the driving factor for the reduction, as described before. Like the PSC load case, it is the interplay of waviness morphology, waviness angle and number of affected 0°-plies ratio in dependence on the impact side, which is a key factor for the final failure evolution. The influencing factors for each load case derived from the test observations are summarized in Table 11.

Influencing factors	**Load cases**		
	PSC	CAI	Interaction
Energy level		✓	✓
Waviness morphology	✓	✓	✓
Waviness angle (Θ)	✓	✓	✓
No. of affected 0°-plies ratio (α_0)	✓	✓	✓
No. of total affected plies ratio (α)			
Thickness	✓		

Table 11: Influencing factors derived from the conducted experiments

5.5 Interaction approach

Four experimentally derived KDFs are introduced in Section 5.1. The aim is on the one hand to identify separately the critical influencing factors in each load case and in interaction, on the other hand to identify how do they influence each other. The comparison of the CAI KDFs with each other and subsequently their comparison with the PSC KDFs provides meaningful physical relation related to the interaction behavior as described below.

Interaction approach of the CAI results

Three CAI KDFs are shown in Figure 93 which are derived by means of failure loads from Section 5.4.2 and the formulas described in Table 9. They are highlighted by dashed rectangles using different colors; the pure impact KDF in green ($KDF_{Imp,\ CAI}$), the pure waviness KDFs in violet ($KDF_{Wav,\ CAI}$) and the interaction KDFs in black ($KDF_{Interaction,\ CAI}$).

$KDF_{Imp,\ CAI}$ and $KDF_{Interaction,\ CAI}$ are normalized by the failure load without impact and waviness ($FL_{No\ Defect}$) which is derived based on Equation (4). $KDF_{Wav,\ CAI}$ is normalized by the impact failure load. The comparison of $KDF_{Imp,\ CAI}$ with $KDF_{Wav,\ CAI}$ shows, that impact is the main driver for the strength reduction and not the waviness.

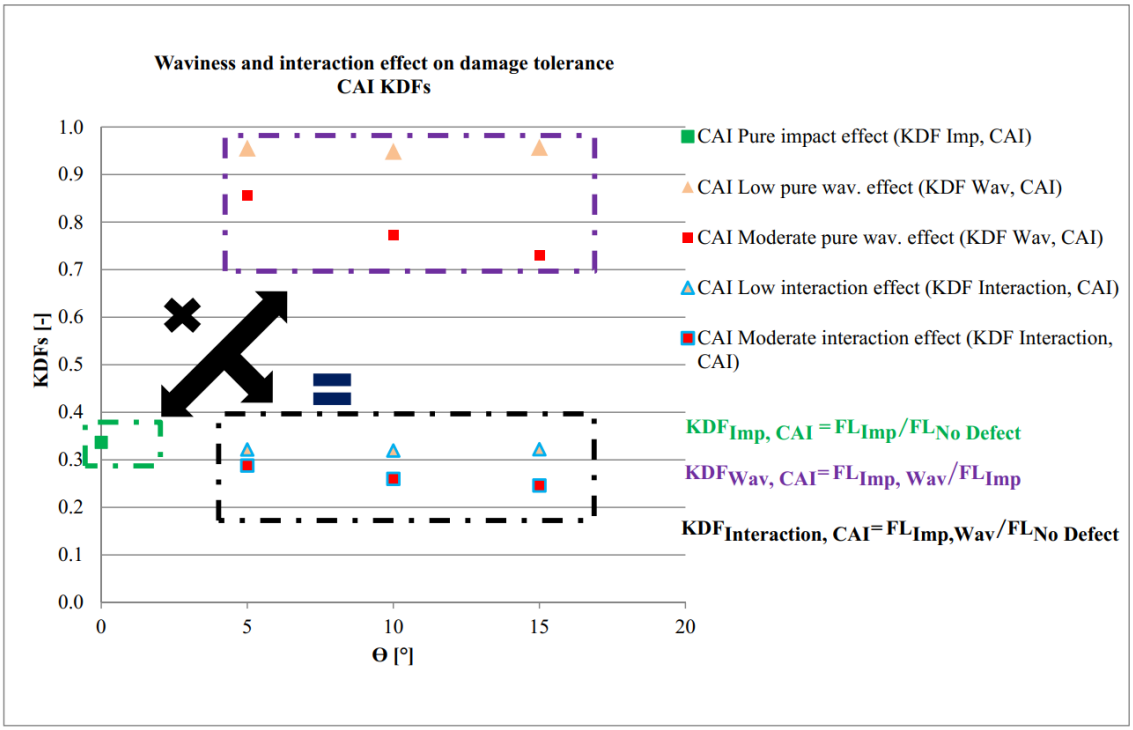

Figure 93: Pure impact, pure waviness and interaction KDFs derived from CAI test – Overview [2]

As highlighted in the KDF illustration, the multiplication (✕) of the CAI pure waviness KDF (violet) with pure impact KDF (green) results in (=) a CAI interaction KDF (black), which is equal to the derived interaction KDF described in Table 9 as shown in equation below:

$$KDF_{Interaction,\ CAI} = KDF_{Imp,\ CAI} * KDF_{Wav,\ CAI} = FL_{Imp,\ Wav}/FL_{No\ Defect} \quad (13)$$

This equation indicates that the interaction behavior represents approximately a multiplicative relation in the investigated cases. The interaction KDF ($KDF_{Interaction,\ CAI}$) provides like $KDF_{Wav,\ CAI}$ the above mentioned two tendencies related to the dependency from the waviness angle (Θ), which are observable in the failure loads, failure membrane strains and the sizes of the projected delamination areas, too.

Even if the interaction KDFs ($KDF_{Interaction,\ CAI}$) are in the same range as the pure impact KDF ($KDF_{Imp,\ CAI}$), as it is observed in case of the low configurations, the waviness effect is still present as observed in the inplane and out of plane distributions. Thus, it can be concluded that waviness effects cannot compensate impact effects or vice versa, thus a multiplicative relation seems reasonable. In the investigated cases, this equation is characterized by the fact that it contains all relevant influencing factors for the strength reduction.

This formula was developed for the following assumptions:

- Symmetrical QI laminate
- No other “macroscopic” defects (e.g. pores, inclusion)
- Impact damage is main driver for the strength reduction (in the investigated case $KDF_{Imp,\ CAI} = 0.34$) resulting in significant strain reduction

- Impact side on the convex shape of the waviness morphology (Figure 92 a and c)

In summary, impact and waviness provoke different failure modes in the event of compression loading as shown in Figure 94 and reported by different authors (refer to Table 2). Out of plane waviness provokes interlaminar stresses. These initiate matrix cracks, delaminations which can be followed by local sub-buckling as well as fiber kinking or fiber fracture. The impact event induces interlaminar stresses causing fiber fracture, matrix cracks as well as delaminations. Under compression loading these delaminations are followed by local sub-buckling, too. Both damages influence the initial position of the neutral axis independently. In case of the waviness, it is shifted due to waviness morphology. In CAI case, it is shifted due to the induced delaminations by the impact event. The displacement of the neutral axis affects the deformation, loading state and consequently the stability behavior. It is assumed that these processes occur simultaneously, so that both damages reinforce the reduction in the compression strength independently. Therefore, a multiplicative relationship seems reasonable.

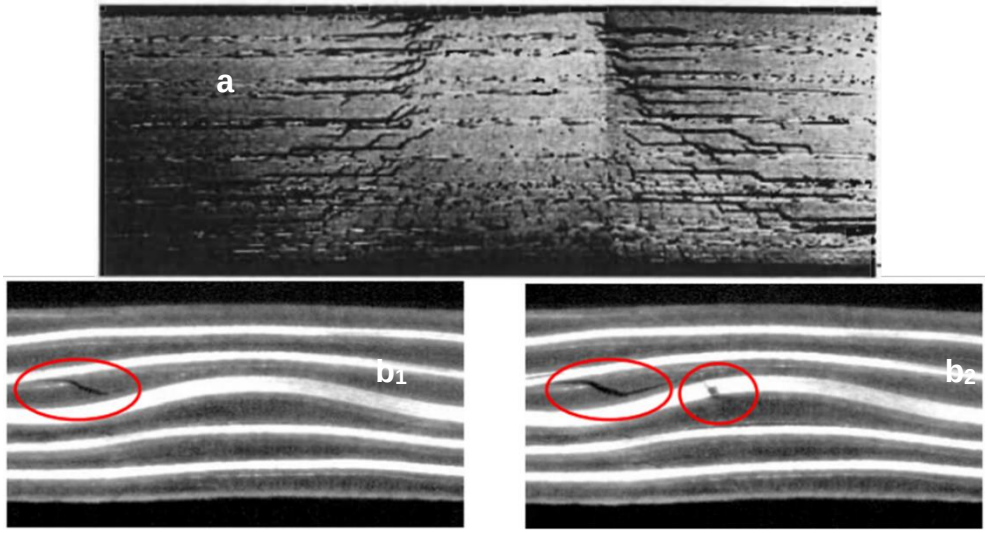

Figure 94: a = Impact failure mode (Delamination), Waviness failure modes b_1 = Matrix crack, delamination and b_2 = Fiber kinking just before final failure [2]

Simplification of the interaction approach based on CAI and PSC results

The PSC and CAI pure waviness effect KDFs are depicted in Figure 95. The CAI pure waviness effect KDFs ($KDF_{Wav, CAI}$) are related to the impact failure load. The PSC waviness effect KDFs ($KDF_{Wav, PSC}$) is related to the failure load without waviness. Based on the comparison between these load cases (PSC and CAI) it is observed, that the PSC KDFs ($KDF_{Wav, PSC}$) are dependent from the waviness angle. In contrast, the CAI KDFs show that the waviness angle comes firstly into play at a certain increased number of affected 0°-plies. At small range of affected 0°-plies there is no significant dependency from waviness angle. In both load cases, there is a significant reduction in the KDFs, when the number of affected 0°-plies is increased. The KDFs of both load cases are in the same range at small waviness angle (5°) and differ at larger waviness angle (15°), nevertheless these KDFs are related to different

strain levels as shown in Figure 96. The CAI strain level is reduced by more than factor 3 in comparison to PSC one due to the impact itself.

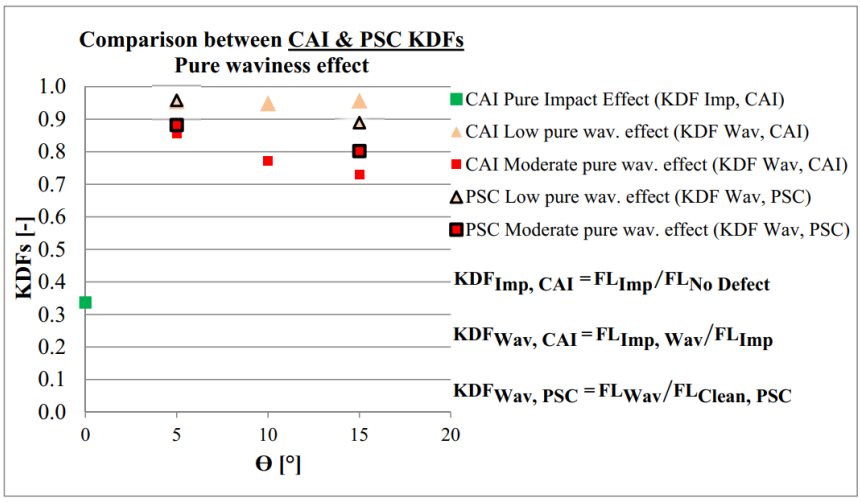

Figure 95: Comparison between the pure waviness effect derived from CAI & PSC tests [2]

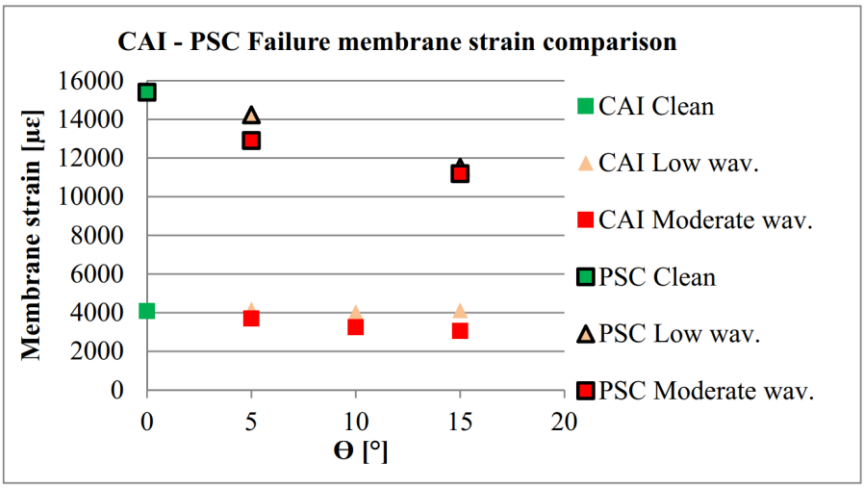

Figure 96: CAI & PSC Failure membrane strain levels [2]

Additionally, it is observed, that the multiplication (✕) of the CAI pure impact KDF ($KDF_{Imp, CAI}$) with the PSC pure Waviness KDFs ($KDF_{Wav, PSC}$) shown in Figure 97 results (=) on the one hand in KDFs that are in the same range as the CAI interaction KDFs ($KDF_{Interaction, CAI}$) shown in Figure 93. On the other hand, it provides a comparable tendency to the moderate configurations. The low configurations tendency is not reproduced, since all resulting PSC KDFs depend on the waviness angle. This observation can be written as the equation given below:

$$KDF_{Interaction} = KDF_{Imp, CAI} * KDF_{Wav, PSC} \quad (14)$$

This equation represents a simplified approximation of Equation (13) which can be a useful mean for preliminary assessment of the interaction behavior between impact and waviness, since each term of this relation $KDF_{Imp,CAI}$ and $KDF_{Wav, PSC}$ comprises independently the driving factors for the reduction. It does not mean that there is no interaction between both

defects. Nevertheless, the joint effect of both, impact and waviness, could be roughly estimated by a superposition of both effects individually. A further benefit of this simplification can be a reduction of the experimental and numerical efforts. Commonly, the investigation of the interaction behavior requires the fabrication of specimen sets with and without defects. The waviness fabrication method as well as conducting CAI tests with specimens having different morphologies can be a big challenge. On the one hand, the fabrication method can strongly affect the relevant waviness parameters, that is why preliminary manufacturing trials were conducted to ensure their consistency as described in Section 4.3. On the other hand, the CAI test fixture is designed for plane specimens, that is why the anti-buckling rails were modified as described in Section 4.4. In contrast, PSC test fixtures are more flexible with regards to the waviness morphology. So that the waviness effect can be investigated by means of conducting PSC tests instead of CAI tests, under the assumption that the impact is the main driver for the reduction.

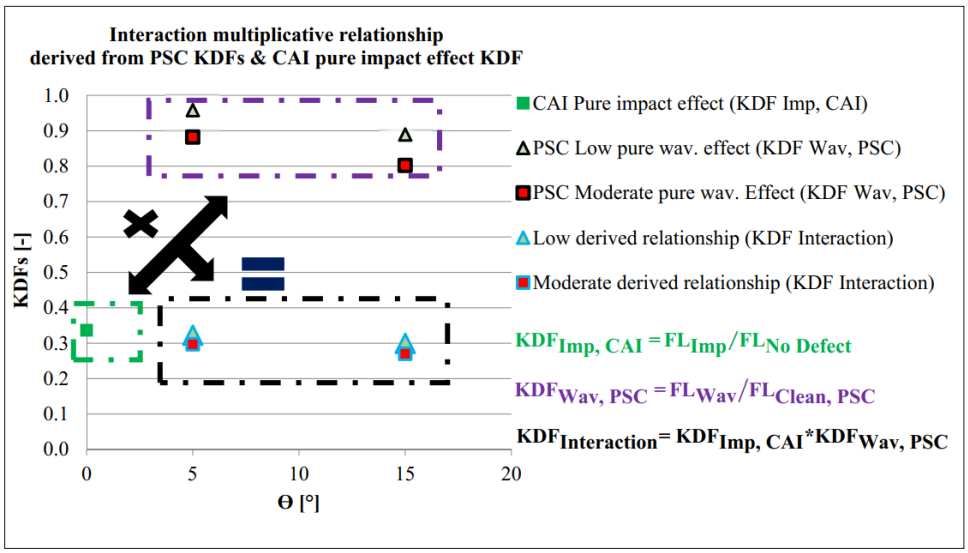

Figure 97: Derived interaction relationship derived from PSC KDFs and pure impact effect KDF [2]

The assumptions for the application of the simplified formula are the already presented observations, which have to be considered; Impact is main driver for the reduction. The difference between the strain levels indicates, that the CAI stiffness is reduced significantly due to the delaminations induced by impact and due to the waviness. The through thickness delamination distribution is a function of the waviness morphology and impact side. The waviness morphology and delamination distribution affect independently the neutral axis position and thus the structure deformation behavior. Waviness affects the local buckling load, which is a function of number of affected 0°-plies and waviness angle.

5.6 Limits of the interaction approach

The multiplicative interaction approach (Equation 13) and its related simplification (Equation 14) help to better understand the physical behavior of both damages, identify the influencing factors as well as the dependencies between them. This reduces for instance the future experimental efforts and help identifying critical cases. On the other hand, the approaches have limits which need to be considered.

Limits of the interaction approach $KDF_{Interaction, CAI}$

In case of interaction, the experimentally observed multiplicative relation Equation (13) is limited to the assumptions given in Section 5.5. Its applicability to other cases like:

- Symmetrical laminate with high percentage of 0°-plies i.e. 60%
- Non-symmetrical laminate
- Impact side opposite on the convex shape of the waviness morphology (Figure 92 b)
- Impact side on the concave shape of the waviness morphology (Figure 92 d)
- Morphology A with wavy plies in flat laminate (Table 1)

requires further experimental investigations, numerical investigations, respectively.

Limits of the simplified interaction approach $KDF_{Interaction}$

Equation (14) represents a simplification for preliminary assessment of the interaction behavior. It considers, that impact is driving the strength reduction and the waviness can lead to an additional reduction, if certain conditions are present as described in Section 5.4.3. Both knock down factors $KDF_{Imp, CAI}$ and $KDF_{Wav, PSC}$ comprise independently the driving factors for the compression strength reduction. Its usage without considering the driving factors and the dependencies mentioned below is not fully rational, because these can underestimate or overestimate the interaction KDFs:

- Waviness effect on the deformation behavior (Figure 98)
- Dependency between waviness morphology and impact side (Figure 99)

Waviness effect on the deformation behavior

Depending on the waviness morphology the initial position of the neutral axis can be shifted as described in Section 5.3. In Figure 98, the initial neutral axis of different morphologies is highlighted in green dashed lines, the shifted one in red dashed lines exemplary for morphology B. The displacement of the neutral axis causes a local bending moment which is superimposed with the global compression load as described in Section 2.7. Depending on the sense of rotation of the bending moment, the longitudinal membrane strain distributions are affected as depicted in Figure 98.

Thor [13] investigated the failure behavior of a structure containing waviness (morphology C) under compression loading as described in Section 2.2. The respective membrane strain distribution is depicted in Figure 98. On its convex side, there is a tension strain (+2800 με). On its concave side, there is a compression strain (-10000με). In case of morphology B with convex shape, there is compression strains on both sides. Nevertheless, the strain on the convex side represents a tension region. In case of morphology B with the concave shape,

there is no published data related to the strain distribution. However, it is expected that the concave side is dominated by larger compression strain than the other two examples. Based on Kaddour [50], the compression strain allowable of IM7-8552 is 11000 με, 1.1 %, respectively. I.e. the strain allowable in case of morphology B is exceeded on the flat side. In case of morphology C, the strain on the concave side is almost critical. In case of morphology B with the concave side, it is expected, that the strain allowable is exceeded on its concave side.

Table 12 provides different $KDF_{Wav,\,PSC}$ in dependence on different waviness morphology and influencing factors which obviously cause strong variation in the KDFs. The described change in the deformation behavior due to the waviness morphology can affect consequently the resulting KDFs ($KDF_{Wav,\,PSC}$) as well as the failure mode and position that is why they have to be considered. Accordingly, rational application of the simplified interaction relation requires a deep physical understanding of the dependencies between the change in the deformation behavior of the structure and the influencing factors.

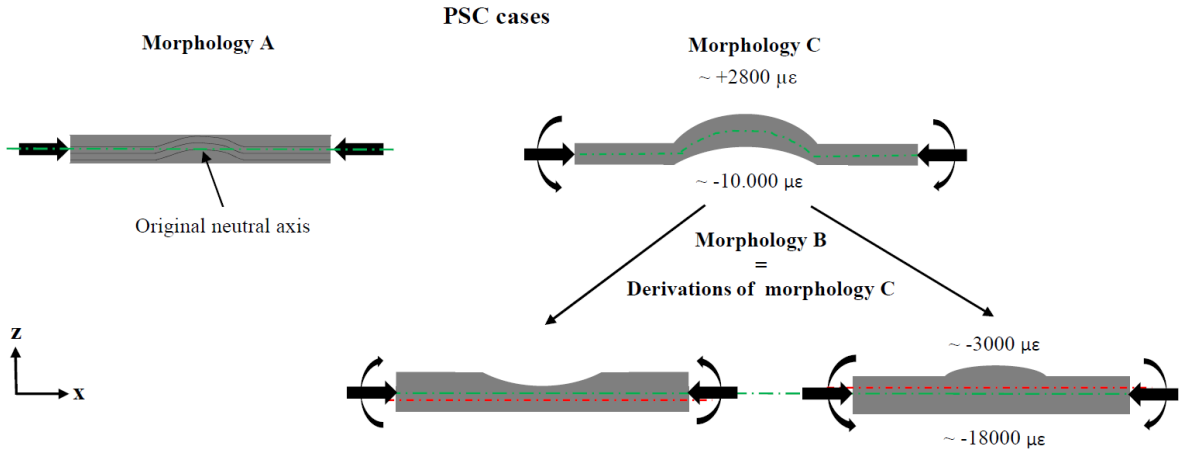

Figure 98: Morphology effect on the deformation behavior. Strain distribution of morphology C based on [13], morphology B with convex shape based on current investigation

PSC KDFs from literature and conducted test						
Morphology type	**A - Uniform**	**A - graded**	**A - centered**	**B - convex**	**B - concave**	**C**
Morphology	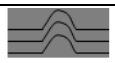					
Reference	Hsiao [5]		Mukhopadhyay [10]	Al-Kathemi [2]	N/A	Thor [13]
Layup	Only 0°-Plies		QI	QI		QI
t [mm]	19.1	9.1	6.0	4.0		5.1
$\alpha_{0°}$ [%]	100	100	33*	41		100
Θ [°]	15	7	12	15		15
$KDF_{Wav,\,PSC}$ [-]	0.24	0.65	0.67	0.80		0.35

Table 12: Variation in the $KDF_{Wav,\,PSC}$ due to the influencing factors and waviness morphologies (* = Affected 0°-plies with 12° waviness angle. Remaining 0°-plies are affected by smaller waviness angle, refer to [10])

Dependency between waviness morphology and impact side

Additionally, it is reasonable, to consider the dependency between the impact side relative to waviness orientation, too. Because it can affect the damage resistance as shown in Figure 99 and consequently the resulting KDFs. Impacting a wavy structure with concave curvature as shown in Table 13 leads to a smaller projected delamination area (300 mm²) in comparison to a wavy structure with convex curvature (1260mm²). Accordingly, in spite of the simplicity of the interaction approach neglecting the above described dependencies between the waviness morphology and deformation behavior as well the waviness morphology and impact side in addition to the role of influencing factors results in strong variation in the interaction KDF limiting its applicability.

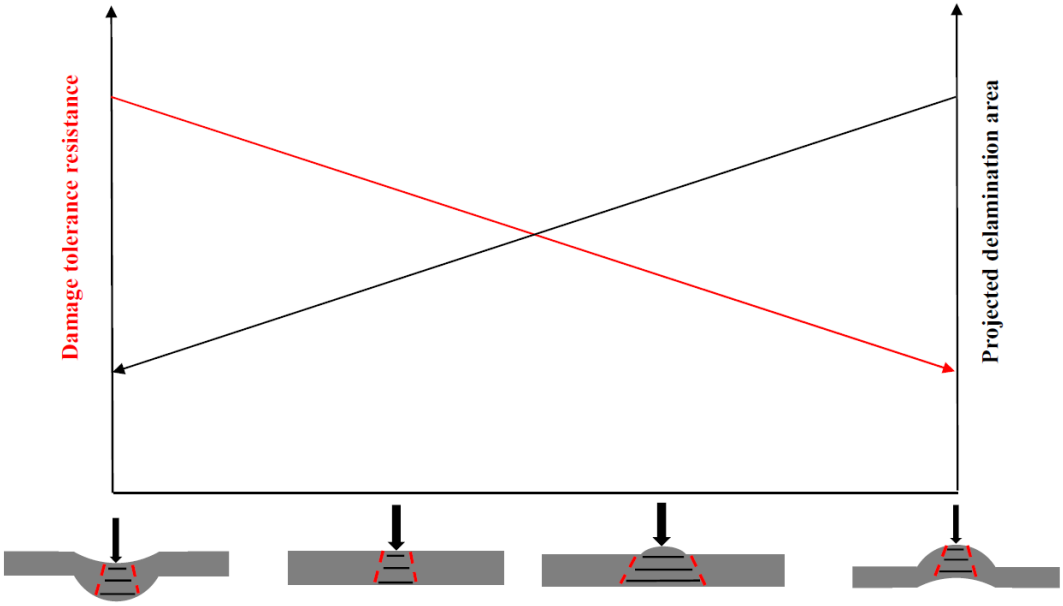

Figure 99: Dependency between waviness morphology and impact side

Morphology type	Reference	Impact energy [J]	$A_{Projected}$ [mm²]
	Ehrlich [36]	9.4	300
	Ehrlich [36] / Current	9.4/ 15	638/ 892
	Current	15	1473
	Ehrlich [36]	9.4	1260

Table 13: Variation in the damage resistance (Projected delamination area $A_{Projected}$) due to the impact side relative to waviness morphologies

6 Experimental verification

The objective of this chapter is to verify the research and working hypotheses given in Section 3.1 by independent experimental works from literature as well as showing the reliability of the current findings.

Working hypothesis 1.a: Effect of waviness morphology (convex, concave and flat geometry) on the damage resistance and damage tolerance
The experimental results of Ehrlich [36] described in Section 2.4 and Section 2.5 are used to verify this working hypothesis.

Table 14 provides an overview of the baseline data of both experimental investigations [2] and [36]. The baseline layup data, geometry of the specimens as well as the impact data are similar, except for layup sequence and impact energy level, which are different. Nevertheless, both layups are quasi-isotropic laminates.

	Baseline data	**Ehrlich** [36]	**Al-Kathemi** [2]
Layup data	Material	IM7-8552	IM7-8552
	Layup	$[[45/0/-45/90]_4]_s$	$[[45/-45/90/45/0/-45/90/0]_2]_s$
	Layup type	QI	QI
	t_{Ply} [mm]	0.125	0.125
	No. Plies	32	32
Geometry	$t_{Nominal}$ [mm]	4	4
	l [mm]	150	150
	B [mm]	100	100
Impact data	Impact Standard	[28]	[28]
	Impactor diameter [mm]	16	16
	Impact energy [J]	6.1; 7.82; 9.36	15
	Impact window	125mm x 75mm	125mm x 75mm

Table 14: Geometry, layup and impact baseline data of the impacted specimens from Ehrlich [36] and Al-Kathemi [2]

The waviness morphology in the current investigation represents morphology B as described in the previous sections and shown in Table 1. It is characterized by an uniform waviness angle, defined number of total affected plies and number of affected 0°-plies as illustrated in Table 5. The impact side represents the waviness side as shown in Figure 56.

The morphology investigated by Ehrlich represents morphology C as shown in Table 1. Different curvature severities (U) were manufactured as depicted in Table 15. Due to the manufacturing process of the curved specimens described in [36], it is reasonable to consider, that the curved specimens are affected by uniform waviness with constant waviness angle in the entire laminate, in which all plies are affected by waviness. Accordingly, assuming a comparable waviness angle, Ehrlich's configurations represent the critical case in comparison to the current investigation, because in his investigated cases the entire laminate is affected by uniform waviness.

Nevertheless, the waviness angles of both works are not directly comparable, because the mathematical description of Ehrlich's specimen waviness shape does not represent a sinusoidal function, which is the case in the current investigation. The difference in the mathematical description of the waviness shape leads to a different waviness angle. Therefore, to enable the comparison between both experimental investigations, the curvature severity (U) of all wavy specimens was measured by means of Keyence microscope according to [36] and as shown in Figure 100**.** The average of U for each wavy configuration is illustrated in Table 15 as well as the investigated U by Ehrlich [36]. It can be seen, that the waviness angle is increased with an increased U. If the waviness curvatures of both investigations have the same mathematical description, they would have the same waviness angle and consequently the same U.

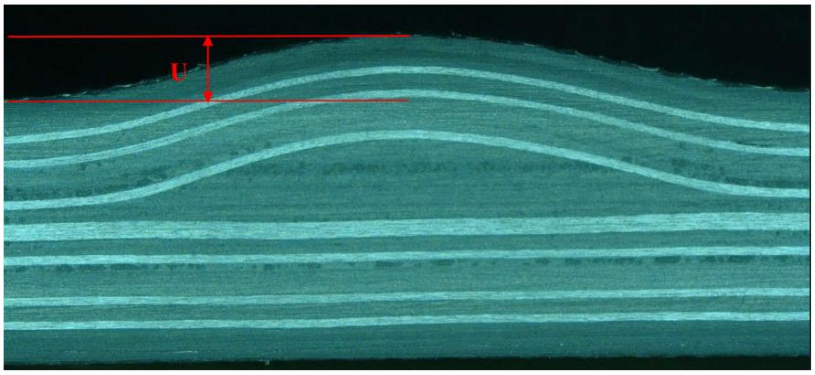

Figure 100: Waviness severity definition, sample of the moderate configuration 15°, U = 0.9mm

	Configurations	**Θ [°]**	**$U_{Average}$ [mm]**	**α [%]**	**$\alpha_{0°}$ [%]**
Current investigation	Clean	0	0	0	0
	Low waviness	5°	0.36	16	13
		10°	0.65		
		15°	0.89		
	Moderate waviness	5°	0.33	41	38
		10°	0.69		
		15°	0.90		
Ehrlich [36]	Clean	0	0	0	0
	Curvature 1	Not	0.6	100	100

Curvature 2	comparable	1.2	100	100
Curvature 3		1.8	100	100

Table 15: Curvature severity data of Ehrlich [36] and current investigation

Based on Ehrlich [36] the curvature of the structure plays a crucial role on the damage resistance of the structure. Convex, concave and plane specimens were impacted with different impact energies as shown in Table 14. In the following, Ehrlich's results based on the impact energy of 9.36 J are only used to compare them with the current experimental work. This energy level is closer to 15 J. The others energy levels provide similar tendencies.

His experimental results show that impacting convex specimens have much greater damage than plane and concave specimens as shown in Figure 23. The projected delamination area of convex specimens is increased with increased curvature severity (U). The reason why convex structures are more critical than plan and concave structures is already described in Section 2.5, see Figure 38, too. Therefore, impacting a convex structure represents the worst case. The average projected delamination areas in dependence on U of the clean, low, moderate configurations as well as Ehrlich's configurations are depicted in Figure 101 and in Figure 102. Two tendencies are obvious: First, the well-known tendency regarding the dependency between the projected delamination area and the impact energy. It is increased with increased impact energy. Second, the current investigation provides the same tendency like Ehrlich regarding the dependency of U. The projected delamination area is increased with increased U.

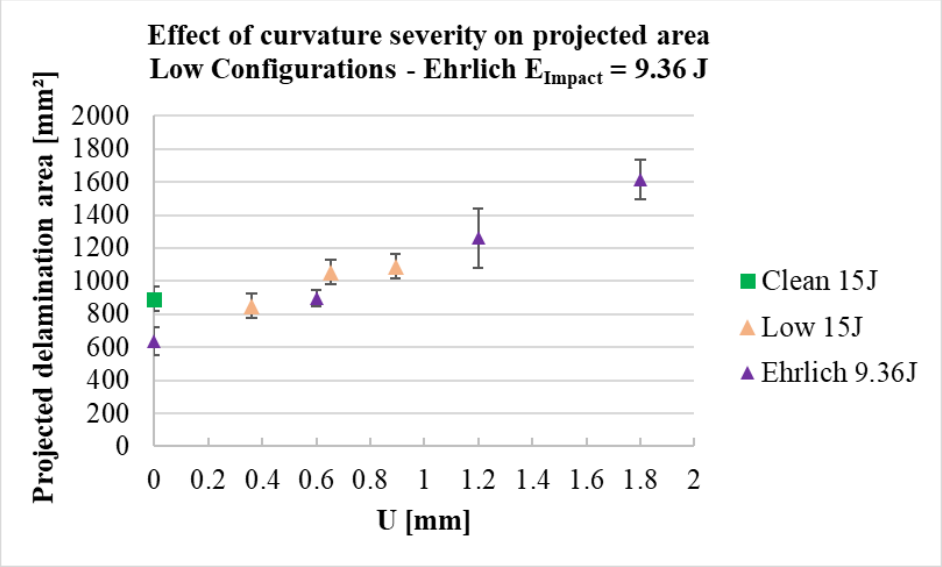

Figure 101: Projected areas comparison between the clean und low configurations of the current study and Ehrlich [36]

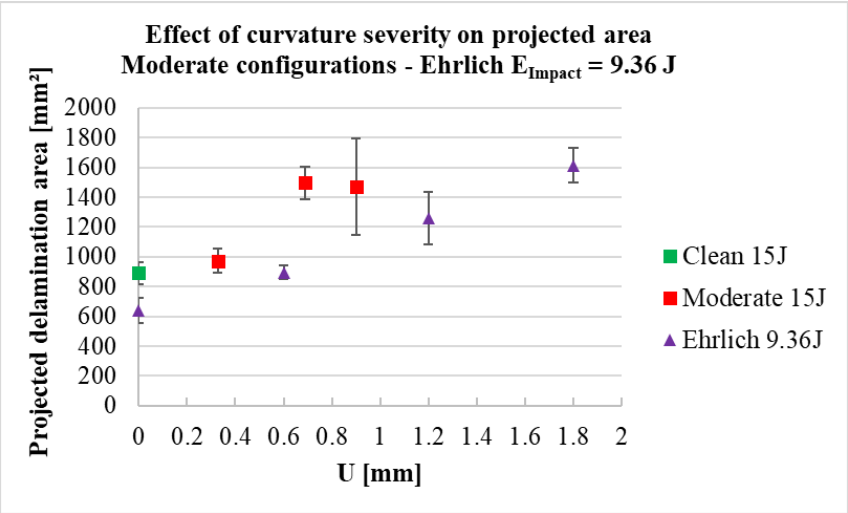

Figure 102: Projected areas comparison between the clean und moderate configurations of the current study and Ehrlich [36]

The maximal impact force of the investigated curved samples by Ehrlich are illustrated in dependence of U in Figure 103. Two dependencies are obvious**.** The maximal impact force depends on U as well as on the orientation of the curved samples. The maximal force in case of the convex samples is generally lower than the flat and concave samples. It is decreased with increased U. This relation reflects the sensitivity of convex structure against impact in comparison to concave impacted structure. The decrease of the maximal impact force with the increase of U is observed in the current investigation as shown in Figure 104, too.

Ehrlich stated, that the significant first force drop shown in Figure 105 provides similar dependencies as the maximal impact force. It is decreased with increasing U. Nevertheless, it can be stated, that these results are almost in the same range and the decrease is not noticeably pregnant as in case of the maximal impact force. In case of the current investigation, the significant first drop of the low and moderate configurations with 15° are slightly higher than the other configurations, nevertheless, it is almost in the same range as shown in Figure 106. No significant dependency with U is observed.

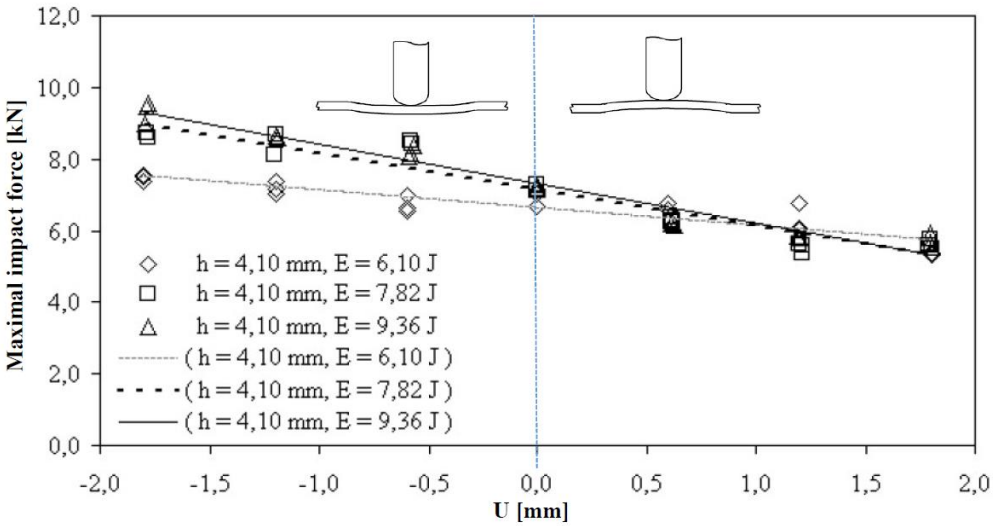

Figure 103: Maximal impact force in dependence of U [36]

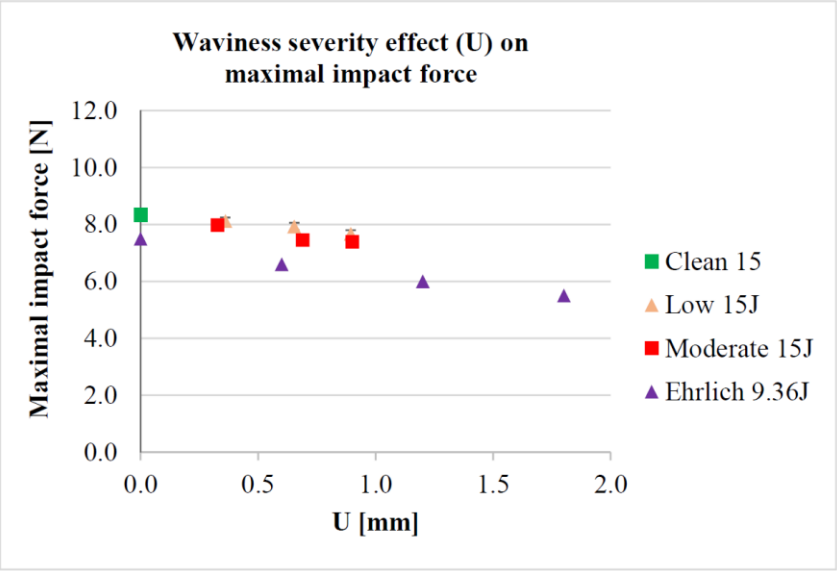

Figure 104: Maximal impact force in dependence on U, comparison between the clean und moderate configurations of the current study and Ehrlich [36]

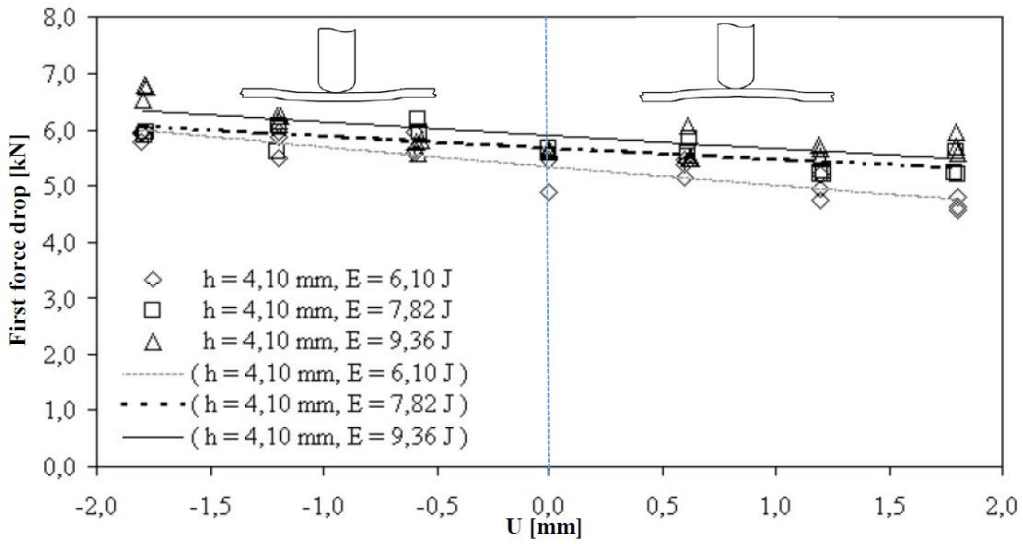

Figure 105: First force drop in dependence on U [36]

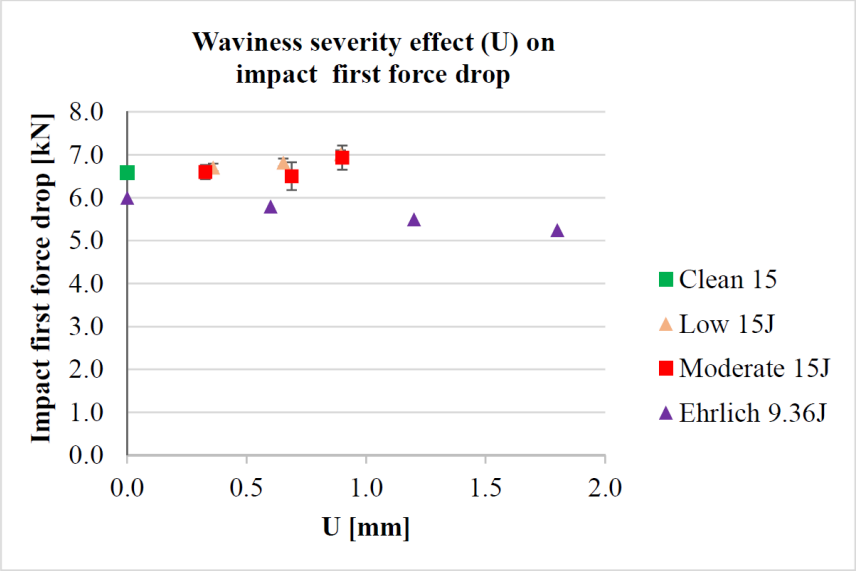

Figure 106: First significant force drop in dependence on U, comparison between the clean und moderate configurations of the current study and Ehrlich [36]

Working hypothesis 1.b: Effect of impact side relative to the orientation of the waviness morphology

The significant difference in the size of the projected delamination areas between the convex and concave specimens shown in Figure 23 indicates, that the impact side relative to the curvature orientation plays a crucial role on the damage resistance of the structure, too. The loading of a curved structure in the opposite direction to the curvature orientation leads to considerable interlaminar peel stresses as well as interlaminar shear stress provoking delaminations as described by Schürmann [40], too, see Figure 37.

In summary, in the event of an impact, waviness morphology and impact side relative to the waviness orientation are significant influencing factors, which affect the damage resistance of the structure and thus the residual strength. It makes a difference whether the waviness has a convex, concave or flat morphology. The experimental findings of Ehrlich and the current investigation provide similar tendencies. Thereby, the above-mentioned working hypotheses are verified.

Working hypothesis 1.c: Effect of impact position relative to the waviness position and waviness severity

By means of Rhead's [37] experimental results, working hypothesis 1.c is verified. Rhead investigated the effect of manufacturing induced tow gaps on the damage resistance and damage tolerance as described in Section 2.4. He demonstrated experimentally that the impact side relative to the defect position within the laminate thickness (= defect depth) as well as the defect geometry have a significant effect on damage resistance and damage tolerance behavior. Impacting a coupon directly over a tow gap (coupon A) produces a larger projected delamination area in comparison to an impacted sample with a tow gap close to the non-impact side (coupon B) as shown in Figure 25 (c and d). The projected delamination area of coupon A is approximately 1500mm², considering a circular area with a diameter of 44 mm. In case of coupon B, the projected delamination area is approximately 804 mm² considering a

diameter of 32 mm as shown in Figure 25 (c - d). That is why the CAI strength for coupon B was 14% higher in comparison to coupon A. That means, impacting a coupon directly over a tow gap represents the critical case.

Although the current investigated manufacturing defect differs from Rhead's defect type, his findings correlate well with the current investigated configurations regarding the criticality of the chosen impact position relative to waviness defect. Consequently, it is expected that impacting the plane side of the wavy specimens would produce a smaller projected delamination area and thus a higher residual strength. Nevertheless, this assumption should be proven numerically or experimentally. Accordingly, the impact side relative the defect position is an influencing factor, which has to be considered in future studies.

Working hypothesis 1.d: Effect of number of affected 0°-plies in dependence on the waviness angle

The findings of the current investigation indicate that waviness morphology, waviness angle and number of affected 0°-plies are influencing factors in both load cases PSC and CAI. The number of affected 0°-plies is a key influencing factor as shown in Figure 61, Figure 87 (b), respectively. The significant role of the number of affected 0°-plies ratio on strength reduction was investigated and demonstrated in the PSC load case by different authors namely Adams [7] and Duangmuan [9] as described in Section 2.2.

Further, relevant waviness parameters as the waviness angle, which are critical for the PSC load case are not automatically critical for the CAI as shown in Figure 95. In case of interaction, besides the identified influencing parameters; waviness morphology, impact side relative to the waviness position as well as impact side relative to the waviness orientation, there is an identified dependency between the waviness angle and number of affected 0°-plies.

From a certain number of affected 0°-plies, there is an additional significant reduction and a dependency from the waviness angle which cannot be neglected as shown in Figure 87 (b). It is challenging to verify these findings by independent data from the literature, because either the configurations are not comparable or there is a lack of relevant information to reliably guarantee comparability. In addition, there is no external literature treating the interaction between OoP and impact damages. Further, the strong dependency of the strength allowable from the manufacturing process quality complicates additionally the comparability with possible existing data. Nevertheless, Rivallant's experimental study described in Section 2.3 and in [29] is used to highlight the significant role of the 0°-plies on the compression after impact strength.

Rivallant used inter alia a QI laminate fabricated from material T700-M21 with the stacking sequence $[0_2,45_2,90_2, 45_2]_s$ and a thickness of 4.16 mm. Due to the impact, cracks in the upper 0°-plies under der impactor position were observed. It was found, that the strength reduction is related to the change in rupture mode: the presence of initial cracks in the 0°-plies at the impact location leads to a rupture by propagation of the cracks in the buckled plate. The reported failure stress/ load based on an impact energy of 29.5 J is approximately 150 MPa,

62.4 kN, respectively. The failure load of the clean specimen impacted with 35 J is 70.3 kN as shown in Figure 86, which is higher than Rivallant's impacted specimen.

The strength certainly depends on the respective material properties, which in turn depend on the manufacturing-induced defects that could arise during the manufacturing process. Abir [30] reported, depending on unintentional manufacturing-induced defects such as fiber misalignment, the compression strength in case of T700-M21 can vary widely (1015 MPa – 1465 MPa). Based on Hexcel [44] the compression strength of IM7-8552 is 1690 MPa. Based on Kaddour [50], it is 1590 MPa. Based on Ehrlich [36], it is 1500 MPa, which represents a deviation of 7% between these sources. Despite the notable deviation in compression strengths of both materials, it seems reasonable to assume that the reduction in Rivallant's impacted CAI specimen is more due to the damaged 0 °-plies rather than the discrepancy in the material properties.

Working hypothesis 1.e: Waviness effect on damage tolerance strain allowable
Currently, failure of the structure is prevented by setting a damage tolerance strain allowable for the component below the strain required to cause delamination propagation. However, if any reduction is detected in the damage tolerance strain allowable due to the presence of defects, an appropriate measure must be taken, to avoid structure collapse. Therefore, it is reasonable to investigate whether the damage tolerance strain is affected by the presence of a defect, when it is affected, respectively.

The current investigation shows that impact is the main driver for the strength reduction. It provides two tendencies regarding the damage tolerance strain as shown in Figure 88 (b). At certain conditions described in Section 5.4.2 the damage tolerance strain, failure membrane strain, respectively, is not significantly affected by the waviness and it is in the range of the samples without waviness. But from a certain increased number of affected 0°-plies, there is a significant dependency on the waviness angle followed by significant reduction in the strain level which can no longer be neglected.

Falco [38] investigated the effect of tow-drop gaps on the damage resistance and damage tolerance as described in Section 2.4. The staggered and no staggered gap specimens are illustrated in Figure 27 (a - b). Although his defect type differs from the current investigated defect type, his investigation provides similar tendencies. Impact is the main driver for the strength reduction. The longitudinal strain distributions of the staggered and no staggered gap specimens are affected by the tow-gaps and they differ from the baseline as shown in Figure 30. The longitudinal strain distributions of the low and moderate configurations are affected by the waviness and they differ from clean configuration, too, as shown in Figure 89.

Working hypothesis 1.f: Interaction effect between the thickness, waviness angle and number of affected 0°-plies
In Section 5.3 the thickness effect on the compression strength reduction was demonstrated by comparison performed between the 4 mm and 8 mm KDFs shown in Figure 72. All waviness parameters were identical in these configurations, except for the thickness. It was demonstrated, it is not only the waviness angle that is decisive for the reduction, but also the

thickness, which plays a crucial role in connection with the number of affected 0°-plies, number of unaffected 0°-plies, respectively.

Although, this finding seems to be reasonable, trials were done to verify it by independent data from the literature. To reduce possible influencing parameters to a minimum, investigations based on the same material used in the current investigation as well as a QI laminate were involved as shown in Table 16. Nevertheless, these investigations [10] and [13] differ also from the current investigation in the stacking sequences and the waviness morphology. Additionally, the waviness angle in [10] is different. The related number of affected 0°-plies ratio ($\alpha_{0°}$**)** is an estimation of the main affected 0°-plies in laminate midplane as shown in Figure 107. From this micrograph, it is obvious, that the other 0°-plies are affected by waviness, too. Their respective waviness angle was not reported by the author. As stated in Section 2.2, there is a lack of prior art studies investigating QI laminates, which complicates the verification. Considering all data shown in Table 16, the influence of the thickness cannot be clearly identified. This is due to large variations in the waviness parameters.

Considering Duangmuan's experimental results [9] described in Section 2.2 and Section 5.3, the thickness beneficial effect can be clearly identified. Some of his experimental results, which are based on cross ply laminates are summarized in Table 10. The considered two thicknesses have the same morphology and waviness angle but with different number of affected 0°-plies ratios ($\alpha_{0°}$)**.** In case of thickness 1 (2.79 mm), 60 % of the plies are affected by waviness. In case of thickness 2 (3.81 mm), 71 % of the plies are affected by waviness. Nevertheless, the resulting KDFs are in the same range (0.61) exhibiting the benefit of the thickness and verifying the findings of current investigation.

This comparison shows that the combination of different morphologies and waviness parameters as well as different thicknesses with comparable waviness angles could lead to very conservative KDFs. The worst case KDF based on data shown in Table 16 would be 0.35. As a result, any possible beneficial influence of the thickness can be lost. While comparable waviness morphologies and parameters provide the thickness effect on the KDFs reasonably.

Source	**Material**	**Layup**	**$t_{Nominal}$ [mm]**	**Morphology**	**Θ [°]**	**$\alpha_{0°}$ [%]**	**α [%]**	**KDFs [-]**
Current investigation	IM7–8552	$[[45/-45/90/45/0/-45/90/0]_2]s$	4.0	B	15	13	16	0.89
			4.0		15	25	25	0.86
			4.0		15	38	41	0.80
		$[[45/-45/90/45/0/-45/90/0]_4]s$	8.0		15	13	13	0.95
[13]	IM7–8552	$[[0/45/-45/90]_5]s$	5.1	C	15	100	100	0.35
[10]	IM7–8552	$[[45/90/45/0]_3]s$	6.0	A	10	33	N/A	0.67
					12	33	N/A	0.67

Table 16: KDFs of QI-laminates related to different morphologies and thicknesses

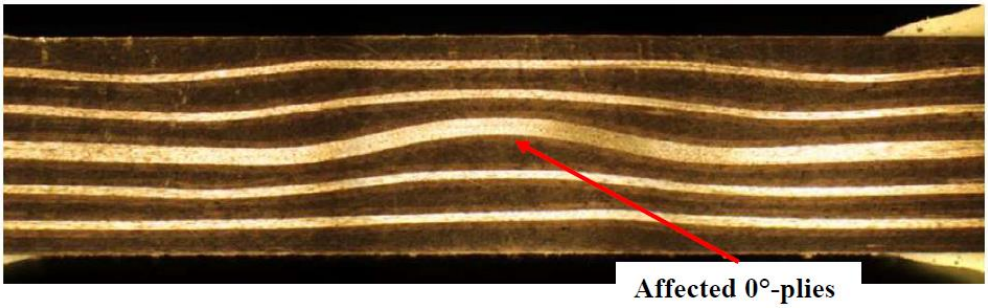

Figure 107: Mukhopadhyay's wavy specimen with centralized waviness in laminate midplane, morphology A [10]

Working hypothesis 2.: Main influencing factors of waviness defects, impact and the effect of their combinations

The second working hypothesis regarding defining and the assessment of the main influencing factors of waviness, impact and the effect of their combinations on the residual strength is verified by the current experimental investigation and the experimental data from the literature. Based on that, the influencing factors are summarized in Table 17.

Influencing factors	Reference	Load cases		
		PSC	CAI only impact	CAI Interaction
Energy level	[23], [2]		✓	✓
Waviness morphology (Convex, concave or flat)	[36], [2]	✓		✓
Impact side relative to the orientation of the waviness morphology	[36], [2]			✓
Impact position relative to the waviness position	[37], [2]			✓
Curvature severity (U)	[36], [2]		✓	✓
Waviness angle (Θ)	Different	✓		✓
No. of affected 0°-plies ratio (α_0)	[7], [9], [2]	✓	✓	✓
No. of total affected plies ratio (α)				
Thickness (t)	[9], [2], [23]	✓	✓	N/A
Thickness dependency from Θ and α_0	[7], [9], [2]	✓		N/A

Table 17: Influencing factors derived from the current experimental investigation and literature

Working hypothesis 3.: Derivation of a simplified physical interaction relation of out of plane waviness and impact

The third working hypothesis regarding the derivation of a simplified physical interaction relation of out of plane waviness and impact (Equation 14) is verified by the current investigation as described in Section 5.5. The simplified interaction relation assumes that impact is main driver for strength reduction.

Falco [38] investigated the effect of tow-drop gaps on the damage resistance and damage tolerance using different impact energy levels as described in details in Section 2.5. He found out, that the compression strength reduction is driven by the impact itself rather than by the influence of manufacturing-induced defects. His experimental findings correlate well with the current investigation. First, impact is the main driver for the strength reduction. Accordingly, the main assumption on which the simplified interaction relation based on, is verified. Second, the effect of defect depends on the energy level and defect parameters (waviness parameters).

Although, there is no information related to the gap density or data describing the gap geometry, it was observed by Falco [38] with comparable impact energy of 15 J to current investigation, that the delamination shape of both investigated gap configurations is comparable to the sample without gaps as shown in Figure 28 and Figure 29. The residual CAI strength of defective specimens does not present significant differences to the gap free samples. Falco's observations correlate well with observations done in the low configurations. The delamination shape of the low configurations is similar to the clean configuration (without waviness) as shown in Figure 81 to Figure 82. Their corresponding failure loads were in the similar range as the clean configuration as shown in Figure 87 (b).

In contrast, Ghayour's [39] experimental investigation on the effect of periodically induced gaps on the impact response described in Section 2.4 showed that an 8 % of gap percentage in the whole laminate can change the shape of the projected delamination pattern and increase the delamination area up to 50 % as shown in Figure 32. The change in the shape of the projected delamination pattern and the increase in the projected delamination area were observed in the moderate waviness configurations as shown in Figure 80 (Size of projected delamination area) and Figure 83 to Figure 84 (Shape of delamination areas of configurations with 10° and 15°).

In spite of the difference in the defect types, the material used as well as layup sequences both works [38] and [39] provide independently the identified two tendencies described in Section 5.4 confirming the link between the energy level and defect parameters. Further, these works confirm that the chosen impact energy level for the current experimental work to investigate the waviness effect on the damage resistance and damage tolerance was suitable. Because it enabled to show the dependency between the impact energy level and waviness angle in dependence on the number of affected 0°-plies as well as the waviness effect on the strain level and stability behaviour.

The research and working hypotheses are successfully verified by the current experimental and external investigations. The physical interaction effect between out of plane waviness and impact is demonstrated as shown in Section 5.4. This interaction represents a multiplicative relation, in which the OoP waviness effects cannot compensate impact effects or vice versa due to the structural mechanical aspects described in Section 5.5. Nevertheless, the observability of the interaction depends on the energy level and waviness parameters, defect parameters, respectively, as observed implicitly by Rhead [37], Falco [38] and Ghayour [39], too. A simplified interaction relation is derived and its limits are given in Section 5.6.

The considered external literature, especially Ehrlich's work [36] reveal that in the current experimental campaign selected impact side relative to waviness position and orientation are chosen rational, because they represent critical influencing parameters. Based on the current and the external investigations, the main influencing factors are identified and summarized in Table 17.

Finally, an important finding is observed; gathering different waviness morphologies, waviness parameters, different thickness and different impact sides relative to waviness orientation and position can lead to a very conservative KDFs as shown in this investigation, Table 16, respectively. This would underestimate the structure capacity. Consequently, building distinction cases based on the identified influencing factors given in Table 17 would reduce possible conservatisms in case of interaction between OoP waviness and impact damages an. Additionally, the identified influencing factors can server as distinction cases catalogue to identify critical cases.

7 Final remarks

7.1 Main conclusions and benefits

Within the present experimental investigation, a test campaign with 105 specimens that examines the interaction effect between out of plane (OoP) waviness and low velocity impact on the compression strength of a quasi-isotropic laminates (QI) was conducted. Undamaged (plain strength compression = PSC) and impacted (compression after impact = CAI) specimens were fabricated with and without OoP waviness. This test campaign differs from existing experimental studies by examining the above-mentioned interaction, as well as treating relevant parameters as numbers of affected plies and 0°-affected plies in dependence on waviness angles (Θ).

To derive empirical understanding of the interaction behavior and the role of the relevant parameters in each load case, different knock down factors (KDFs) were introduced. The pure waviness effect in an undamaged and impacted structure is defined by ($KDF_{Wav,\ PSC}$) and ($KDF_{Wav,\ CAI}$), respectively. $KDF_{Wav,\ PSC}$ is normalized by the PSC failure load without waviness. $KDF_{Wav,\ CAI}$ is normalized by the CAI failure load without waviness. Additional KDFs were provided for the pure impact ($KDF_{Imp,\ CAI}$) and the interaction effect ($KDF_{Interaction,\ CAI}$). $KDF_{Imp,\ CAI}$ and $KDF_{Interaction,\ CAI}$ are normalized by the failure load without impact and waviness damages. $KDF_{Imp,\ CAI}$ provides the reduction in the compression strength due to the impact event itself. In contrast, $KDF_{Interaction,\ CAI}$ provides the strength reduction due to the simultaneously presence of waviness and impact damages.

In the PSC load case ($KDF_{Wav,\ PSC}$), the waviness morphology, waviness angle and number of affected 0°-plies in dependence on the thickness are the relevant influencing factors which can lead to a significant reduction in the compression strength. A larger thickness can have a beneficial effect on the residual strength comparing two laminates with similar waviness influencing factors. However, the combination of different morphologies, waviness parameters as well as different thicknesses with even comparable waviness angles can lead to conservative KDFs underestimating the structure capacity. As a result, any possible beneficial influence of the thickness can be lost.

In the CAI case without waviness ($KDF_{Imp,\ CAI}$), the reduction in the strength depends on the impact energy. This affects the projected delamination size, shape and delamination distribution within the laminate thickness. Consequently, the stability behavior of the structure and thus the final failure load and failure modes depend also on the impact energy level.

Comparing the pure impact KDF ($KDF_{Imp,\ CAI}$) with the CAI pure waviness KDF ($KDF_{Wav,\ CAI}$) show that impact itself is the main driver for the strength reduction. Nevertheless, waviness can lead to an additional strength reduction which depends on the number of affected 0°-plies. $KDF_{Wav,\ CAI}$ shows two tendencies. In the first one, it is characterized by negligible dependency on the waviness angle and strength reduction. In the second tendency, from a certain number of affected 0°-plies, there is an additional significant

strength reduction and a dependency from waviness angle which cannot be neglected. The compression strength is decreased with increased waviness angle. Consequently, there is a dependency between the number of affected 0°-plies and the waviness angle.

In the interaction case ($KDF_{Interaction,\ CAI}$), a distinction with regards to the impact direction relative to the waviness orientation and waviness position has to be made. These influencing parameters affect the damage resistance response of the structure and consequently the interaction KDF, too. The same two tendencies are observed as for $KDF_{Wav,\ CAI}$. In the tendency with negligible dependency on the waviness angle, the $KDF_{Interaction,\ CAI}$ and failure membrane strains (far field strains) are in the range of the impacted structure without waviness ($KDF_{Imp,\ CAI}$). Nevertheless, the inplane strain distribution and out of plane deformation are affected by the waviness. The reason for these observed tendencies is related to the increased number of affected 0°-plies. The dependency on the affected 0°-plies is a result of the local sub-buckling mode and load.

The comparison of these KDFs reveals that the waviness effect in the investigated impact energy level is present, even if this effect is not always evident in the KDFs. Accordingly, the evaluation of the experimental study indicates, that the interaction behavior represents approximately a multiplicative relation in the investigated cases. Waviness effects cannot compensate impact effects or vice versa, thus a multiplicative relation seems reasonable.

The comparison of the pure waviness effect KDF of an undamaged ($KDF_{Wav,\ PSC}$) and impacted structure ($KDF_{Wav,\ CAI}$) shows that both KDFs are in a comparable range. Nevertheless, $KDF_{Wav,\ CAI}$ shows the above mentioned two tendencies compared to $KDF_{Wav,\ PSC}$, which depends on the waviness angle. This comparison shows that the identified multiplicative relation can be further approximated by means of the two knock down factors $KDF_{Imp,\ CAI}$ and $KDF_{Wav,\ PSC}$. This simplification is a useful mean for preliminary assessment of the interaction behavior, since both KDFs comprise independently the driving factors for the strength reduction. It does not mean that there is no interaction between both defects. Nevertheless, the joint effect of both, impact and waviness, could be roughly estimated by superposition of both individually determined effects.

This simplified approach provides also valuable benefits in terms of reducing the experimental and numerical efforts. Usually, the investigation of the interaction behavior requires the fabrication of defective and pristine specimens. The waviness fabrication method as well as conducting CAI tests with specimens having different morphologies can be a big challenge. On the one hand, the fabrication method can strongly affect the relevant waviness parameters. On the other hand, the CAI test fixture is designed for plane specimens. In contrast, PSC test fixtures are more flexible with regards to the waviness morphology. So that the waviness effect can be investigated by means of conducting PSC tests instead of CAI tests, under the assumption that impact is the main driver for the strength reduction. Nevertheless, it has to be considered that both damages provoke independently different failure modes under compression loading. Besides the impact induced delaminations, waviness affects the delamination shape, size and distribution. Both damages affect independently the initial position of the neutral axis inducing a change in the deformation,

loading state and the stability behavior. It is assumed that these processes occur simultaneously, so that both damages reinforce the compression strength reduction.

In this thesis, distinction cases developed helped to identify the relevant influencing factors separately and in interaction as well as the dependencies between them. These distinction cases are related to the differentiation between the waviness morphology in dependence on the impact side relative to the waviness orientation, impact position as well as the waviness parameters. Considering these distinction cases serve as a guideline for achieving targeted findings by designing a suitable experimental campaign as well as reducing the numerical efforts. They also could be an opportunity for weight saving by means of designing more damage tolerant structures, reducing conservatisms in design methods and consequently a way forward minimizing repair. These aspects could offer economic benefits for the industrial applications.

The current investigation and reviewed works enabled the demonstration of the link between the impact energy level and the relevant defect parameters. The chosen impact energy level for the current experimental investigation was suitable, because it enables to reveal the dependency between the impact energy level and role of the relevant influencing factors on the CAI strength reduction. Despite big waviness angle in case of the low waviness configurations, the strength decreased was negligible. Therefore, it is reasonable putting the waviness angle in context to the other influencing parameters. Such considerations could help in the future to design more damage tolerant structures. Nevertheless, further investigations are required.

In summary, it can be stated, that it is the interplay between the waviness morphology, number of affected 0°-plies and waviness angles that are the relevant variables in dependence on the impact energy and impact direction relative to waviness orientation and position for reducing the compression strength and not just the waviness angle alone and projected delamination areas. These interrelationships have not been formulated or published with such clarity by other authors yet.

7.2 Critical assessment of the interaction approach

The conducted experimental investigation indicates that the interaction behavior represents approximately a multiplicative relation in the investigated cases. Impact and waviness provoke different failure modes in the event of compression loading. They occur independently of each other and each of them reduces the final compressive failure load independently.

For the investigated layup, material, impact scenario and waviness morphology, the derived CAI interaction KDF formula ($KDF_{Interaction,\ CAI}$) provides the dependencies between these influencing factors on the strength reduction. Although, it is reasonable to assume that the multiplicative relation would be valid for other layups, material, impact scenario and waviness morphology, nevertheless, the role of each influencing factors has to be investigated. For instance, the already identified dependency between the impact side and waviness morphology which strongly affects the damage resistance. Altmann [19] also found, that matrix properties strongly affect the failure mechanism of wavy structure under compression loading and consequently the compression strength in the interaction case, too. The dependencies between the individual influencing factors must be examined more intensively in order to quantify the effect of each factor more precisely.

The simplified interaction KDF formula ($KDF_{Interaction}$) can be a useful mean for preliminary assessment of the interaction behavior and for reducing the experimental effort, since each KDF ($KDF_{Imp,\ CAI}$ and $KDF_{wav,\ PSC}$) comprises independently the driving factors for the reduction. Nevertheless, it has to be stated that $KDF_{Imp,\ CAI}$ is derived from a standard specimen without curvature. Although, impact is the main driver for reduction, the damage resistance and consequently the residual strength depends on the impact side relative to the waviness orientation. Out of plane waviness with convex shape is less damage tolerant in comparison to out of plane waviness with concave shape. For the case that the available $KDF_{Imp,\ CAI}$ is derived from a wavy specimen with concave shape to cover a convex impacted wavy specimen, the resulting interaction KDF would be not conservative, because it overestimates the residual compression strength. Further, it has to be taken into the account that the pure waviness KDF ($KDF_{wav,\ PSC}$) depends on the waviness angle. In contrast, the CAI pure waviness KDFs show ($KDF_{wav,\ CAI}$) that the waviness angle comes firstly into play at a certain increased number of affected 0°-plies. At small range of affected 0°-plies there is no significant dependency from waviness angle. But, there is a significant reduction in the KDFs, when the number of affected 0°-plies is increased. Also, the interplay between the waviness morphology and the deformation behavior strongly affects the resulting interaction KDF, failure mode and position.

These limits demonstrate the need for additional investigations described in the next section.

7.3 Future works

Different influencing factors and dependencies are identified in the investigated load cases. Nevertheless, further investigations given below would be beneficial, which would strengthen the physical understanding of the interaction behavior, so that the derived relations would be generalized for covering more cases. In addition, it would help to reduce the experimental and numerical efforts by considering the relevant influencing factors and dependencies.

Numerical verification

The experimentally derived interaction approach should be verified numerically by considering the tested configurations and their fabrication method. In the plain strength compression (PSC) and interaction load cases, the focus of the numerical analysis should be directed towards the dependencies between the waviness morphology, waviness angle and number of affected 0°-plies. Additionally, in the interaction load case, the focus of the analysis needs to be directed towards the waviness effect on the delamination shape, size of the projected delamination area, the through the thickness delamination distribution as well as the changed stability behavior due to the waviness and dependency on the number of affected 0°-plies, too.

These outputs determine the quality of the numerical simulation. Once, the numerical verification is successfully completed, the applicability of the interaction approaches to other cases given in Section 5.6 should be investigated.

Analytical simplification

The current experimental investigation provides improved phenomenological understanding of the interaction behavior between out of plane waviness and impact damages. In the long term, it should be aimed to reduce the numerical and experimental efforts. This goal can be achieved by the derivation of more specific and robust analytical relations which require further investigations:

- Experimental or numerical investigations with further stepwise increased number of affected 0°-plies in dependence on different waviness morphologies (A, B and C) as well as impact side relative to the waviness orientation would be recommendable.
- Investigate whether the identified dependency between the curvature induced by the waviness and the impact side is present in a flat specimen affected by waviness (morphology A). This distinction within morphology A enables a better physical understanding of the interaction behavior and a check, whether the variation in the residual strength is a consequence of this dependency.
- The PSC experimental results indicate that larger thickness have beneficial effect on the compression strength. The literature lacks CAI tests with thick laminates. The majority of the investigated specimens are in the range of 4 mm to 5 mm. In addition, there is no CAI test related to thick specimens with out of plane waviness. Based on Abrate [23] the thickness has a significant effect on the magnitude of the maximum contact force which affect the extent of the damage induced. Thin laminates respond primarily by bending, which causes high tensile stresses in the outer ply leading to an increased delamination area in the direction of the impacted side (reversed pine tree). For thicker laminates, damage is initiated by high contact stresses and propagates

downwards in the direction of the non-impacted side building a pine tree distribution. Therefore, there is a need to better understand the waviness effect in thick impacted laminates.

KDFs on structural level

Different KDFs are derived experimentally in this investigation on coupon level. The captured effect of defect by these coupons represents only local effects. It is assumed that the transfer on the structural level would be not significant. However, it is recommendable to perform experiments and numerical simulations on structural level to quantify the interaction effect on the compression strength reduction on real components.

References

[1] F. Heineck und C. Willberg, „Manufacturing-Induced Imperfections in Composite Parts manufactured via Automated Fiber Placement," Journal of composites Science, 2 June 2019.

[2] N. Al-Kathemi, T. Wille, R. D. F. Heinecke und M. Wiedemann, „Interaction Effect of Out of Plane Waviness and Impact Damages on composite structures – An Experimental Study," Composite Sructures, 2021.

[3] G. Fernlund, J. Wells, L. Fahrang, J. Kay und A. Poursartip, „Causes and remedies for porosity in composite manufacturing," in 37th Riso International Symposium on Material Science, 2016.

[4] G. W. Ehrenstein, Faserverbund-Kunststoffe, Hanser.

[5] H. Hsiao und I. Daniel, „Effect of Fiber Waviness on Stiffness and Strength Reduction of Unidirectional Composite under Compressive Loading," Compsote Science and Technology 56, pp. 581-593, February 1996.

[6] H. Hsiao und I. Daniel, „Elastic properties of composites with fiber waviness," Composites Part A, pp. 27(10) 931-941, 1996.

[7] O. D. Adams und S. J. Bell, „Compression Strength Reductions in Composite Laminates due to Multiple Layer Waviness," Compsite Science and Technology Vol. 53, pp. 207-212, 1995.

[8] H.-J. Chun und I. M. D. Jai-Yoon Shin, „Effects of material and geometric nonlinearities on the tensile and compressive behavior of composite materials with fiber waviness," Composite Science and technology 61, pp. 125-134, August 2000.

[9] P. Duangmuan, „Layer Waviness Effects on Comression Strength of Composite Laminates: Progressive Failure Analysis and Experimental Validation," August 2012. [Online]. Available: https://core.ac.uk/download/pdf/276266518.pdf.

[10] S. Mukhopadhyay, M. I. Jones und S. R. Hallett, „Modelling of out-of-plane fibre waviness; Tension and compression tests," in IV ECCOMAS Thematic Conference on the Mechanical Response of Composites, 2013.

[11] I. A. Khattab, A Noval Numerical Approach and Experimental study on the Waviness Defects in Composite Structures, Braunschweig, 2013.

[12] A. P. J. Altmann, „Matrix dominated effects of defects on the mechanical properties of wind turbines blades," 04 May 2015. [Online]. Available: https://mediatum.ub.tum.de/doc/1233442/1233442.pdf.

[13] M. Thor, U. Mandel, M. Nagler, F. Maier, J. Tauchner, M. Sause und R. Hinterhölzl, „Numerical and experimental investigation of out of plane fiber waviness on the mechanical properties of composite materials," 17 1 2020. [Online]. Available: https://link.springer.com/content/pdf/10.1007/s12289-020-01540-5.pdf.

[14] H. Rai, C. W. Rogers und D. Crane, „Mechnics of Curved Fiber Composites," Journal of Reinforced Plastics and Composites Vol.11, pp. 552-566, May 1992.

[15] T. A. Bogetti, J. W. Gillespie und J. a. M. A. Lamontia, „Influence of Ply Waviness on the Stiffness and Strength Reduction on Composite Laminates," Journal of Thermoplastic Composite Materials Vol. 5, pp. 344-369, October 1992.

[16] T. A. Bogetti, J. W. Gillespie und J. a. M. A. Lamontia, „The Influence of Ply Waviness with Nonlinear Shear on the Stiffness and Strength Reduction of Composite Laminates," Journal of Thermoplastic Compsote Materials Vol. 7, pp. 76-90, April 1994.

[17] M. R. Garnich und G. Karami, „Finite Element Micromechnics for stiffness and strength of wavy fiber Composites," Journl of Composite Materials, pp. 273-292, 2004.

[18] P. Gesell, „Einfluss von Welligkeiten in Faserverbunwerkstoffen auf Steifigkeiten und Festigkeiten," 25 July 2013. [Online]. Available: https://www.researchgate.net/publication/299424984_Einfluss_von_Faserwelligkeit_in_Faserverbundwerkstoffen_auf_Steifigkeit_und_Festigkeit#fullTextFileContent.

[19] A. Altmann und P. Gesell, „Strength prediction of ply waviness in composite materials considering matrix dominated effects," Composite Structure, pp. 127:51-59, March 2016.

[20] S. Eskandari, F. Andrade Pires, P. Camanho und A. Marques, „Damage analysis of out of plane undulated fiber composites," Composite Structures, pp. 464-476, May 2016.

[21] S. Mukhopadhyay, I. J. Mike und S. R. Hallett, „Tensile failure of laminates containing an embedded wrinkle; numerical and experimentall study," Composite: Part A, pp. 219-228, July 2015.

[22] [Online]. Available: www.airliners.net.

[23] S. Abrate, Impact on Composite Structure, Cambridge University Press, 1998.

[24] J. Baaran, L. Kärger und A. Wetzel, „Efficient Prediction of Composite Damage Tolerance," 2006. [Online]. Available: https://elib.dlr.de/47206/1/Efficient_prediction.pdf.

[25] L. Kärger, „Effiziente Simulation von Schlagsschädigungen in Faserverbund-Sandwichstrukturen," 2007. [Online]. Available: https://elib.dlr.de/53070/1/dissertation.pdf.

[26] P. Mendes und M. Donadon, „Numerical Prediction of Compression After Impact behavior of Woven Composite Laminates," Composite Structures 113, pp. 476-491, 2014.

[27] S. Rivallant, C. Bouvet und N. Hongkarnjanakul, „Failure analysis of CFRP laminates subjected to compression after impact: FE simulation using discrete interface elements," Nr. Vol. 55, pp. 83-93, 2013.

[28] A. T. Method, Determination of Compression Strength after Impact, Airbus, Hrsg., 2005.

[29] S. Rivallant, C. Bouvet, E. A. Abdallah, B. Broll und J.-J. Barrau, „Experimental analysis of CFRP laminates subjected to compression after impact: The role of impact-induced cracks in failure," Composite Structures 111 , p. 147–157, 2014.

[30] M. Abir, T. Tay, M. Ridha und H. Lee, „Modelling Damage Growth in Composites

subjected to Impact and Compression After Impact," Composite Structures 168, pp. 13-35, 2017.

[31] W. Tan, B. G. Falzon, L. N. Chiu und M. Price, „Predicting Low Velocity Impact Damage and Compression After Impact (CAI) behaviour of Composite laminates," Composites: Part A 71, pp. 212-226, 2015.

[32] R. Bogenfeld, J. Kreikemeier und T. Wille, „An Analytical Approach for Low-Velocity Impact on Composite Structure," Composite Structures 187, pp. 71-84, 2018.

[33] R. Bogenfeld, J. Kreikemeier und T. Wille, „Review and Benchmark study on the Analysis of Low-Velocity Impact on Composite Laminates," Engineering Failure Analysis 86, pp. 72-99, 2018.

[34] K. Huang, A. d. Boer und R. Akkermann, „Analytical Modelling of Impact Resistance and Damage Tolerance of Laminated Composite Plates," AIAA Journal Vol. 46, No.11, pp. 2760-2772, November 2008.

[35] A. T. Rhead, R. Butler und G. W. Hunt, „Compressive strength of composite laminates with delamination-induced interaction of panel and sublaminate buckling modes," Composite Structures, pp. 326-334, 6 March 2017.

[36] I. Ehrlich, „Impactverhalten schwach gekrümmter Strukturen aus faserverstärkten Kunststoffen," December 2004. [Online]. Available: https://d-nb.info/973886102/34.

[37] A. Rhead, T. Dodwell und R. Butler, „The effect of tow gaps on compression after impact strength of robotically laminated structures," Computers, Materials & Continua, Nr. volume 35 , pp. 1-16, 2013.

[38] O. Falco, C. Lopes, J. Mayugo, N. Gascons und J. Renart, „Effect of tow-drop gaps on the damage resistance and tolerance of Variable-Stiffness Panels," pp. 94-103, 19 May 2014.

[39] M. Ghayour, M. Hojjati und R. Ganesan, „Effect of tow gaps on impact strength of thin composite laminates made by Automated Fiber Placement: Experimental and semi-analytical approaches," Composite Structures 248 (2020) 112536, 30 05 2020.

[40] H. Schürmann, Konstruieren mit Faser-Kunststoff Verbunden, Springer, 2007.

[41] R. Roos, Model for interlaminar normal stresses in doubly curved laminates, S. F. I. o. T. Zurich, Hrsg., 2008.

[42] K. Manikarnika, „Compression Strength of Wrinkled Composite Laminate," DTU Wind Energy - Department of wind energy, 2016.

[43] A. T. M. Method, Determination of Plain, Open Hole and Filled Hole Compression Strength, 2015.

[44] Hexcel, HexPly 8552 Epoxy matrix (180°C/356°F curing matrix).

[45] K. Hoffmann, Eine Einführung in die Technik des Messen mit Dehnungsmessstreifen, Darmstadt : Hottinger Baldwin Messtechnik, 1987.

[46] HBM, „www.hbm.com," 2020. [Online]. Available: https://www.hbm.com/de/6021/tipps-fuer-die-experimentelle-spannungsanalyse/.

[47] S. Neßlinger, „Analyse von reinfiltrierten Schäden in Faserverbundkunstoffen," 2016. [Online]. Available: https://docplayer.org/59798008-Masterarbeit-analyse-von-

reinfiltrierten-schaeden-in-faserverbundkunststoffen-sebastian-nesslinger.html.

[48] S. Sanchez-Saez, E. Barbero, R. Zaera und C. Navarro, „Compression after impact of thin composite laminates,“ Spain.

[49] M. Gaedke, „Methodology for residual strength of damaged laminated composites,“ 1997.

[50] A. S. Kaddour, M. J. Hinton, S. Lic und P. A. Smith, „Failure exercises: How can composites design and manufacture communities build their strength,“ in ECCM16 - 16TH European conference on composite materials, Sevilla, Spain, 2014.